The Higgs decay and dark matter in the gauge-Higgs unification

Ph.D. thesis

Shuichiro Funatsu

Department of Physics, Osaka University,
Toyonaka, Osaka 560-0043, Japan
funatsu@het.phys.sci.osaka-u.ac.jp

22nd February 2016

Abstract

The scenario of gauge-Higgs unification solves the fine-tuning problem associated with the Higgs boson mass. In particular, the $SO(5) \times U(1)$ gauge-Higgs unification is phenomenologically viable. The Higgs boson is unified with the gauge bosons as the fifth-dimensional component of the gauge fields. The Higgs boson appears as a fluctuation mode of the Wilson line phase θ_H along the fifth dimension. The observed Higgs boson with mass 125 GeV is realised with $SO(5)$-spinor fermions in addition to the $SO(5)$-vector quark-lepton multiplets. The constraint for this model is obtained from the Z' signals at the LHC in dilepton events. Candidates for the Z' are the first Kaluza-Klein modes of Z, Z_R and γ and the allowed region of Z' mass is found to be $4 \sim 9$ TeV for θ_H from 0.2 to 0.07. The model possesses the universality under which various physical quantities such as the Kaluza-Klein scale and the Higgs self couplings are determined by θ_H.

In this thesis, the Higgs boson decay and the dark matter candidate in this model are studied. The decay processes $H \to \gamma\gamma$ and $H \to Z\gamma$ occur at the one-loop level. In spite of the presence of an infinite number of the Kaluza-Klein modes in the loops, the corrections turn out finite and the deviations of these decay rates from the standard model become approximately $O(1)\%$. The branching ratios of the Higgs boson are consistent with the standard model. The lowest mode of the $SO(5)$-spinor fermions, which couples to $SU(2)_L$ very weakly and is stable, becomes a candidate for the dark matter. The observed relic density of the dark matter is reproduced with the Breit-Wigner enhancement in the annihilation processes. From the direct detection experiments, the allowed region of their mass is from 2.6 to 3.1 TeV, which corresponds to $0.07 < \theta_H < 0.09$ ($9.0 < m_{\rm KK} < 10.4$ TeV).

Contents

1. Introduction

In 2012, the Higgs boson was discovered at the Large Hadron Collider (LHC) by the ATLAS group [1] and the CMS group [2]. As of 2015, the combined result of the Higgs mass with the ATLAS and the CMS is $m_H = 125.09 \pm 0.24$ GeV [3]. By the discovery of the Higgs boson, all of the particles in the standard model (SM) were discovered. The measured branching ratios of the Higgs boson is consistent with those in the SM [4, 5] and no particles beyond the SM have been discovered [6, 7]. Although the SM have been successful so far, it is not complete. There is the so-called fine-tuning problem. The radiative correction to the Higgs boson mass squared is proportional to the square of the cutoff parameter. If the cutoff scale of the SM is far larger than the electroweak (EW) scale, the bare Higgs boson mass must be fine-tuned to produce the observed Higgs boson mass. Hence the more fundamental theory will appears in the high energy scale which is not far larger than the EW scale. The LHC has started run 2 from 2015. By this run, the properties of the Higgs boson are measured and physics beyond the SM is expected to be observed.

The other problem of the SM is that there are no candidates of the dark matter (DM) in the SM. The Planck data [8] indicate the existence of the DM. In contrast, the DM has not been detected by the direct detection experiments such as the LUX experiment [9,10] so far. The DM might be detected by the 300 live-days result of the LUX experiment or future experiments such as the XENON 1T experiment.

To solve the fine-tuning problem and to explain the existence of the DM, the more fundamental theory beyond the SM is necessary. The fine-tuning problem of the Higgs boson mass is one of the keys to study the more fundamental theory. The fine-tuning problem occurs because the Higgs boson mass is not protected by symmetry in the SM. Therefore one of the approach to solve the fine-tuning problem is to protect the Higgs boson mass by some symmetry. The gauge-Higgs unification is one of the scenario which can solve the fine-tuning problem. In gauge-Higgs unification, the Higgs boson mass is unified with the gauge boson as an extra-dimensional component of the gauge field [11–19]. Therefore the Higgs boson mass is protected by the gauge symmetry in GHU scenario. In five-dimensional GHU, the Higgs boson does not have the potential at the tree level. By radiative corrections, the Higgs boson acquires the mass and the vacuum expectation value (VEV) which minimise the effective potential. This VEV is physical because the VEV can not be gauged away. The Higgs boson appears as a fluctuation mode of the Wilson line phase θ_H along the fifth-dimension. The one more important point is that the acquired Higgs mass is found to be finite at the one loop level. This is the so-called Hosotani mechanism [11, 12].

In particular, the $SO(5) \times U(1)$ GHU model is a viable model of the scenario beyond the SM [20–25]. In the model, the Lagrangian has the $SO(5) \times U(1)_X$ symmetry. The $SO(5)$ symmetry is broken to $SO(4)$ symmetry by the boundary condition and the Higgs doublet appears as $SO(5)/SO(4)$ element. The remaining $SO(4) \times U(1)_X \simeq$

$SU(2)_L \times SU(2)_R \times U(1)_X$ symmetry is broken to $SU(2)_R \times U(1)_Y$ symmetry by the brane interaction. Finally, $SU(2)_R \times U(1)_Y$ symmetry is broken to $U(1)_{\rm EM}$ by the Hosotani mechanism.

The effective potential has minimum at $\theta_H = \frac{\pi}{2}$ in the minimal model with the quarks and leptons in the $SO(5)$-vector multiplets [23]. The Higgs boson coupling to the SM particles are approximately suppressed from the SM value by $\cos\theta_H$ [24]. Therefore $\theta_H = \frac{\pi}{2}$ leads to the stable Higgs boson and contradicts the experiments. Thus the value $\theta_H \neq \frac{\pi}{2}$ is required and it is realised by adding the $SO(5)$-spinor fermions. The parameter sets which realise the observed Higgs boson with mass 126 GeV are obtained in [26]. In the paper, the non-trivial relation between the Kaluza-Klein (KK) scale and the θ_H is found. The relation is called the universality and later more concretely studied in [27]. By this universality, this model is very predictive. In the paper [27], the Z' signal at the LHC is predicted. In this model, the Z' is the KK Z, Z_R and γ where Z_R is the neutral $SU(2)_R$ gauge boson and does not have zero mode. By the constraint from the 8 TeV LHC result, the Z' mass must be larger than about 4 TeV. By the universality, it corresponds to $\theta_H < 0.2$.

One of the topics covered in this thesis is the study of the Higgs decay in the $SO(5) \times U(1)$ GHU. The decay rates of the Higgs decay $H \to b\bar{b},\ \tau\bar{\tau},\ WW,\ ZZ$ are given by the SM value times $\cos^2\theta_H$ because these processes occur at the tree level. In contrast, the $H \to \gamma\gamma,\ gg$ processes occur at the loop level and an infinite number of the KK modes contribute to the processes. However, the cancellations between the KK mode contributions occur [26]. The infinite sum of the KK mode contributions converge and their contributions turn out negligible. The $H \to Z\gamma$ process also occur at the loop level [29]. The KK number in the loop can change through the interaction with the Z boson. Nevertheless, summing up all of the KK mode contributions, the cancellation among the KK mode contributions occurs. The summation of their contributions converge and is negligible as in the $H \to \gamma\gamma$ case. As a result, the production cross section $\sigma(gg \to H)$ and the decay rate $\Gamma(H \to \gamma\gamma)$, $\Gamma(H \to Z\gamma)$ are approximated as the SM value times $\cos^2\theta_H$. Therefore the branching ratio of the Higgs decay is almost equal to the SM value. and the deviation of the signal strength from the SM value is approximately $1 - \cos^2\theta_H \simeq O(1)\%$.

The $SO(5) \times U(1)$ GHU model can solve the fine-tuning problem. In addition, one of the fermions in the $SO(5)$-spinor representation, which called as dark fermions becomes the candidate of the DM [28]. The study of this DM candidate is another topic of this thesis. Its annihilation cross section seems to be small by the naive estimation. However, the Breit-Wigner enhancement occurs in the annihilation processes and there are the region in which the relic density of the dark fermion matches to the observed relic density of the DM. In the region, the elastic scattering cross section of the dark fermion off the nucleon is smaller than the experimental limit from the LUX 85-live days result and larger than the expected limit of the LUX 300-live days result. Its mass range is from 2.6 to 3.1 TeV.

In section 2, the $SO(5) \times U(1)$ GHU model is reviewed. In section 3, the decay rate of the $H \to \gamma\gamma$ and the $H \to Z\gamma$ process are evaluated in the model. In section 4, the relic density and the elastic scattering cross section off the nucleon of the neutral dark fermion are evaluated. Section 5 is devoted to the Summary and discussions. In the appendices, the $SO(5)$ algebra and the triple and quartic gauge boson couplings, the couplings of the Higgs boson to the gauge bosons, the couplings of the gauge and the Higgs boson to the SM fermions and the couplings of the gauge and the Higgs boson to the dark fermions are summarised.

2. Model

2.1. Hosotani mechanism

In this subsection, the Hosotani mechanism [11, 12] is reviewed. Theories on spacetime with compactified extra dimension(s) are defined by the Lagrangian and the boundary conditions. Some of the boundary conditions are equivalent because they can be changed each other by the gauge transformation. In addition, vacuum expectation value (VEV) of extra dimensional component of gauge field is physical quantity. The VEV might not be gauged away from the theory without changing the boundary conditions. To consider the VEV of the gauge field, the radiative corrections play important role. By radiative corrections, the gauge boson acquires the VEV which minimise the effective potential. This mechanism of symmetry breaking is called the Hosotani mechanism.

Consider the $SU(N)$ theory on the $M^4 \times S^1$ spacetime. The Lagrangian is given by

$$\mathcal{L} = \mathrm{Tr}\left[-\frac{1}{4}F_{MN}F^{MN} - \frac{1}{2\xi}\left(\partial_M A^M\right)^2\right] + \overline{\psi}\left(\Gamma^M D_M - m\right)\psi \ , \tag{2.1}$$

where

$$F_{MN} = \partial_M A_N - \partial_N A_M - ig\left[A_M, A_N\right] \ , \tag{2.2}$$

$$D_M = \partial_M - igA_M \ . \tag{2.3}$$

The Lagrangian has the gauge symmetry and is invariant under the gauge transformation

$$A'_M = \Omega\left(A_M + ig^{-1}\partial_M\right)\Omega^\dagger \ . \tag{2.4}$$

Next, consider the boundary condition. Because the fifth dimensional coordinate y and $y + 2\pi R$ is same point, set the boundary condition as

$$A_M(x^\mu, y + 2\pi R) = UA_M(x^\mu, y)U^\dagger \ , \tag{2.5}$$

$$\psi(x^\mu, y + 2\pi R) = U\psi(x^\mu, y) \ , \tag{2.6}$$

where U is a element of $SU(N)$. In the new gauge transformed by (2.4), $A'_M(x^\mu, y+2\pi R)$ is written as

$$A'_M(x^\mu, y+2\pi R) = U' A'_M(x^\mu, y) U'^\dagger - ig^{-1} (\partial_M U') U'^\dagger \ , \tag{2.7}$$

where

$$U' = \Omega(x^\mu, y+2\pi R) U \Omega^\dagger(x^\mu, y) \ . \tag{2.8}$$

If $\partial_M U' = 0$ is satisfied, $A'_M(x^\mu, y+2\pi R) = U' A'_M(x^\mu, y) U'^\dagger$ is the boundary condition in the new gauge. Simultaneously, $\psi'(x^\mu, y+2\pi R) = U'\psi'(x^\mu, y)$ is satisfied. Therefore as shown above, the boundary condition is also changed by the gauge transformation. Some of the boundary conditions are related to each other through the gauge transformation. It implies that VEV is physical because in general the VEV cannot be cancelled away from the theory. By the gauge transformation, the VEV can always be gauged away from the Lagrangian. However, the VEV appears in the new boundary condition.

2.2. Action

The $SO(5) \times U(1)$ GHU is defined on the Randall-Sundrum metric [30].

$$ds^2 = e^{-2\sigma(y)} \eta_{\mu\nu} dx^\mu dx^\nu + dy^2 \ , \tag{2.9}$$

where $-L \leq y \leq L$, $\sigma(y) = k|y|$ and $\eta_{\mu\nu} = \mathrm{diag}(-1,1,1,1)$. Therefore $y = L$ and $y = -L$ are identified as the same point, so that this metric has $S^1/\mathbf{Z_2}$ symmetry for the fifth dimensional coordinate. The so-called conformal coordinate is defined for the region $0 \leq y \leq L$ as

$$ds^2 = z^{-2} \left\{ \eta_{\mu\nu} dx^\mu dx^\nu + k^{-2} dz^2 \right\} \ , \tag{2.10}$$

where $z = e^{ky}$ and $1 \leq z \leq z_L = e^{kL}$. The $y = 0 (z = 1)$ and $y = L (z = z_L)$ brane is called the Planck brane and TeV brane respectively. This $e^{kL} = z_L$ is called the "warp factor" and it is assumed that $z_L \gg 1$.

The bulk Lagrangian has the $SU(3)_c \times SO(5) \times U(1)_X$ symmetry. $SU(3)$ symmetry is the color symmetry and $SO(5) \times U(1)_X$ symmetry is finally broken to $U(1)_{\mathrm{EM}}$ symmetry. The gauge fields of $SU(3)$, $SO(5)$ and $U(1)_X$ are denoted by G_M, A_M and B_M, respectively. The matter fields in the bulk are Ψ_a and Ψ_{F_i}. Ψ_a is the fermion multiplet in the $SO(5)$-vector representation and Ψ_{F_i} is the fermion multiplet in the $SO(5)$-spinor representation.

The bulk action is given by

$$
\begin{aligned}
S_{\rm bulk} = \int d^5x\sqrt{-G}\,\Big[&-{\rm Tr}\Big(\frac{1}{4}F^{(A)MN}F^{(A)}_{MN}+\frac{1}{2\xi_A}(f^{(A)}_{\rm gf})^2+\mathcal{L}^{(A)}_{\rm gh}\Big)\\
&-\Big(\frac{1}{4}F^{(B)MN}F^{(B)}_{MN}+\frac{1}{2\xi_B}(f^{(B)}_{\rm gf})^2+\mathcal{L}^{(B)}_{\rm gh}\Big)\\
&-{\rm Tr}\Big(\frac{1}{4}F^{(G)MN}F^{(G)}_{MN}+\frac{1}{2\xi_C}(f^{(G)}_{\rm gf})^2+\mathcal{L}^{(G)}_{\rm gh}\Big)\\
&+\sum_a\overline{\Psi}_a\mathcal{D}(c_a)\Psi_a+\sum_{i=1}^{n_F}\overline{\Psi}_{F_i}\mathcal{D}(c_{F_i})\Psi_{F_i}\Big],\\
F^{(A)}_{MN} = \partial_M A_N-\partial_N A_M-ig_A\big[A_M,A_N\big]\ ,&\quad F^{(B)}_{MN}=\partial_M B_N-\partial_N B_M\ ,\\
F^{(G)}_{MN} = \partial_M G_N-\partial_N G_M-ig_C\big[G_M,G_N\big]\ ,&\\
\mathcal{D}(c) = \Gamma^A e_A{}^M\Big(\partial_M+\frac{1}{8}\omega_{MBC}[\Gamma^B,\Gamma^C]-ig_AA_M-ig_BQ_XB_M-ig_CQ_CG_M)\Big)-c\sigma'(y)\ ,&
\end{aligned}
\tag{2.11}
$$

where $f_{\rm gf}$ are the gauge-fixing terms, $\mathcal{L}_{\rm gh}$ are the ghost Lagrangian, $\overline{\Psi}\equiv i\Psi^\dagger\Gamma^0$ and gamma matrices are given by

$$
\Gamma^\mu=\begin{pmatrix}&\sigma^\mu\\ \bar\sigma^\mu&\end{pmatrix}\ ,\quad \Gamma^5=\begin{pmatrix}1&\\&-1\end{pmatrix}\ ,\quad \sigma^\mu=(1,\ \vec\sigma)\ ,\quad \bar\sigma^\mu=(-1,\ \vec\sigma)\ .
\tag{2.12}
$$

$e_A{}^M$ is the vielbein and ω_{MAB} is the spin connection. $\omega_M\equiv\frac{1}{8}\omega_{MAB}[\Gamma^A,\Gamma^B]$ on the RS metric is given by

$$
(\omega_\mu,\omega_y)=\Big(-\frac{1}{2}ke^{-\sigma}\eta_{\mu\nu}\Gamma^\nu\Gamma^5,0\Big)\,.
\tag{2.13}
$$

The boundary conditions at $y_0=0$ and $y_1=L$ are set by

$$
\begin{aligned}
\begin{pmatrix}A_\mu(x,y_j-y)\\ A_y(x,y_j-y)\end{pmatrix}=&P\begin{pmatrix}A_\mu(x,y_j+y)\\ -A_y(x,y_j+y)\end{pmatrix}P^{-1}\ ,\\
\begin{pmatrix}B_\mu(x,y_j-y)\\ B_y(x,y_j-y)\end{pmatrix}=&\begin{pmatrix}B_\mu(x,y_j+y)\\ -B_y(x,y_j+y)\end{pmatrix}\ ,\\
\begin{pmatrix}G_\mu(x,y_j-y)\\ G_y(x,y_j-y)\end{pmatrix}=&\begin{pmatrix}G_\mu(x,y_j+y)\\ -G_y(x,y_j+y)\end{pmatrix}\ ,\\
\Psi_a(x,y_j-y)=&\,P_{\rm vec}\Gamma^5\Psi_a(x,y_j+y)\ ,\\
\Psi_{F_i}(x,y_j-y)=&\,\eta_{F_i}(-1)^jP_{\rm sp}\Gamma^5\Psi_{F_i}(x,y_j+y)\\
P_{\rm vec}={\rm diag}(-1,-1,-1,-1,\ 1),&\ P_{\rm sp}={\rm diag}(-1,-1,\ 1,\ 1)
\end{aligned}
\tag{2.14}
$$

By the above boundary condition, the $SO(5)$ symmetry is broken to $SO(4)$ and A_y in the $SO(5)/SO(4)$ have the zero modes. In contrast, the $SU(3)$ and $U(1)$ symmetries are

preserved and G_y and B_y do not have zero modes. Therefore only A_y in the $SO(5)/SO(4)$ part can have the VEV and this part corresponds to the Higgs doublet in the SM.

The $SO(5)$ can be divided by $SO(4) \simeq SU(2)_L \times SU(2)_R$ and $SO(5)/SO(4)$. Correspondingly, the gauge boson can be denoted as

$$A_M = \sum_{a=1}^{3} A_M^{a_L} T^{a_L} + \sum_{a=1}^{3} A_M^{a_R} T^{a_R} + \sum_{a=1}^{4} A_M^{\hat{a}} T^{\hat{a}} \ . \tag{2.15}$$

The VEV of the Higgs boson is taken to $\langle A_z^{\hat{a}} \rangle = v \cdot \delta^{a4} u_H(z)$, where $u_H(z) \equiv \sqrt{\frac{2}{k(z_L^2-1)}} z$. and the Wilson line phase is given by

$$\exp\left\{ \frac{i}{2} \theta_H 2\sqrt{2} T^{\hat{4}} \right\} = \exp\left\{ i g_A \int_1^{z_L} dz \langle A_z \rangle \right\} \ . \tag{2.16}$$

In this notation, v can be rewritten as $v = f_H \theta_H$, where

$$f_H \equiv \frac{2}{g_A} \sqrt{\frac{k}{z_L^2 - 1}} \ . \tag{2.17}$$

The four dimensional effective Lagrangian is obtained by integrating the five-dimensional Lagrangian by the fifth coordinate. The four-dimensional gauge couplings of the strong and weak interactions and the electroweak charge are given by

$$g_s = \frac{g_C}{\sqrt{L}}, \ g_w = \frac{g_A}{\sqrt{L}}, \ e = \frac{g_A g_B}{\sqrt{(g_A^2 + 2g_B^2)L}}, \tag{2.18}$$

respectively.

Considering the $SO(5)$-vector fermion multiplets, the multiplets can be written as $\Psi = (\Psi_1 \ \ \Psi_2 \ \ \Psi_3 \ \ \Psi_4 \ \ \Psi_5)^T$. For convenience, $\hat{\Psi}$ is defined as

$$\hat{\Psi} = \begin{pmatrix} \hat{\Psi}_{11} & \hat{\Psi}_{12} \\ \hat{\Psi}_{21} & \hat{\Psi}_{22} \end{pmatrix} \equiv \frac{1}{\sqrt{2}} \begin{pmatrix} -i\Psi_1 - \Psi_2 & i\Psi_3 + \Psi_4 \\ i\Psi_3 - \Psi_4 & i\Psi_1 - \Psi_2 \end{pmatrix} \ . \tag{2.19}$$

then $(\hat{\Psi}_{11} \ \ \hat{\Psi}_{21})^T$ and $(\hat{\Psi}_{12} \ \ \hat{\Psi}_{22})^T$ are $SU(2)_L$ doublets and $(\hat{\Psi}_{11} \ \ \hat{\Psi}_{12})^T$ and $(\hat{\Psi}_{21} \ \ \hat{\Psi}_{22})^T$ are $SU(2)_R$ doublets. For each generation, Ψ_a are donated as

$$\begin{aligned} &\hat{\Psi}_1 = \begin{pmatrix} T & t \\ B & b \end{pmatrix} \ , \quad \left(\Psi_1\right)_5 = t' \ , \quad \hat{\Psi}_2 = \begin{pmatrix} U & X \\ D & Y \end{pmatrix} \ , \quad \left(\Psi_2\right)_5 = b' \ , \\ &\hat{\Psi}_3 = \begin{pmatrix} \nu_\tau & L_{1X} \\ \tau & L_{1Y} \end{pmatrix}, \left(\Psi_3\right)_5 = \tau' \ , \quad \hat{\Psi}_4 = \begin{pmatrix} L_{2X} & L_{3X} \\ L_{2Y} & L_{3Y} \end{pmatrix}, \left(\Psi_4\right)_5 = \nu'_\tau \ . \end{aligned} \tag{2.20}$$

The electromagnetic charges of each particles are

$$T : \frac{5}{3}\ , \quad U,\ B,\ t,\ t' : \frac{2}{3}\ , \quad D,\ X,\ b,\ b' : -\frac{1}{3}\ , \quad Y : -\frac{4}{3}\ ,$$
$$L_{2X} : 1\ , \quad L_{2Y},\ \nu_\tau,\ \nu'_\tau,\ L_{3X} : 0\ , \quad L_{3Y},\ \tau,\ \tau', \quad L_{1X},\ : -1\ , \quad L_{1Y} : -2\ , \tag{2.21}$$

because the electric charge is $Q_{\rm EM} = T^{3_L} + T^{3_R} + Q_X$ as shown later. The bulk mass parameters are set such that $c_1 = c_2$ and $c_3 = c_4$ in each generation. With the boundary condition in (2.14), zero modes appear in

$$\left[Q_{1L} = \begin{pmatrix} T_L \\ B_L \end{pmatrix}, q_L = \begin{pmatrix} t_L \\ b_L \end{pmatrix},\ t'_R \right], \ \left[Q_{2L} = \begin{pmatrix} U_L \\ D_L \end{pmatrix}, Q_{3L} = \begin{pmatrix} X_L \\ Y_L \end{pmatrix},\ b'_R \right],$$
$$\left[\ell_L = \begin{pmatrix} \nu_{\tau L} \\ \tau_L \end{pmatrix}, L_{1L} = \begin{pmatrix} L_{1XL} \\ L_{1YL} \end{pmatrix},\ \tau'_R \right], \ \left[L_{2L} = \begin{pmatrix} L_{2XL} \\ L_{2YL} \end{pmatrix}, L_{3L} = \begin{pmatrix} L_{3XL} \\ L_{3YL} \end{pmatrix},\ \nu'_{\tau R} \right]. \tag{2.22}$$

Considering the $SO(5)$-spinor fermion multiplets, top two components are $SU(2)_L$ doublet and bottom 2 components are $SU(2)_R$ doublet. From the boundary condition, Ψ_{F_i} do not have zero modes.

To break the $SO(4)$ symmetry spontaneously and reproduce the mass difference between the fermions in same generations, the brane action is added. The brane scalar $\hat{\Phi}$, the brane fermions $\hat{\chi}^q_{aR}$ and $\hat{\chi}^l_{aR}$ $(a = 1, 2, 3)$ are localised on the Planck brane. $\hat{\chi}^q_{aR}$ and $\hat{\chi}^l_{aR}$ are $SU(2)_L$ doublet and denoted as

$$\hat{\chi}^q_{1R} = \begin{pmatrix} \hat{T}_R \\ \hat{B}_R \end{pmatrix}_{7/6}, \quad \hat{\chi}^q_{2R} = \begin{pmatrix} \hat{U}_R \\ \hat{D}_R \end{pmatrix}_{1/6}, \quad \hat{\chi}^q_{3R} = \begin{pmatrix} \hat{X}_R \\ \hat{Y}_R \end{pmatrix}_{-5/6},$$
$$\hat{\chi}^l_{1R} = \begin{pmatrix} \hat{L}_{1XR} \\ \hat{L}_{1YR} \end{pmatrix}_{-3/2}, \quad \hat{\chi}^l_{2R} = \begin{pmatrix} \hat{L}_{2XR} \\ \hat{L}_{2YR} \end{pmatrix}_{1/2}, \quad \hat{\chi}^l_{3R} = \begin{pmatrix} \hat{L}_{3XR} \\ \hat{L}_{3YR} \end{pmatrix}_{-1/2}, \tag{2.23}$$

where the subscripts denote $U(1)$ charge Q_X. The brane action is given by

$$
\begin{aligned}
S_{\rm brane} = \int d^5x\sqrt{-G}\,\delta(y)\Big\{ & -(D_\mu\hat{\Phi})^\dagger D^\mu\hat{\Phi} - \lambda_{\hat{\Phi}}(\hat{\Phi}^\dagger\hat{\Phi}-w^2)^2 \\
& + \sum_{\alpha=1}^{3}\left(\hat{\chi}^{q\dagger}_{\alpha R}\, i\bar{\sigma}^\mu D_\mu\hat{\chi}^{q}_{\alpha R} + \hat{\chi}^{l\dagger}_{\alpha R} i\bar{\sigma}^\mu D_\mu\hat{\chi}^{l}_{\alpha R}\right) \\
& - i\Big[\kappa^q_1\hat{\chi}^{q\dagger}_{1R}\hat{\Psi}_{1L}\hat{\tilde{\Phi}} + \tilde{\kappa}^q\hat{\chi}^{q\dagger}_{2R}\hat{\Psi}_{1L}\hat{\Phi} + \kappa^q_2\hat{\chi}^{q\dagger}_{2R}\hat{\Psi}_{2L}\hat{\tilde{\Phi}} + \kappa^q_3\hat{\chi}^{q\dagger}_{3R}\hat{\Psi}_{2L}\hat{\Phi} - ({\rm h.c.})\Big] \\
& - i\Big[\tilde{\kappa}^l\hat{\chi}^{l\dagger}_{3R}\hat{\Psi}_{3L}\hat{\tilde{\Phi}} + \kappa^l_1\hat{\chi}^{l\dagger}_{1R}\hat{\Psi}_{3L}\hat{\Phi} + \kappa^l_2\hat{\chi}^{l\dagger}_{2R}\hat{\Psi}_{4L}\hat{\tilde{\Phi}} + \kappa^l_3\hat{\chi}^{l\dagger}_{3R}\hat{\Psi}_{4L}\hat{\Phi} - ({\rm h.c.})\Big]\Big\}\ , \\
D_\mu\hat{\Phi} = & \left(\partial_\mu - ig_A\sum_{a_R=1}^{3}A^{a_R}_\mu T^{a_R} - ig_B\frac{B_\mu}{2}\right)\hat{\Phi}\ , \\
D_\mu\hat{\chi}_{\alpha R} = & \left(\partial_\mu - ig_A\sum_{a_L=1}^{3}A^{a_L}_\mu T^{a_L} - iQ_X g_B B_\mu - ig_C Q_C G_\mu\right)\hat{\chi}_{\alpha R}, \qquad (2.24)
\end{aligned}
$$

where $\hat{\tilde{\Phi}} = i\sigma_2\hat{\Phi}^*$. $\langle\hat{\Phi}\rangle = (0,w)^t \neq 0$ breaks $SU(2)_R\times U(1)_X$ to $U(1)_Y$. Assume $w \gg O(M_{\rm KK})$, then the brane scalar is heavy and negligible. By the VEV of the brane scalar, the brane action is rewritten as

$$
\begin{aligned}
S^{\rm mass}_{\rm brane} = \int d^5x\sqrt{-G}\,\delta(y)\Big\{ & -\frac{1}{4}g_A^2w^2\left(A^{1_R}_\mu A^{1_R\mu} + A^{2_R}_\mu A^{2_R\mu}\right) \\
& - \frac{1}{4}w^2\left(g_A A^{3_R}_\mu - g_B B_\mu\right)\left(g_A A^{3_R\mu} - g_B B^\mu\right) \\
& - \sum_{\alpha=1}^{3} i\mu^q_\alpha(\hat{\chi}^{q\dagger}_{\alpha R}Q_{\alpha L} - Q^\dagger_{\alpha L}\hat{\chi}^q_{\alpha R}) - i\tilde{\mu}^q(\hat{\chi}^{q\dagger}_{2R}q_L - q^\dagger_L\hat{\chi}^q_{2R}) \\
& - \sum_{\alpha=1}^{3} i\mu^l_\alpha(\hat{\chi}^{l\dagger}_{\alpha R}L_{\alpha L} - L^\dagger_{\alpha L}\hat{\chi}^l_{\alpha R}) - i\tilde{\mu}^l(\hat{\chi}^{l\dagger}_{3R}\ell_L - \ell^\dagger_L\hat{\chi}^l_{3R})\Big\}, \\
& \frac{\mu^q_\alpha}{\kappa^q_\alpha} = \frac{\tilde{\mu}^l}{\tilde{\kappa}^q} = \frac{\mu^l_\alpha}{\kappa^l_\alpha} = \frac{\tilde{\mu}^l}{\tilde{\kappa}^l} = w\ . \qquad (2.25)
\end{aligned}
$$

Therefore define that

$$
\begin{pmatrix} A^{3'_R}_\mu \\ B'_\mu \end{pmatrix} = \begin{pmatrix} c_\phi & -s_\phi \\ s_\phi & c_\phi \end{pmatrix}\begin{pmatrix} A^{3_R}_\mu \\ B_\mu \end{pmatrix}\ , \qquad (2.26)
$$

where

$$
c_\phi = \frac{g_A}{\sqrt{g_A^2+g_B^2}},\quad s_\phi = \frac{g_B}{\sqrt{g_A^2+g_B^2}}\ . \qquad (2.27)
$$

By this definition, the brane mass term of the gauge fields are written as

$$S^{\rm mass}_{\rm brane} \supset \int d^5x\sqrt{-G}\,\delta(y)\Big\{ -\frac{g_A^2 w^2}{4}\left(A_\mu^{1_R}A^{1_R\mu}+A_\mu^{2_R}A^{2_R\mu}\right)-\frac{g_A^2+g_B^2}{4}w^2 A_\mu^{3'_R}A^{3'_R\mu}\Big\}, \tag{2.28}$$

and by this brane mass term, the boundary condition for $A_\mu^{1_R}$, $A_\mu^{2_R}$ and $A_\mu^{3'_R}$ are changed to

$$A_\mu^{1_R}=A_\mu^{2_R}=A_\mu^{3'_R}\simeq 0\ , \tag{2.29}$$

for $m_n \ll O(M_{\rm Planck})$ modes. Therefore the $SO(4)\times U(1)_X$ symmetry is broken to $SO(2)\times U(1)_Y$. For simplicity, the boundary condition for $A_\mu^{1_R}$, $A_\mu^{2_R}$ and $A_\mu^{3'_R}$ is written as $A_\mu^{1_R}=A_\mu^{2_R}=A_\mu^{3'_R}=0$ in the following.

The Higgs VEV can be removed from the Lagrangian by the gauge transformation

$$\Omega(y)=\exp\left(ig_A\int_y^L dy'\langle A_y\rangle\right) \tag{2.30}$$

where the phase is determined by the condition $\Omega(L)=1$. By this gauge transformation, the boundary condition at $y=0$ is changed to

$$P_0'=\Omega(-y)P_0\Omega^\dagger(y)\ . \tag{2.31}$$

From $\{T^{\hat{4}},P_0\}=0$, P_0 can be written as

$$\tilde{P}_0=\begin{pmatrix} -1 & & & & & \\ & -1 & & & & \\ & & -1 & & & \\ & & & -\cos 2\theta_H & \sin 2\theta_H \\ & & & \sin 2\theta_H & \cos 2\theta_H \end{pmatrix}, \tag{2.32}$$

in the vector representation and

$$\tilde{P}_0=\begin{pmatrix} \cos\theta_H & -i\sin\theta_H & & \\ i\sin\theta_H & -\cos\theta_H & & \\ & & \cos\theta_H & -i\sin\theta_H \\ & & i\sin\theta_H & -\cos\theta_H \end{pmatrix}, \tag{2.33}$$

in the spinor representation. This gauge in which $\langle\tilde{A}_z\rangle=0$ is called the twisted gauge.

2.3. Mode functions of the gauge fields

In this subsection, the mode functions and the mass spectra is considered. At first, the KK decomposition of the Abelian gauge field is considered as a example [31]. The action is given by

$$S = \int d^4x \int_1^{z_L} dz \ \sqrt{-G} \left(-\frac{1}{4} F_{MN} F^{MN} - \frac{1}{2\xi} (f_{\rm gf})^2 \right), \tag{2.34}$$

where $f_{\rm gf}$ is gauge-fixing term

$$f_{\rm gf} = z^2 \left\{ \eta^{\mu\nu} \partial_\mu B_\mu + \xi k^2 z \partial_z (z^{-1} B_z) \right\}. \tag{2.35}$$

Here, the 't Hooft-Feynman gauge $\xi = 1$ is taken. Therefore the equation of motion is obtained by

$$\begin{aligned} S = & \int d^4x \int_1^{z_L} \frac{dz}{kz} \ \left(\frac{1}{2} \eta^{\mu\rho} B_\mu \left\{ \eta^{\nu\sigma} \partial_\sigma \partial_\nu B_\rho + k^2 z \partial_z \left(z^{-1} \partial_z B_\rho \right) \right\} \right) \\ & + \int d^4x \int_1^{z_L} \frac{dz}{kz} \ \left(\frac{1}{2} k^2 B_z \left\{ \eta^{\mu\rho} \partial_\mu \partial_\rho B_z + k^2 \partial_z \left(z \partial_z (z^{-1} B_z) \right) \right\} \right) \end{aligned} \tag{2.36}$$

where $B_\mu \partial_z B_\rho = B_z (\partial_\mu B_\rho) = B_z \partial_z (z^{-1} B_z) = 0$ are imposed. As the scalar case, the gauge bosons are decomposed to

$$B_\mu(x,z) = \sum_n B_\mu^{(n)}(x) \frac{f_g^{(n)}(z)}{\sqrt{r_{g^{(n)}}}}, \tag{2.37}$$

$$B_z(x,z) = \sum_n B_z^{(n)}(x) \frac{f_h^{(n)}(z)}{\sqrt{r_{h^{(n)}}}}, \tag{2.38}$$

where r_g, r_h are the normalisation factors

$$r_{g^{(n)}} = \int_1^L \frac{dz}{kz} \ f_g^{(n)}(z)^2 \ , \tag{2.39}$$

$$r_{h^{(n)}} = \int_1^L \frac{dz}{kz} z^{-2} \ f_h^{(n)}(z)^2 \ . \tag{2.40}$$

The eigenstate of $f_g^{(n)}(y), f_h^{(n)}(y)$ are determined by

$$k^2 \partial_z \left(z^{-1} \partial_z f_g^{(n)} \right) = -m_n^2 f_g^{(n)} \tag{2.41}$$

$$k^2 \partial_z \left(z \partial_z (z^{-1} f_h^{(n)}) \right) = -m_n^2 f_h^{(n)}. \tag{2.42}$$

To solve the equation, $z^{-1}f_g^{(n)} = \bar{f}_g^{(n)}$ is defined as the scalar case. By rewriting the equation, we obtain

$$\left\{z^2\partial_z^2 + z\partial_z + z^2(\lambda_n^2 - 1)\right\}\bar{f}_g^{(n)} = 0 \ , \tag{2.43}$$

where $\lambda_n \equiv m_n/k$ is defined. Therefore, the solution of this equation $\bar{f}_g^{(n)}$ is written by the Bessel function

$$f_g^{(n)}(\lambda_n z) \propto z\left\{a_n J_1(\lambda_n z) + b_n Y_1(\lambda_n z)\right\} . \tag{2.44}$$

Similarly, $f_h^{(n)}(y)$ is obtained as

$$f_h^{(n)}(\lambda_n z) \propto z^2\left\{a_n J_0(\lambda_n z) + b_n Y_0(\lambda_n z)\right\} . \tag{2.45}$$

The coefficients and the mass eigenvalues are determined by the boundary condition.

For convenience, the functions are defined

$$F_{\alpha,\beta}(u,v) \equiv J_\alpha(u)Y_\beta(v) - Y_\alpha(u)J_\beta(v) \ . \tag{2.46}$$

$$\begin{aligned} C(z;\lambda) &= \frac{\pi}{2}\lambda z z_L F_{1,0}(\lambda z, \lambda z_L) \ , \quad C'(z;\lambda) = \frac{\pi}{2}\lambda^2 z z_L F_{0,0}(\lambda z, \lambda z_L) \ , \\ S(z;\lambda) &= -\frac{\pi}{2}\lambda z F_{1,1}(\lambda z, \lambda z_L) \ , \quad S'(z;\lambda) = -\frac{\pi}{2}\lambda^2 z F_{0,1}(\lambda z, \lambda z_L) \ , \\ \hat{S}(z;\lambda) &= \frac{C(1;\lambda)}{S(1;\lambda)} S(z;\lambda) \ . \end{aligned} \tag{2.47}$$

Here the formulas

$$xZ'_\alpha(x) + \alpha Z_\alpha(x) = xZ_{\alpha-1}(x) \ , \tag{2.48}$$

$$xZ'_\alpha(x) - \alpha Z_\alpha(x) = -xZ_{\alpha+1}(x) \ , \tag{2.49}$$

are shown for convenience.

Imposing the Neumann condition $\partial_z A_\mu = 0$, A_μ has the zero mode. In the case, $f_g^{(0)}/\sqrt{r_{g^{(0)}}} = 1/\sqrt{L}$. The non-zero mode which satisfies the Neumann condition at the $z = z_L$, $f_g^{(n)}$ can be written as

$$\begin{aligned} f_g^{(n)}(\lambda_n z) &= \frac{\pi}{2}\lambda z z_L\left\{J_1(\lambda_n z)Y_0(\lambda_n z_L) - Y_1(\lambda_n z)J_0(\lambda_n z_L)\right\} \\ &= C(z;\lambda) \ , \end{aligned} \tag{2.50}$$

and imposing the Dirichlet condition $A_z = 0$ at the $z = z_L$, $f_h^{(n)}$ is written as

$$f_h^{(n)}(\lambda_n z) = C'(z;\lambda) \ . \tag{2.51}$$

Imposing the Dirichlet condition $A_\mu = 0$ at the $z = z_L$, $f_g^{(n)}$ is written as

$$f_g^{(n)}(\lambda_n z) = S(z;\lambda) \ . \tag{2.52}$$

and imposing the Neumann condition $\partial_z(z^{-1}A_z) = 0$ at the $z = z_L$, A_z has zero mode. From the boundary condition, $f_h^{(0)} = z$ and

$$r_{h^{(n)}} = \int_1^L \frac{dz}{kz} z^2 = \frac{z_L^2 - 1}{2k} \ . \tag{2.53}$$

For non-zero mode, $f_h^{(n)}$ is written as

$$f_h^{(n)}(\lambda_n z) = S'(z;\lambda) \ . \tag{2.54}$$

Considering the gauge bosons in the $SO(5)\times U(1)$ GHU model, $A_\mu(x,z)$ and $B_\mu^X(x,z)$ are expanded as follows.

$$\tilde{A}_\mu(x,z) + \frac{g_B}{g_A} B_\mu(x,z) T_B = \hat{W}_\mu^- + \hat{W}_\mu^+ + \hat{Z}_\mu + \hat{A}_\mu^\gamma + \hat{W}_{R\mu}^- + \hat{W}_{R\mu}^+ + \hat{Z}_{R\mu} + \hat{A}_\mu^{\hat{4}} \ , \tag{2.55}$$

where

$$\begin{aligned}
\hat{W}_\mu^\mp &= \sum_n W_\mu^{(n)\mp}(x) \left\{ h^L_{W^{(n)}} \frac{T^{1_L} \mp i T^{2_L}}{\sqrt{2}} + h^R_{W^{(n)}} \frac{T^{1_R} \mp i T^{2_R}}{\sqrt{2}} + \hat{h}_{W^{(n)}} \frac{T^{\hat{1}} \mp i T^{\hat{2}}}{\sqrt{2}} \right\} \ , \\
\hat{Z}_\mu &= \sum_n Z_\mu^{(n)}(x) \left\{ h^L_{Z^{(n)}} T^{3_L} + h^R_{Z^{(n)}} T^{3_R} + \hat{h}_{Z^{(n)}} T^{\hat{3}} + \frac{g_B}{g_A} h^B_{Z^{(n)}} T_B \right\} \ , \\
\hat{A}_\mu^\gamma &= \sum_n A_\mu^{\gamma(n)}(x) \left\{ h^L_{\gamma^{(n)}} T^{3_L} + h^R_{\gamma^{(n)}} T^{3_R} + \frac{g_B}{g_A} h^B_{\gamma^{(n)}} T_B \right\} \ , \\
\hat{W}_{R\mu}^\mp &= \sum_n W_{R\mu}^{(n)\mp}(x) \left\{ h^L_{W_R^{(n)}} \frac{T^{1_L} \mp i T^{2_L}}{\sqrt{2}} + h^R_{W_R^{(n)}} \frac{T^{1_R} \mp i T^{2_R}}{\sqrt{2}} \right\} \ , \\
\hat{Z}_{R\mu} &= \sum_n Z_{R\mu}^{(n)}(x) \left\{ h^L_{Z_R^{(n)}} T^{3_L} + h^R_{Z_R^{(n)}} T^{3_R} + \frac{g_B}{g_A} h^B_{Z_R^{(n)}} T_B \right\} \ , \\
\hat{A}_\mu^{\hat{4}} &= \sum_n A_\mu^{\hat{4}(n)}(x) \hat{h}_{A^{\hat{4}(n)}} T^{\hat{4}} \ , \\
\hat{W}^\pm &= \frac{\hat{W}^1 \mp i\hat{W}^2}{\sqrt{2}} \ , \quad \hat{W}_R^\pm = \frac{\hat{W}_R^1 \mp i\hat{W}_R^2}{\sqrt{2}} \ .
\end{aligned} \tag{2.56}$$

The weak mixing angle θ_W is given by

$$\cos\theta_W = \frac{1}{\sqrt{1+s_\phi^2}} \ . \tag{2.57}$$

The KK spectrum and corresponding wave functions for each tower are summarised as

follows.

W boson tower

The mass spectrum of the W boson tower is given by

$$2S(1;\lambda_{W^{(n)}})C'(1;\lambda_{W^{(n)}}) + \lambda_{W^{(n)}}\sin^2\theta_H = 0 \ . \tag{2.58}$$

This equation has the solution which corresponds to the SM W boson. For $\lambda_{W^{(0)}} z_L \ll 1$, the solution of Eq. (2.58) is obtained by the approximations $S(1;\lambda_{W^{(0)}}) \simeq -\lambda_{W^{(0)}} z_L/2$ and $C'(1;\lambda_{W^{(0)}}) \simeq \lambda_{W^{(0)}}^2 z_L \ln z_L$. Thus the mass of the SM W boson is obtained by

$$m_W \simeq k z_L^{-1} \frac{\sin\theta_H}{\sqrt{kL}} \simeq m_{\rm KK}\frac{\sin\theta_H}{\pi\sqrt{kL}} \ . \tag{2.59}$$

For zero mode, $W^{(0)}$ is denoted by W for simplicity. Their mode function is given by

$$\begin{aligned}
\begin{pmatrix} h^L_{W^{(n)}}(z) \\ h^R_{W^{(n)}}(z) \\ \hat{h}_{W^{(n)}}(z) \end{pmatrix} &= \frac{1}{\sqrt{r_{W^{(n)}}}\sqrt{2}} \begin{pmatrix} (1+\cos\theta_H)C(z;\lambda_{W^{(n)}}) \\ (1-\cos\theta_H)C(z;\lambda_{W^{(n)}}) \\ -\sqrt{2}\sin\theta_H \hat{S}(z;\lambda_{W^{(n)}}) \end{pmatrix} \ , \\
r_{W^{(n)}} &= \int_1^{z_L} \frac{dz}{kz}\left\{(1+\cos^2\theta_H)C(z;\lambda_{W^{(n)}})^2 + \sin^2\theta_H \hat{S}(z;\lambda_{W^{(n)}})^2\right\} \ .
\end{aligned} \tag{2.60}$$

Z boson tower

The mass spectrum of the Z boson tower is given by

$$2S(1;\lambda_{Z^{(n)}})C'(1;\lambda_{Z^{(n)}}) + (1+s_\phi^2)\lambda_{Z^{(n)}}\sin^2\theta_H = 0 \ , \tag{2.61}$$

This equation also has the solution for $\lambda z_L \ll 1$ as the W boson tower and it corresponds to the SM Z boson. The mass of the SM Z boson is obtained by

$$m_Z \simeq k z_L^{-1} \frac{\sin\theta_H}{\sqrt{kL}} \frac{1}{\cos\theta_W} \ . \tag{2.62}$$

For zero mode, $Z^{(0)}$ is denoted by Z for simplicity. Their mode function is given by

$$\begin{aligned}
\begin{pmatrix} h^L_{Z^{(n)}}(z) \\ h^R_{Z^{(n)}}(z) \\ \hat{h}_{Z^{(n)}}(z) \\ h^B_{Z^{(n)}} \end{pmatrix} &= \frac{1}{\sqrt{1+s_\phi^2}} \frac{1}{\sqrt{r_{Z^{(n)}}}\sqrt{2}} \begin{pmatrix} \left\{(1+s_\phi^2)(1+\cos\theta_H) - 2s_\phi^2\right\}C(z;\lambda_{Z^{(n)}}) \\ \left\{(1+s_\phi^2)(1-\cos\theta_H) - 2s_\phi^2\right\}C(z;\lambda_{Z^{(n)}}) \\ -\sqrt{2}(1+s_\phi^2)\sin\theta_H \hat{S}(z;\lambda_{Z^{(n)}}) \\ -2s_\phi c_\phi C(z;\lambda_{Z^{(n)}}) \end{pmatrix} \ , \\
r_{Z^{(n)}} &= \int_1^{z_L} \frac{dz}{kz}\left\{c_\phi^2 C(z;\lambda_{Z^{(n)}})^2 + (1+s_\phi^2)\left[\cos^2\theta_H C(z;\lambda_{Z^{(n)}})^2 + \sin^2\theta_H \hat{S}(z;\lambda_{Z^{(n)}})^2\right]\right\} \ .
\end{aligned} \tag{2.63}$$

γ (photon) tower

The mass spectrum of the photon tower is given by

$$C'(1; \lambda_{\gamma^{(n)}}) = 0 \ , \tag{2.64}$$

and the mode function is given by

$$\begin{pmatrix} h^L_{\gamma^{(n)}}(z) \\ h^R_{\gamma^{(n)}}(z) \\ h^B_{\gamma^{(n)}} \end{pmatrix} = \frac{1}{\sqrt{1+s_\phi^2}} \frac{1}{\sqrt{r_{\gamma^{(n)}}}} \begin{pmatrix} s_\phi \\ s_\phi \\ c_\phi \end{pmatrix} C(z; \lambda_{\gamma^{(n)}}) \ ,$$
$$r_{\gamma^{(n)}} = \int_1^{z_L} \frac{dz}{kz} C(z; \lambda_{\gamma^{(n)}})^2 \ . \tag{2.65}$$

For the photon $\gamma = \gamma^{(0)}$,

$$h^L_\gamma(z) = h^R_\gamma(z) = \frac{1}{\sqrt{(1+s_\phi^2)L}} s_\phi = t_\phi h^B_\gamma \ . \tag{2.66}$$

Therefore the electric charge is

$$Q_{\rm EM} = T^{3_L} + T^{3_R} + Q_X \ . \tag{2.67}$$

W_R boson tower

The mass spectrum of the W_R boson tower is given by $C(1; \lambda_{W_R^{(n)}}) = 0$. Their mode function is given by

$$\begin{pmatrix} h^L_{W_R^{(n)}}(z) \\ h^R_{W_R^{(n)}}(z) \end{pmatrix} = \frac{1}{\sqrt{r_{W_R^{(n)}}}\sqrt{2}} \begin{pmatrix} 1-\cos\theta_H \\ -1-\cos\theta_H \end{pmatrix} C(z; \lambda_{W_R^{(n)}}) \ ,$$
$$r_{W_R^{(n)}} = \int_1^{z_L} \frac{dz}{kz} C(z; \lambda_{W_R^{(n)}})^2 \ . \tag{2.68}$$

Z_R boson tower

The mass spectrum of the Z boson tower is given by $C(1; \lambda_{Z_R^{(n)}}) = 0$, Their mode function is given by

$$\begin{pmatrix} h^L_{Z_R^{(n)}}(z) \\ h^R_{Z_R^{(n)}}(z) \\ h^B_{Z_R^{(n)}} \end{pmatrix} = \frac{1}{\sqrt{1+(1+2t_\phi^2)\cos^2\theta_H}\sqrt{r_{Z_R^{(n)}}}\sqrt{2}} \begin{pmatrix} -1-\cos\theta_H \\ 1-\cos\theta_H \\ 2t_\phi \cos\theta_H \end{pmatrix} C(z; \lambda_{Z_R^{(n)}}) \ ,$$
$$r_{Z_R^{(n)}} = \int_1^{z_L} \frac{dz}{kz} C(z; \lambda_{Z_R^{(n)}})^2 = r_{W_R^{(n)}} \ , \quad t_\phi \equiv \frac{s_\phi}{c_\phi} \ . \tag{2.69}$$

$A^{\hat{4}}$ tower

The mass spectrum of the $A^{\hat{4}}$ tower is given by $S(1;\lambda_{A^{\hat{4}(n)}})=0$, Their mode function is given by

$$h_{A^{\hat{4}(n)}}(z)=\frac{1}{\sqrt{r_{A^{\hat{4}(n)}}}}S(z;\lambda_{A^{\hat{4}(n)}}),\quad r_{A^{\hat{4}(n)}}=\int_1^{z_L}\frac{dz}{kz}S(z;\lambda_{A^{\hat{4}(n)}})^2\ . \tag{2.70}$$

$A_z(x,z)$ and $B_z(x,z)$ are expanded as

$$\begin{aligned}
\tilde{A}_z(x,z)&=\sum_{a=1}^{3}\sum_{a=1}^{3}\hat{G}^a+\hat{D}^a+\hat{H}\ ,\\
\hat{D}^a&=\sum_n D^{a(n)}(x)\left\{u^L_{D^{(n)}}T^{a_L}+u^R_{D^{(n)}}T^{a_R}+\hat{u}_{D^{(n)}}T^{\hat{a}}\right\}\ ,\\
\hat{G}^a&=\sum_n G^{a(n)}(x)\left\{u^L_{G^{(n)}}T^{a_L}+u^R_{G^{(n)}}T^{a_R}\right\}\ ,\\
\hat{H}\ &=\sum_n H^{(n)}(x)u_{H^{(n)}}T^{\hat{4}}\ ,\\
B_z&=\sum_n B^{(n)}(x)u_{B^{(n)}}T_B\ .
\end{aligned} \tag{2.71}$$

D tower

The mass spectrum of the D tower is given by

$$C(1;\lambda_{D^{(n)}})S'(1;\lambda_{D^{(n)}})-\lambda_{D^{(n)}}\cos^2\theta_H=0\ . \tag{2.72}$$

Their mode functions are given by

$$\begin{aligned}
\begin{pmatrix}h^L_{D^{(n)}}(z)\\ h^R_{D^{(n)}}(z)\\ \hat{h}_{D^{(n)}}(z)\end{pmatrix}&=\frac{1}{\sqrt{r_{D^{(n)}}}\sqrt{2}}\begin{pmatrix}\cos\theta_H C'(z;\lambda_{D^{(n)}})\\ -\cos\theta_H C'(z;\lambda_{D^{(n)}})\\ -\sqrt{2}\sin\theta_H\hat{S}'(z;\lambda_{D^{(n)}})\end{pmatrix}\ ,\quad \hat{S}'(z;\lambda)=\frac{C(1;\lambda)}{S(1;\lambda)}S'(z;\lambda)\ ,\\
r_{D^{(n)}}&=\int_1^{z_L}\frac{kdz}{z}\left\{\cos^2\theta_H C'(z;\lambda_{D^{(n)}})^2+\sin^2\theta_H\hat{S}'(z;\lambda_{D^{(n)}})^2\right\}\ .
\end{aligned} \tag{2.73}$$

G tower

The G boson mass spectrum and mode functions are given by

$$C'(1;\lambda_{G^{(n)}})=0\ , \tag{2.74}$$

$$\begin{aligned}
u^L_{G^{(n)}}=u^R_{G^{(n)}}&=\frac{1}{\sqrt{2}}\frac{1}{\sqrt{r_{G^{(n)}}}}C'(z;\lambda_{G^{(n)}})\ ,\\
r_{G^{(n)}}&=\int_1^{z_L}\frac{kdz}{z}C'(z;\lambda_{G^{(n)}})^2\ .
\end{aligned} \tag{2.75}$$

H (Higgs) tower

The mass spectrum of the Higgs tower is determined by

$$S(1;\lambda_{H^{(n)}}) = 0 \ . \tag{2.76}$$

For the zero mode which is the 4D Higgs boson $H = H^{(0)}$, $\lambda_{H^{(n)}} = 0$. The mode functions are

$$u_{H^{(0)}}(z) = u_H(z) = \sqrt{\frac{2}{k(z_L^2-1)}}\ z \ , \tag{2.77}$$

for the 4D Higgs boson, and

$$u_{H^{(n)}}(z) = \frac{1}{\sqrt{r_{H^{(n)}}}} S'(z;\lambda_{H^{(n)}}), \quad r_{H^{(n)}} = \int_1^{z_L} \frac{kdz}{z} S'(z;\lambda_{H^{(n)}})^2 \ , \tag{2.78}$$

for KK-excited states ($n \geq 1$).

B tower

The B tower mass spectrum and the mode functions are given by

$$C'(1;\lambda_{B^{(n)}}) = 0 \ , \tag{2.79}$$

$$u_{B^{(n)}} = \frac{1}{\sqrt{r_{B^{(n)}}}} C'(z;\lambda_{B^{(n)}}) \ , \quad r_{B^{(n)}} = \int_1^{z_L} \frac{kdz}{z} C'(z;\lambda_{B^{(n)}})^2 \ . \tag{2.80}$$

2.4. Mode functions of the $SO(5)$-vector fermions

In this subsection, the mass spectra and the mode functions of the $SO(5)$-vector fermions are summarised [32]. Consider the free fermion,

$$S = \int d^4x \int dy \sqrt{-G}\ \bar{\psi}\ \Gamma^A e_A{}^M \Big(\partial_M + \frac{1}{8}\omega_{MBC}[\Gamma^B,\Gamma^C] - c\sigma'(y)\Big)\psi \ , \tag{2.81}$$

then the equation of motion is written as

$$\begin{pmatrix} -kD_-(c) & \sigma^\mu\partial_\mu \\ \bar{\sigma}^\mu\partial_\mu & -kD_+(c) \end{pmatrix} \check{\psi}(x,z) = 0 \ , \tag{2.82}$$

where $\psi = z^2\check{\psi}$ are defined and

$$D_\pm(c) = \pm\frac{d}{dz} + \frac{c}{z} \ . \tag{2.83}$$

Consider the KK decomposition of the fermion and substitute it to the equation of motion to obtain the wave function of the KK modes. The fermion is decomposed to

$$\check{\psi}(x,z) = \sum_n \frac{1}{\sqrt{r_{f^{(n)}}}} \begin{pmatrix} \check{\psi}_R^{(n)}(x) f_R^{(n)}(z) \\ \check{\psi}_L^{(n)}(x) f_L^{(n)}(z) \end{pmatrix} , \tag{2.84}$$

where $\sqrt{r_{f^{(n)}}}$ is the normalisation factor

$$r_{f^{(n)}} = \int_1^{Z_L} \frac{dz}{kz}\, z f_R^{(n)}(z)^2 = \int_1^{z_L} \frac{dz}{kz}\, z f_L^{(n)}(z)^2 . \tag{2.85}$$

Considering the eigenvalue equation

$$kD_-(c) f_R^{(n)}(z) = m_n f_L^{(n)}(z) , \tag{2.86}$$

$$kD_+(c) f_L^{(n)}(z) = m_n f_R^{(n)}(z) , \tag{2.87}$$

the eigenvalue m_n becomes the KK mass. These equations (2.86) and (2.87) are rewritten as

$$\{z^2\partial_z^2 + z\partial_z + (\lambda_n z)^2 - (c-1/2)^2\} z^{-\frac{1}{2}} f_R^{(n)}(z) = 0 \tag{2.88}$$

$$\{z^2\partial_z^2 + z\partial_z + (\lambda_n z)^2 - (c+1/2)^2\} z^{-\frac{1}{2}} f_L^{(n)}(z) = 0 . \tag{2.89}$$

Therefore $f_R^{(n)}(z)$, $f_L^{(n)}(z)$ is written as

$$f_R^{(n)}(z) \propto z^{\frac{1}{2}} \left\{ a_n J_{c-\frac{1}{2}}(\lambda_n z) + b_n Y_{c-\frac{1}{2}}(\lambda_n z) \right\} \tag{2.90}$$

$$f_L^{(n)}(z) \propto z^{\frac{1}{2}} \left\{ a_n J_{c+\frac{1}{2}}(\lambda_n z) + b_n Y_{c+\frac{1}{2}}(\lambda_n z) \right\} \tag{2.91}$$

From the boundary condition, either $f_R^{(n)}$ or $f_L^{(n)}$ must satisfy the Dirichlet boundary condition. Therefore, the normalisation factor satisfies the condition (2.85):

$$\begin{aligned} r_{f^{(n)}} &= \int_1^{Z_L} \frac{dz}{k} f_R^{(n)2} \\ &= \int_1^{Z_L} \frac{dz}{\lambda_n k} f_R^{(n)} D_+ f_L^{(n)} \\ &= \frac{1}{\lambda_n k} \left[f_R^{(n)} f_L^{(n)} \right]_{z=1}^{z=z_L} + \int_1^{Z_L} \frac{dz}{\lambda_n k} D_- \left(f_R^{(n)} \right) f_L^{(n)} = \int_1^{Z_L} \frac{dz}{k} f_L^{(n)}(z)^2 . \end{aligned} \tag{2.92}$$

For convenience, we define

$$\begin{aligned} C_L(z;\lambda,c) = &\quad \frac{\pi}{2}\lambda\sqrt{zz_L}F_{c+\frac{1}{2},c-\frac{1}{2}}(\lambda z,\lambda z_L)\ ,\ S_L(z;\lambda,c) = -\frac{\pi}{2}\lambda\sqrt{zz_L}F_{c+\frac{1}{2},c+\frac{1}{2}}(\lambda z,\lambda z_L)\ , \\ C_R(z;\lambda,c) = &-\frac{\pi}{2}\lambda\sqrt{zz_L}F_{c-\frac{1}{2},c+\frac{1}{2}}(\lambda z,\lambda z_L)\ ,\ S_R(z;\lambda,c) = \quad \frac{\pi}{2}\lambda\sqrt{zz_L}F_{c-\frac{1}{2},c-\frac{1}{2}}(\lambda z,\lambda z_L)\ . \end{aligned} \tag{2.93}$$

By imposing the Dirichlet boundary condition for $f_L^{(n)}(z_L) = 0$, $D_- f_R^{(n)}(z)|_{z=z_L} = 0$ must be satisfied simultaneously from the Eq. (2.86). In the case, $f_R^{(n)}$ and $f_L^{(n)}$ is expressed by using $F_{\alpha\beta}$ as

$$f_R^{(n)}(z) = C_R(\lambda_n z, \lambda_n z_L)\ , \tag{2.94}$$

$$f_L^{(n)}(z) = S_L(\lambda_n z, \lambda_n z_L)\ , \tag{2.95}$$

respectively. Similarly by imposing the Neumann boundary condition for $f_R^{(n)}(z_L) = 0$, $D_+ f_L^{(n)}(z)|_{z=z_L} = 0$ must be satisfied simultaneously from the Eq. (2.87). In the case, $f_R^{(n)}$ and $f_L^{(n)}$ is expressed as

$$f_R^{(n)}(z) = S_R(\lambda_n z, \lambda_n z_L)\ , \tag{2.96}$$

$$f_L^{(n)}(z) = C_L(\lambda_n z, \lambda_n z_L)\ , \tag{2.97}$$

respectively. From the orthogonality of the Bessel function, the effective potential becomes the infinite sum of the fermions with mass $m_n = k\lambda_n$.

$Q_{\mathsf{EM}} = \frac{5}{3}$ sector

From the boundary condition (2.14), T must satisfies $D_+(z^{-2}T_L) = 0$, at $z = z_L$. Therefore T_L is decomposed by $z^2 C_L$. At $z = 1$, from the boundary condition (2.14) and brane mass (2.24),

$$\lambda S_R - \frac{(\mu_1^q)^2}{2k}\, C_L = 0\ , \tag{2.98}$$

must be satisfied where $C_L = C_L(1,\lambda,c)$, etc. For $\mu_1^q \gg \sqrt{k\lambda}$, the first term of the LHS is negligible and the zero mode does not exist.

$Q_{\mathsf{EM}} = \frac{2}{3}$ sector

To calculate in the twisted gauge, $\tilde{B}, \tilde{t}, \tilde{t}'$ are defined as

$$\begin{pmatrix} \tilde{B} \\ \tilde{t} \\ \tilde{t}' \end{pmatrix} = \tilde{\Omega} \begin{pmatrix} B \\ t \\ t' \end{pmatrix}\ ,\quad \tilde{\Omega} = \begin{pmatrix} \frac{1}{2}(1+c) & \frac{1}{2}(1-c) & \frac{-1}{\sqrt{2}}s \\ \frac{1}{2}(1-c) & \frac{1}{2}(1+c) & \frac{1}{\sqrt{2}}s \\ \frac{1}{\sqrt{2}}s & -\frac{1}{\sqrt{2}}s & c \end{pmatrix}\ , \tag{2.99}$$

where $c = \cos\theta(z)$, $s = \sin\theta(z)$. From the boundary condition (2.14), $\tilde{U}, \tilde{B}, \tilde{t}, \tilde{t}'$ must satisfy

$$D_+(z^{-2}\tilde{U}_L) = D_+(z^{-2}\tilde{B}_L) = D_+(z^{-2}\tilde{t}_L) = \tilde{t}'_L = 0 \tag{2.100}$$

at $z = z_L$. Therefore U_L, B_L, t_L, t'_L are decomposed as

$$\begin{pmatrix} \tilde{U}_L(x,z) \\ \tilde{B}_L(x,z) \\ \tilde{t}_L(x,z) \\ \tilde{t}'_L(x,z) \end{pmatrix} = \frac{\sqrt{k}z^2}{\sqrt{r_{t^{(n)}}}} \begin{pmatrix} a_U^{(n)} C_L(z,\lambda_{t^{(n)}}) \\ a_B^{(n)} C_L(z,\lambda_{t^{(n)}}) \\ a_t^{(n)} C_L(z,\lambda_{t^{(n)}}) \\ a_{t'}^{(n)} S_L(z,\lambda_{t^{(n)}}) \end{pmatrix} t_L^{(n)}(x) \ , \tag{2.101}$$

Here $C_L(z,\lambda_{t^{(n)}}) = C_L(z;\lambda_{t^{(n)}},c)$ and $S_L(z,\lambda_{t^{(n)}}) = S_L(z;\lambda_{t^{(n)}},c)$. From the boundary condition (2.14) and brane mass (2.24) at $z = 1$,

$$\begin{aligned} s_H(\tilde{B}_L - \tilde{t}_L) - \sqrt{2}c_H\tilde{t}'_L = 0 \ , \\ \left(D_+ - \frac{\mu_2^2}{2k}\right)\left(z^{-2}\tilde{U}_L\right) - \frac{\tilde{\mu}\mu_2}{4k}z^{-2}(\tilde{B}_L + \tilde{t}_L) + \frac{\tilde{\mu}\mu_2}{4c_H k}z^{-2}(\tilde{B}_L - \tilde{t}_L) = 0 \ , \\ -\frac{\tilde{\mu}\mu_2}{2k}z^{-2}\tilde{U}_L + \left(D_+ - \frac{\mu_1^2+\tilde{\mu}^2}{4k}\right)z^{-2}(\tilde{B}_L + \tilde{t}_L) - \frac{\mu_1^2-\tilde{\mu}^2}{4c_H k}z^{-2}(\tilde{B}_L - \tilde{t}_L) = 0 \ , \\ \frac{\tilde{\mu}\mu_2}{2k}z^{-2}\tilde{U}_L - \frac{\mu_1^2-\tilde{\mu}^2}{4k}z^{-2}(\tilde{B}_L + \tilde{t}_L) \\ + \left(c_H D_+ - \frac{\mu_1^2+\tilde{\mu}^2}{4c_H k}\right)z^{-2}(\tilde{B}_L - \tilde{t}_L) + \sqrt{2}s_H D_+(z^{-2}\tilde{t}'_L) = 0 \ , \end{aligned} \tag{2.102}$$

must be satisfied where $c_H = \cos\theta_H$ and $s_H = \sin\theta_H$. For simplicity, the superscripts of the brane masses are abbreviated. By (2.101), this condition is rewritten as

$$\begin{pmatrix} 0 & 0 & \sqrt{2}s_H c_H C_L & -c_H S_L \\ \lambda S_R - \frac{\mu_2^2}{2k}C_L & -\frac{\tilde{\mu}\mu_2}{2k}C_L & \frac{\tilde{\mu}\mu_2}{2k}C_L & 0 \\ -\frac{\mu_2^2}{2k}C_L & 2\lambda S_R - \frac{\tilde{\mu}^2+\mu_1^2}{2k}C_L & \frac{\tilde{\mu}^2-\mu_1^2}{2k}C_L & 0 \\ \frac{\mu_2^2}{2k}C_L & \frac{\tilde{\mu}^2-\mu_1^2}{2k}C_L & 2c_H^2\lambda S_R - \frac{\tilde{\mu}^2+\mu_1^2}{2k}C_L & \sqrt{2}s_H\lambda C_R \end{pmatrix} \begin{pmatrix} a_U^{(n)} \\ \frac{a_B^{(n)}+a_t^{(n)}}{2} \\ \frac{a_B^{(n)}-a_t^{(n)}}{2c_H} \\ a_{t'}^{(n)} \end{pmatrix} = 0 \ . \tag{2.103}$$

The above equation have the nontrivial solution when

$$C_L^2\left\{\tilde{\mu}^2 S_L S_R + \mu_2^2 S_L S_R + s_H^2\frac{\mu_2^2}{2}\right\} = 0 \tag{2.104}$$

is satisfied where $\mu^1, \mu^2, \tilde{\mu} \gg \sqrt{\lambda k}$ is assumed. Therefore the mass spectrum of the

$Q_{\rm EM} = \frac{2}{3}$ fermion is determined by

$$\left(\frac{\tilde{\mu}^2}{\mu_2^2} + 1\right) S_L S_R + \frac{s_H^2}{2} = 0 \ . \tag{2.105}$$

For $0 < c < 1/2$, the solution for $\lambda z_L \ll 1$ is obtained by approximating $S_L \simeq -\lambda z_L^{1+c}/(1+2c)$ and $S_R \simeq \lambda z_L^{1-c}/(1-2c)$, as

$$m_t \simeq \frac{k z_L^{-1} \sin\theta_H}{\sqrt{2}} \frac{\sqrt{1-4c_t^2}}{\sqrt{1+(\tilde{\mu}^2/\mu_2^2)}} \ . \tag{2.106}$$

For $1/2 < c$, the solution for $\lambda z_L \ll 1$ is obtained by approximating $S_L \simeq -\lambda z_L^{1+c}/(1+2c)$ and $S_R \simeq \lambda z_L^{c}/(2c-1)$, as

$$m_u \simeq \frac{k z_L^{-1} \sin\theta_H}{\sqrt{2}} \frac{\sqrt{4c_u^2-1}}{z^{c-1/2}\sqrt{1+(\tilde{\mu}^2/\mu_2^2)}} \ . \tag{2.107}$$

The coefficients are obtained as

$$\begin{pmatrix} a_U^{(n)} \\ a_B^{(n)} \\ a_t^{(n)} \\ a_{t'}^{(n)} \end{pmatrix} = \begin{pmatrix} -\sqrt{2}\ \tilde{\mu}^q/\mu_2^q \\ (1-\cos\theta_H)/\sqrt{2} \\ (1+\cos\theta_H)/\sqrt{2} \\ -\sin\theta_H C_L/S_L \end{pmatrix} . \tag{2.108}$$

The mode functions of the right-handed components $\tilde{U}_R, \tilde{B}_R, \tilde{t}_R, \tilde{t}'_R$ are obtained by replacing $C_L \to S_R$ and $S_L \to C_R$. Thus the mode functions are written as

$$\begin{aligned}
\begin{pmatrix} \tilde{U}_L(x,z) \\ \tilde{B}_L(x,z) \\ \tilde{t}_L(x,z) \\ \tilde{t}'_L(x,z) \end{pmatrix} &= \frac{\sqrt{k}z^2}{\sqrt{r_{t^{(n)}}}} \begin{pmatrix} a_U^{(n)} C_L(z,\lambda_{t^{(n)}}) \\ a_B^{(n)} C_L(z,\lambda_{t^{(n)}}) \\ a_t^{(n)} C_L(z,\lambda_{t^{(n)}}) \\ a_{t'}^{(n)} S_L(z,\lambda_{t^{(n)}}) \end{pmatrix} t_L^{(n)}(x) \equiv \sqrt{k}z^2 \begin{pmatrix} f_{U_L}^{(n)}(z) \\ f_{B_L}^{(n)}(z) \\ f_{t_L}^{(n)}(z) \\ f_{t'_L}^{(n)}(z) \end{pmatrix} t_L^{(n)}(x) \ , \\
\begin{pmatrix} \tilde{U}_R(x,z) \\ \tilde{B}_R(x,z) \\ \tilde{t}_R(x,z) \\ \tilde{t}'_R(x,z) \end{pmatrix} &= \frac{\sqrt{k}z^2}{\sqrt{r_{t^{(n)}}}} \begin{pmatrix} a_U^{(n)} S_R(z,\lambda_{t^{(n)}}) \\ a_B^{(n)} S_R(z,\lambda_{t^{(n)}}) \\ a_t^{(n)} S_R(z,\lambda_{t^{(n)}}) \\ a_{t'}^{(n)} C_R(z,\lambda_{t^{(n)}}) \end{pmatrix} t_R^{(n)}(x) \equiv \sqrt{k}z^2 \begin{pmatrix} f_{U_R}^{(n)}(z) \\ f_{B_R}^{(n)}(z) \\ f_{t_R}^{(n)}(z) \\ f_{t'_R}^{(n)}(z) \end{pmatrix} t_R^{(n)}(x) \ , \\
r_{t^{(n)}} &= \int_1^{z_L} dz \Big\{ a_U^{(n)2} C_L(z,\lambda_{t^{(n)}})^2 + (a_B^{(n)2} + a_t^{(n)2}) C_L(z,\lambda_{t^{(n)}})^2 + a_{t'}^{(n)2} S_L(z,\lambda_{t^{(n)}})^2 \Big\} \\
&= \int_1^{z_L} dz \Big\{ a_U^{(n)2} S_R(z,\lambda_{t^{(n)}})^2 + (a_B^{(n)2} + a_t^{(n)2}) S_R(z,\lambda_{t^{(n)}})^2 + a_{t'}^{(n)2} C_R(z,\lambda_{t^{(n)}})^2 \Big\} \ ,
\end{aligned} \tag{2.109}$$

$Q_{\rm EM} = -\frac{1}{3}$ sector

To consider the $Q_{\rm EM} = -\frac{1}{3}$ fermions, the equations are obtained from the $Q_{\rm EM} = \frac{2}{3}$ sector by replacing

$$\begin{pmatrix} \tilde{U} \\ \tilde{B} \\ \tilde{t} \\ \tilde{t}' \end{pmatrix} \to \begin{pmatrix} \tilde{b} \\ \tilde{X} \\ \tilde{D} \\ -\tilde{b}' \end{pmatrix} \tag{2.110}$$

$$\mu_2 \leftrightarrow \tilde{\mu} \ . \tag{2.111}$$

Therefore the mass spectrum of the $Q_{\rm EM} = -\frac{1}{3}$ fermion is determined by

$$\left(\frac{\mu_2^2}{\tilde{\mu}^2} + 1 \right) S_L S_R + \frac{s_H^2}{2} = 0 \ . \tag{2.112}$$

and the solution for $\lambda z_L \ll 1$ is obtained as

$$m_b \simeq \frac{k z_L^{-1} \sin\theta_H}{\sqrt{2}} \frac{\sqrt{1-4c_t^2}}{\sqrt{1+(\mu_2^2/\tilde{\mu}^2)}} \ , \tag{2.113}$$

for $0 < c < 1/2$. The ratio of this mass to the top mass is expressed as

$$\frac{m_b}{m_t} \simeq \frac{\sqrt{1+(\tilde{\mu}^2/\mu_2^2)}}{\sqrt{1+(\mu_2^2/\tilde{\mu}^2)}} = \frac{\tilde{\mu}}{\mu_2} \ . \tag{2.114}$$

Thus the mass ratio of the top quark and the bottom quark is reproduced by adjusting the brane mass parameters This relation is also satisfied for the first and the second generations.

The quarks with $Q_{\rm EM} = -\frac{1}{3}$ are decomposed as

$$\begin{aligned}
\begin{pmatrix} \tilde{b}_L(x,z) \\ \tilde{X}_L(x,z) \\ \tilde{D}_L(x,z) \\ \tilde{b}'_L(x,z) \end{pmatrix} &= \frac{\sqrt{k}z^2}{\sqrt{r_{b^{(n)}}}} \begin{pmatrix} a_b^{(n)} C_L(z,\lambda_{b^{(n)}}) \\ a_X^{(n)} C_L(z,\lambda_{b^{(n)}}) \\ a_D^{(n)} C_L(z,\lambda_{b^{(n)}}) \\ a_{b'}^{(n)} S_L(z,\lambda_{b^{(n)}}) \end{pmatrix} b_L^{(n)}(x) \equiv \sqrt{k}z^2 \begin{pmatrix} f_{b_L}^{(n)}(z) \\ f_{X_L}^{(n)}(z) \\ f_{D_L}^{(n)}(z) \\ f_{b'_L}^{(n)}(z) \end{pmatrix} b_L^{(n)}(x) \ , \\
\begin{pmatrix} \tilde{b}_R(x,z) \\ \tilde{X}_R(x,z) \\ \tilde{D}_R(x,z) \\ \tilde{b}'_R(x,z) \end{pmatrix} &= \frac{\sqrt{k}z^2}{\sqrt{r_{b^{(n)}}}} \begin{pmatrix} a_b^{(n)} S_R(z,\lambda_{b^{(n)}}) \\ a_X^{(n)} S_R(z,\lambda_{b^{(n)}}) \\ a_D^{(n)} S_R(z,\lambda_{b^{(n)}}) \\ a_{b'}^{(n)} C_R(z,\lambda_{b^{(n)}}) \end{pmatrix} b_R^{(n)}(x) \equiv \sqrt{k}z^2 \begin{pmatrix} f_{b_R}^{(n)}(z) \\ f_{X_R}^{(n)}(z) \\ f_{D_R}^{(n)}(z) \\ f_{b'_R}^{(n)}(z) \end{pmatrix} b_R^{(n)}(x) \ , \\
r_{b^{(n)}} &= \int_1^{z_L} dz \Big\{ a_b^{(n)2} C_L(z,\lambda_{b^{(n)}})^2 + (a_X^{(n)2} + a_D^{(n)2}) C_L(z,\lambda_{b^{(n)}})^2 + a_{b'}^{(n)2} S_L(z,\lambda_{b^{(n)}})^2 \Big\} \\
&= \int_1^{z_L} dz \Big\{ a_b^{(n)2} S_R(z,\lambda_{b^{(n)}})^2 + (a_X^{(n)2} + a_D^{(n)2}) S_R(z,\lambda_{b^{(n)}})^2 + a_{b'}^{(n)2} C_R(z,\lambda_{b^{(n)}})^2 \Big\} \ ,
\end{aligned} \tag{2.115}$$

where

$$\begin{pmatrix} a_b^{(n)} \\ a_X^{(n)} \\ a_D^{(n)} \\ a_{b'}^{(n)} \end{pmatrix} = \begin{pmatrix} -\sqrt{2}\mu_2^q/\tilde{\mu}^q \\ (1-\cos\theta_H)/\sqrt{2} \\ (1+\cos\theta_H)/\sqrt{2} \\ \sin\theta_H C_L/S_L \end{pmatrix} \ . \tag{2.116}$$

$Q_{\rm EM} = -\frac{4}{3}$ sector

To consider the $Q_{\rm EM} = -\frac{4}{3}$ fermion, the equations are obtained from the $Q_{\rm EM} = \frac{5}{3}$ sector by replacing

$$T \to Y \tag{2.117}$$

$$\mu_1 \to \mu_3 \ . \tag{2.118}$$

The mass spectrum is determined by

$$\lambda S_R - \frac{(\mu_3^q)^2}{2k} \, C_L = 0 \ , \tag{2.119}$$

therefore Y does not have zero mode.

For a lepton multiplet (ν_τ, τ), the wave functions are given by the following replace-

ment rules;

$$\begin{pmatrix} U \\ B \\ t \\ t' \end{pmatrix} \to \begin{pmatrix} \nu_\tau \\ L_{2Y} \\ L_{3X} \\ \nu'_\tau \end{pmatrix} , \quad \begin{pmatrix} b \\ D \\ X \\ b' \end{pmatrix} \to \begin{pmatrix} L_{3Y} \\ \tau \\ L_{1Y} \\ \tau' \end{pmatrix} , \tag{2.120}$$

$$(\tilde{\mu}^q, \mu_2^q) \to (\mu_3^\ell, \tilde{\mu}^\ell) , \quad (\mu_3^q, \mu_1^q) \to (\mu_1^\ell, \mu_2^\ell) , \tag{2.121}$$

$$c_1 \to c_3 . \tag{2.122}$$

2.5. Mode functions of the $SO(5)$-spinor fermions

The mass spectra and the mode functions of the dark fermions are written in this subsection. The $SO(5)$-spinor multiplet consists of four fermions. The above two components are $SU(2)_L$ doublet and the below two components are $SU(2)_R$ doublet. Therefore the $SO(5)$-spinor multiplet are denoted as

$$\Psi_{F_i} = \begin{pmatrix} \Psi_{F_i,l} \\ \Psi_{F_i,r} \end{pmatrix} = \begin{pmatrix} \psi_{F_i,l1} \\ \psi_{F_i,l2} \\ \psi_{F_i,r1} \\ \psi_{F_i,r2} \end{pmatrix} . \tag{2.123}$$

The electric charges are $\frac{1}{2} + Q_{X_{F_i}}$ for $\psi_{F_i,l1}$ and $\psi_{F_i,r1}$ and $\frac{1}{2} - Q_{X_{F_i}}$ for $\psi_{F_i,l2}$ and $\psi_{F_i,r2}$. The $\tilde{\Psi}_{F_i}$ is defined as $\tilde{\Psi}_{F_i} \equiv z^{-2}\Psi_{F_i}$ in the twisted gauge. From the boundary condition at $z = z_L$,

$$\begin{aligned} &\tilde{\Psi}_{F_i,lR}(z_L) = 0 , \quad D_+\tilde{\Psi}_{F_i,lL}(z_L) = 0 , \\ &D_-\tilde{\Psi}_{F_i,rR}(z_L) = 0 , \quad \tilde{\Psi}_{F_i,rL}(z_L) = 0 , \end{aligned} \tag{2.124}$$

for $\eta_{F_i} = +1$ and

$$\begin{aligned} &D_+\tilde{\Psi}_{F_i,lR}(z_L) = 0 , \quad \tilde{\Psi}_{F_i,lL}(z_L) = 0 , \\ &\tilde{\Psi}_{F_i,rR}(z_L) = 0 , \quad D_-\tilde{\Psi}_{F_i,rL}(z_L) = 0 , \end{aligned} \tag{2.125}$$

for $\eta_{F_i} = -1$. In the following, $Q_{X_{F_i}} = \frac{1}{2}$ and $\eta_{F_i} = +1$ are adopted.

The $SO(5)$-spinor fermions are decomposed as

$$\Psi^{(n)}_{F_i,R}(x,z) = \sqrt{k}z^2 \left\{ \begin{pmatrix} f^{(n)}_{i,lR}(z) \\ 0 \\ f^{(n)}_{i,rR}(z) \\ 0 \end{pmatrix} F^{+(n)}_{i,R}(x) + \begin{pmatrix} 0 \\ f^{(n)}_{i,lR}(z) \\ 0 \\ f^{(n)}_{i,rR}(z) \end{pmatrix} F^{0(n)}_{i,R}(x) \right\} ,$$
$$\Psi^{(n)}_{F_i,L}(x,z) = \sqrt{k}z^2 \left\{ \begin{pmatrix} f^{(n)}_{i,lL}(z) \\ 0 \\ f^{(n)}_{i,rL}(z) \\ 0 \end{pmatrix} F^{+(n)}_{i,L}(x) + \begin{pmatrix} 0 \\ f^{(n)}_{i,lL}(z) \\ 0 \\ f^{(n)}_{i,rL}(z) \end{pmatrix} F^{0(n)}_{i,L}(x) \right\} . \tag{2.126}$$

From the boundary condition, the $f^{(n)}_i$'s are proportional to

$$\begin{pmatrix} f^{(n)}_{i,lL}(z) \\ f^{(n)}_{i,lR}(z) \end{pmatrix} \propto \begin{pmatrix} C_L(z) \\ S_R(z) \end{pmatrix} , \quad \begin{pmatrix} f^{(n)}_{i,rL}(z) \\ f^{(n)}_{i,rR}(z) \end{pmatrix} \propto \begin{pmatrix} S_L(z) \\ C_R(z) \end{pmatrix} ,$$

respectively. The boundary condition at $z = 1$ is

$$\begin{aligned} \cos\frac{\theta_H}{2}\tilde{\Psi}_{F_i,lL}(1) - i\sin\frac{\theta_H}{2}\tilde{\Psi}_{F_i,rL}(1) = 0 , \\ -i\sin\frac{\theta_H}{2}\tilde{\Psi}_{F_i,lR}(1) + \cos\frac{\theta_H}{2}\tilde{\Psi}_{F_i,rR}(1) = 0 . \end{aligned} \tag{2.127}$$

From the boundary condition at $z = 1$, the mass spectrum $\{m_{F_i,n} = k\lambda_{i,n}\}$ is determined by

$$C_L(1;\lambda_{i,n},c_{F_i})C_R(1;\lambda_{i,n},c_{F_i}) - \sin^2\frac{\theta_H}{2} = 0 . \tag{2.128}$$

The mode functions are given by

$$\begin{aligned} \begin{pmatrix} f^{(n)}_{i,lL}(z) \\ f^{(n)}_{i,lR}(z) \end{pmatrix} = \frac{i\sin\frac{\theta_H}{2}S_L(1)}{\sqrt{r^{(n)}_i}} \begin{pmatrix} C_L(z) \\ S_R(z) \end{pmatrix} = \frac{\cos\frac{\theta_H}{2}C_R(1)}{\sqrt{r'^{(n)}_i}} \begin{pmatrix} C_L(z) \\ S_R(z) \end{pmatrix} , \\ \begin{pmatrix} f^{(n)}_{i,rL}(z) \\ f^{(n)}_{i,rR}(z) \end{pmatrix} = \frac{\cos\frac{\theta_H}{2}C_L(1)}{\sqrt{r^{(n)}_i}} \begin{pmatrix} S_L(z) \\ C_R(z) \end{pmatrix} = \frac{i\sin\frac{\theta_H}{2}S_R(1)}{\sqrt{r'^{(n)}_i}} \begin{pmatrix} S_L(z) \\ C_R(z) \end{pmatrix} , \end{aligned} \tag{2.129}$$

with $\lambda = \lambda_{i,n}$. The normalisation factors $r^{(n)}_i$ and $r'^{(n)}_i$ are determined by the condition

$$\int_1^{z_L} dz\Big\{|f^{(n)}_{lL}|^2 + |f^{(n)}_{rL}|^2\Big\} = \int_1^{z_L} dz\Big\{|f^{(n)}_{lR}|^2 + |f^{(n)}_{rR}|^2\Big\} = 1 \tag{2.130}$$

to be

$$
\begin{aligned}
r_i^{(n)} &= \int_1^{z_L} dz \Big\{ \sin^2 \frac{\theta_H}{2} S_L(1)^2 C_L(z)^2 + \cos^2 \frac{\theta_H}{2} C_L(1)^2 S_L(z)^2 \Big\} \\
&= \int_1^{z_L} dz \Big\{ \sin^2 \frac{\theta_H}{2} S_L(1)^2 S_R(z)^2 + \cos^2 \frac{\theta_H}{2} C_L(1)^2 C_R(z)^2 \Big\}, \\
r_i'^{(n)} &= \int_1^{z_L} dz \, \Big\{ \cos^2 \frac{\theta_H}{2} C_R(1)^2 C_L(z)^2 + \sin^2 \frac{\theta_H}{2} S_R(1)^2 S_L(z)^2 \Big\} \\
&= \int_1^{z_L} dz \Big\{ \cos^2 \frac{\theta_H}{2} C_R(1)^2 S_R(z)^2 + \sin^2 \frac{\theta_H}{2} S_R(1)^2 C_R(z)^2 \Big\}. \qquad (2.131)
\end{aligned}
$$

The electric charges are 1 for $F_i^{+(n)}$ and 0 for $F_i^{(n)0}$.

In the case of the boundary condition for Ψ_{F_i} with $\eta_{F_i} = -1$ in (2.14), the corresponding mode functions and masses are obtained from the above formulas by the replacement

$$
c_H \leftrightarrow i s_H \ , \quad C_L \leftrightarrow S_L \ , \quad S_R \leftrightarrow C_R \ . \qquad (2.132)
$$

The spectrum is determined by the same equation as in (2.128).

With $\eta_{F_i} = +1$ for Ψ_{F_i}, the odd KK number modes $F_i^{+(n)}, F_i^{0(n)}$ (n: odd) are mostly $SU(2)_R$ doublets, containing $SU(2)_L$ doublets slightly. The even KK number modes $F_i^{+(n)}, F_i^{0(n)}$ (n: even) are mostly $SU(2)_L$ doublets. Consequently the first KK modes $F_i^{+(1)}, F_i^{0(1)}$ couple to the $SU(2)_L$ gauge bosons (W and Z) very weakly. On the other hand, with $\eta_{F_i} = -1$, $F_i^{+(n)}, F_i^{0(n)}$ (n: odd) are mostly $SU(2)_L$ doublets, and the first KK modes $F_i^{+(1)}, F_i^{0(1)}$ couple to W and Z with the standard weak coupling strengths.

At the tree level the masses of the first KK modes $F_i^{+(1)}$ and $F_i^{0(1)}$ are same value which is about 1.5 TeV to 4 TeV. The charged dark fermions $F_i^{+(1)}$ receive radiative correction by photon and becomes heavier than the neutral ones $F_i^{0(1)}$. Their mass difference is estimated to be about $\alpha \cdot m_F$. Thus $F_i^{+(1)}$ eventually decays into $F_i^{0(1)}$ and SM particles. The lightest modes $F_i^{0(1)}$'s are absolutely stable. Their relic densities and the constraints from the direct detection experiments are discussed in Sec. 4.

2.6. Effective potential and the parameters

By the radiative corrections, the Higgs boson acquires the VEV which minimise the effective potential. The way to calculate the effective potential was developed in Ref. [33, 34]. Contributions of the each particle to the effective potential is written as the following form

$$
V = \pm \frac{N}{2} \sum_n \int \frac{d^4 p_E}{(2\pi)^4} \log \left(p_E^2 + m_n^2 \right) \ , \qquad (2.133)
$$

where the sign + and − are assigned for boson and fermion respectively and N is a degrees of freedom of each particle. Suppose that m_n depends on $\langle A_y \rangle$. To calculate the

$\langle A_y \rangle$ dependence of the effective potential,

$$\frac{N}{2}\sum_n \int \frac{d^d p_E}{(2\pi)^d} \log\left(p_E^2\right) \tag{2.134}$$

are neglected because it does not depend on $\langle A_y \rangle$ and Eq. (2.133) is calculated by the dimensional regularisation.

$$\frac{N}{2}\sum_n \int \frac{d^d p_E}{(2\pi)^d} \log\left(1+\frac{m_n^2}{p_E^2}\right) = N\frac{1}{(4\pi)^{d/2}\Gamma(\frac{d}{2})}\frac{\pi}{d\sin(\pi d/2)}\sum_n m_n^d \ , \tag{2.135}$$

where $d = 4+\epsilon$. Consider the function $\rho(w)$ where the mass spectrum of m_n is determined by the condition $\rho(m_n) = 0$ and $\rho(w)$ is chosen so that $\rho(w)$ is a holomorphic function of w, $\lim_{|w|\to\infty}\rho(w) = 0$ and $\rho(iv) = \rho(-iv)$ when v is real. Suppose that all of the points which satisfies $\rho(m_n) = 0$ is on the real axis. Consider the contribution of the W boson tower. The mass spectrum of the W boson tower is determined by (2.58). Thus $\rho(w)$ is chosen as

$$\begin{aligned}\rho(w) &= 1 + \frac{w}{2kS(1;w/k)C'(1;w/k)}\sin^2\theta_H \\ &= 1 - \left(\frac{2}{\pi}\right)^2 \frac{k^2}{w^2 z_L F_{0,0}(w/k, wz_L/k)F_{1,1}(w/k, wz_L/k)}\frac{\sin^2\theta_H}{2} \ .\end{aligned} \tag{2.136}$$

Because the $\rho(w)$ is a holomorphic function of w, the summation can be rewritten as

$$\sum_n m_n^d = \frac{1}{2\pi i}\oint_c dw\ w^d \frac{\rho'(w)}{\rho(w)}, \tag{2.137}$$

where contour c is taken so that all of m_n is inside the contour. It can be expressed as

$$\begin{aligned}\sum_n m_n^d &= -\frac{1}{2\pi}\left(\int_0^\infty dv\ (iv)^d \frac{\rho'(iv)}{\rho(iv)} + \int_{-\infty}^0 dv\ (iv)^d \frac{\rho'(iv)}{\rho(iv)}\right) \\ &= \frac{d}{\pi}\sin\left(\frac{\pi d}{2}\right)\int_0^\infty dv\ v^{d-1}\log\left(\rho(iv)\right) \ .\end{aligned} \tag{2.138}$$

Therefore the $\langle A_y \rangle$ dependent part of Eq. (2.133) is written as

$$V = \pm\frac{N}{2}\sum_n \int \frac{d^d p_E}{(2\pi)^d}\log\left(1+\frac{m_n^2}{p_E^2}\right) = \pm N\frac{1}{(4\pi)^2}\int_0^\infty dv\ v^3\log\left(\rho(iv)\right) \ , \tag{2.139}$$

where the limit $\epsilon \to 0$ is taken in the last equality. Therefore without knowing the every value of m_n, the effective potential is calculated by this method. Again consider the contribution of the W boson tower. Define $q \equiv vz_L/k$, then the W boson tower

contribution is rewritten as

$$V_{\rm eff}^{W} = 2(3-\xi^2)\frac{(kz_L^{-1})^4}{(4\pi)^2}\int_0^\infty dq\ q^3 \log\Big(\rho(iq)\Big)\ , \tag{2.140}$$

where

$$\rho(iq) = 1 + \left(\frac{2}{\pi}\right)^2 \frac{z_L}{q^2 F_{0,0}(iqz_L^{-1}, iq) F_{1,1}(iqz_L^{-1}, iq)} \frac{\sin^2\theta_H}{2}\ . \tag{2.141}$$

The entire effective potential is calculated by using the above formula. The relevant part of the $V_{\rm eff}(\theta_H)$ is given by

$$\begin{aligned}
V_{\rm eff}(\theta_H, z_L, k, c_t, r_t, c_F, n_F, \xi) &= V_{\rm eff}^{\rm gauge}(\theta_H, z_L, k, \xi) + V_{\rm eff}^{\rm fermion}(\theta_H, z_L, k, c_t, r_t, c_F, n_F),\\
V_{\rm eff}^{\rm gauge}(\theta_H, z_L, k, \xi) &= 2(3-\xi^2) I[Q_W] + (3-\xi^2) I[Q_Z] + 3\xi^2 I[Q_S],\\
V_{\rm eff}^{\rm fermion}(\theta_H, z_L, k, c_t, r_t, c_F, n_F) &= -12\Big\{I[Q_{\rm top}] + I[Q_{\rm bottom}]\Big\} - 8 n_F I[Q_F]\ ,\\
I[Q(q;\theta_H)] &= \frac{(kz_L^{-1})^4}{(4\pi)^2}\int_0^\infty dq\ q^3 \ln\{1+Q(q;\theta_H)\},\\
Q_W &= \cos^2\theta_W Q_Z = \frac{1}{2} Q_S = \frac{1}{2} Q_0[q;\frac{1}{2}]\sin^2\theta_H,\\
Q_{\rm top} &= \frac{Q_{\rm bottom}}{r_t} = \frac{Q_0[q;c_t]}{2(1+r_t)}\ \sin^2\theta_H,\\
Q_F &= Q_0[q;c_F]\cos^2\frac{1}{2}\theta_H\ ,\\
Q_0[q;c] &= \frac{z_L}{q^2 \hat{F}_{c-\frac{1}{2},c-\frac{1}{2}}(qz_L^{-1}, q)\hat{F}_{c+\frac{1}{2},c+\frac{1}{2}}(qz_L^{-1}, q)}\ ,
\end{aligned} \tag{2.142}$$

where $r_t = \tilde{\mu}^2/\mu_2^2$, $\hat{F}_{\alpha,\beta}(u,v) = I_\alpha(u)K_\beta(v) - e^{-i(\alpha-\beta)\pi}K_\alpha(u)I_\beta(v)$, and I_α, K_α are the modified Bessel functions. $F_{\alpha,\beta}(u,v)$ is expressed by using $\hat{F}_{\alpha,\beta}(u,v)$ as $F_{\alpha,\beta}(u,v) = (2/\pi)^2\hat{F}_{\alpha,\beta}(u,v)$. The contributions of the up quarks, down quarks, charm quarks, strange quarks and leptons are found to be negligible.

The gauge boson contributions to the effective potential, $I[Q_W]$ and $I[Q_Z]$ have the minimum at $\theta_H = 0, \pi$ and the maximum at $\theta_H = \frac{\pi}{2}$ as shown in Fig. 1(a). For the fermions, the quark contributions, $I[Q_{\rm top}]$ and $I[Q_{\rm bottom}]$ have the minimum at $\theta_H = \frac{\pi}{2}$ and the maximum at $\theta_H = 0, \pi$ and the dark fermion contributions $I[Q_F]$ have the minimum at $\theta_H = 0$ and the maximum at $\theta_H = \pi$ as shown in Fig. 1(b). Therefore the effective potential has the minimum at $\theta_H = 0$, π or $\frac{\pi}{2}$ when no dark fermions are in the Lagrangian. However the value $\theta_H = 0$, π and $\frac{\pi}{2}$ is disfavoured phenomenologically. In the case of $\theta_H = 0$ or π, the electroweak symmetry is not broken. In the case of $\theta_H = \frac{\pi}{2}$, the Higgs boson becomes stable because the Higgs boson coupling to the SM particles are suppressed from the SM value by $\cos\theta_H$ [24]. Therefore the dark fermion is needed to realise the observed Higgs boson.

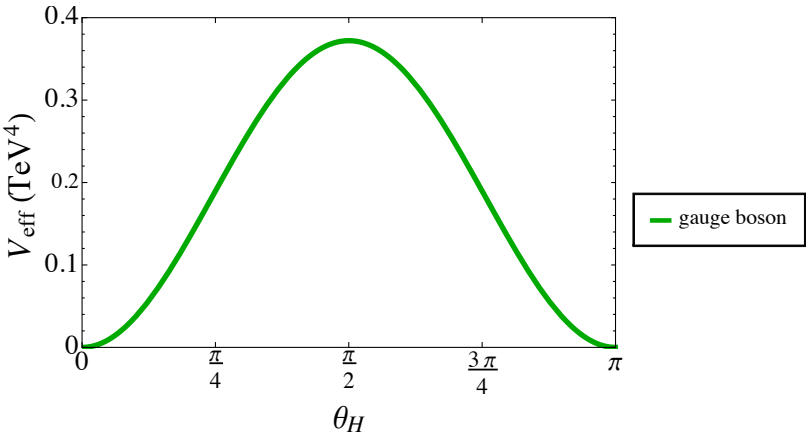

(a) The contribution of the gauge bosons to the effective potential are plotted.

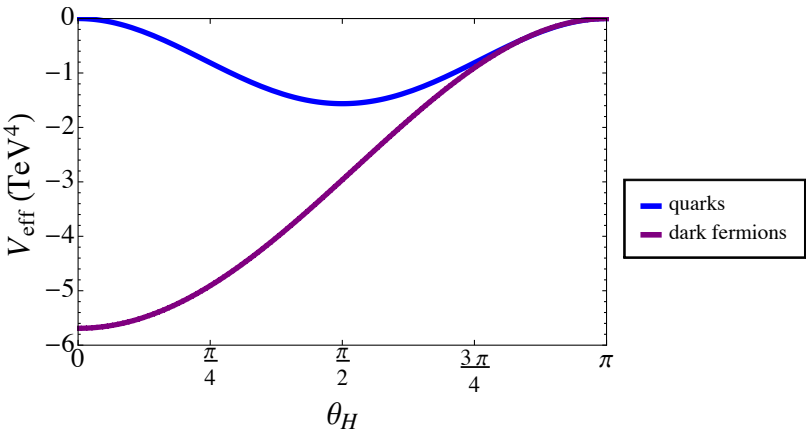

(b) The contribution of the quarks (blue line) and the contribution of the dark fermion (purple line) to the effective potential are plotted.

Figure 1: The contributions to the effective potential of the gauge bosons and the fermions are plotted in Fig. 1(a) and in Fig. 1(b), respectively, in the $n_F = 5$, $z_L = 10^5$, $c_t = 0.227$ and $c_F = 0.382$ case.

The Higgs mass is obtained by the second derivative of the effective potential at the minimum,

$$m_H^2 = \frac{1}{f_H^2} \frac{d^2 V_{\rm eff}}{d\theta_H^2}\bigg|_{\rm min} . \tag{2.143}$$

The Higgs cubic and quartic couplings are obtained by the third and fourth derivatives of the effective potential at the minimum, respectively. The parameters of the effective potential are θ_H, z_L, k, c_t, r_t, c_F and n_F. k, c_t, r_t and c_F are determined to realise the m_W, m_t, m_b and m_H. θ_H is determined by the condition $V'(\theta_H) = 0$. Therefore the free parameters of this model is n_F and z_L.

Table 1: The parameters θ_H, k, c_t, c_F, $m_{F^{(1)}}$ and $m_{Z^{(1)}}$ for z_L and $n_F = 3$, 4, 5 and 6 which realise $m_H = 126$ GeV in the t'Hooft-Feynman gauge.

n_F	z_L	θ_H	k (GeV)	c_t	c_F	$m_{F^{(1)}}$ (TeV)	$m_{Z^{(1)}}$ (TeV)
3	10^8	0.360	9.72×10^{10}	0.357	0.385	0.668	2.41
	10^7	0.258	1.26×10^{10}	0.330	0.353	0.993	3.15
	10^6	0.177	1.69×10^9	0.296	0.309	1.54	4.25
	10^5	0.117	2.32×10^8	0.227	0.235	2.53	5.91
	2×10^4	0.0860	5.87×10^7	0.137	0.127	3.88	7.54
4	10^8	0.355	9.86×10^{10}	0.357	0.423	0.567	2.45
	10^7	0.254	1.28×10^{10}	0.330	0.402	0.834	3.20
	10^6	0.174	1.71×10^9	0.292	0.374	1.27	4.32
	10^5	0.115	2.36×10^8	0.227	0.332	2.03	6.00
	10^4	0.0737	2.29×10^7	0.0366	0.256	3.46	8.52
5	10^8	0.351	9.97×10^{10}	0.357	0.445	0.502	2.48
	10^7	0.251	1.29×10^{10}	0.330	0.430	0.735	3.24
	10^6	0.172	1.74×10^9	0.292	0.410	1.11	4.37
	10^5	0.114	2.38×10^8	0.227	0.382	1.75	6.07
	10^4	0.0730	3.33×10^7	0.0366	0.333	2.91	8.61
6	10^8	0.348	1.01×10^{11}	0.356	0.461	0.455	2.51
	10^7	0.171	1.30×10^{10}	0.330	0.449	0.671	3.29
	10^6	0.171	1.75×10^9	0.292	0.434	1.00	4.43
	10^5	0.113	2.40×10^8	0.227	0.414	1.57	6.16
	10^4	0.0724	3.36×10^7	0.0365	0.379	2.57	8.72

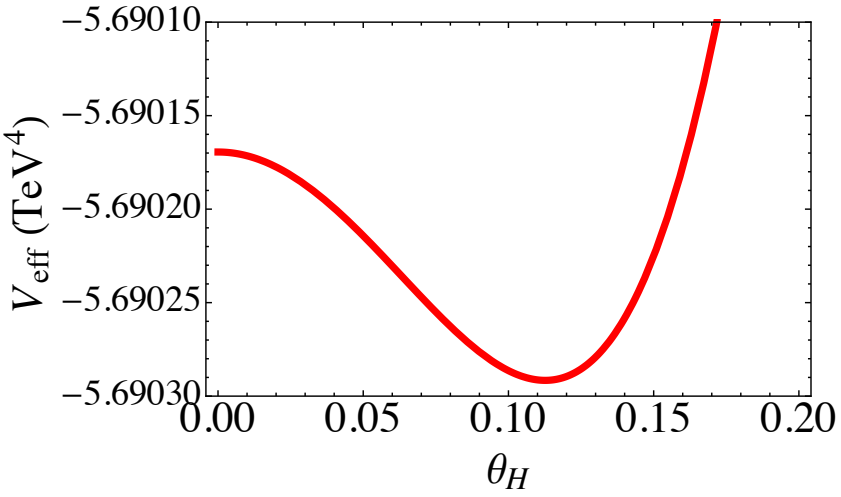

Figure 2: The effective potential $V_{\rm eff}(\theta_H)$ is plotted around the minimum in the $n_F = 5$, $z_L = 10^5$, $c_t = 0.227$ and $c_F = 0.382$ case, where the minimum is $\theta_H = 0.114$.

In the Table 1, the parameter sets which realise the $m_H = 126$ GeV and the $m_{F^{(1)}}$ and $m_{Z^{(1)}}$ are summarised. The bulk mass parameters of the dark fermions need not to be the same value for the each dark fermion. However all bulk mass parameters are set to be same for simplicity. In the case, the dark fermion masses are degenerate. The behaviour of the $V(\theta_H)$ which realise the $m_H = 126$ GeV is plotted in Fig. 2 where the parameters are $n_F = 5$, $z_L = 10^5$, $c_t = 0.227$ and $c_F = 0.382$, so that $\theta_H = 0.114$.

2.7. Universality

As shown in the previous section, the free parameters of this model are n_F and z_L. However the relation among θ_H and the other physical quantities such as $m_{\rm KK}$, $m_{\gamma^{(1)}}$, $m_{Z^{(1)}}$, $m_{Z_R^{(1)}}$, λ_3 and λ_4 are found to be almost independent of n_F, where λ_3 and λ_4 are the Higgs cubic and quartic couplings respectively. Those parameters are well approximated by the function of one parameter θ_H. This is called the universality of this model.

$m_{\rm KK}$, $m_{\gamma^{(1)}}$, $m_{Z^{(1)}}$ and $m_{Z_R^{(1)}}$ are approximated as the function of θ_H by

$$\begin{aligned} m_{\rm KK} &\sim \frac{1352}{(\sin\theta_H)^{0.786}}\ \text{GeV}\ , \\ m_{Z_R^{(1)}} &\sim \frac{1038}{(\sin\theta_H)^{0.784}}\ \text{GeV}\ , \\ m_{Z^{(1)}} &\sim \frac{1044}{(\sin\theta_H)^{0.808}}\ \text{GeV}\ , \\ m_{\gamma^{(1)}} &\sim \frac{1056}{(\sin\theta_H)^{0.804}}\ \text{GeV}\ . \end{aligned} \tag{2.144}$$

The relation between θ_H and $m_{Z^{(1)}}$ is plotted in Fig. 3 for $n_F = 0, 1, 3, 6$. The plotted

points are almost on the same curve and independent of n_F.

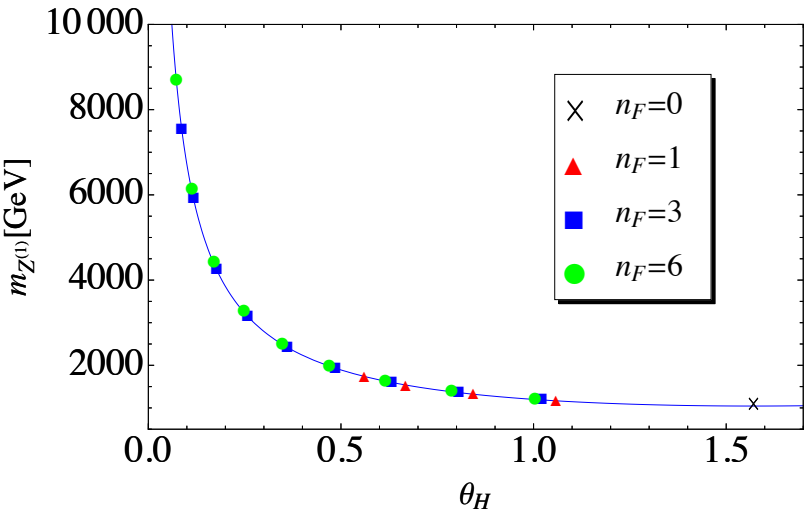

Figure 3: $m_{Z^{(1)}}$ as the function of θ_H for $m_H = 126$ GeV. Reprinted from Ref. [27].

Similarly the Higgs cubic and quartic self-couplings, λ_3 and λ_4 are plotted as the functions of θ_H for $n_F = 0, 1, 3, 9$ in Fig. 4. The fitting curves are given by

$$\begin{aligned} \lambda_3/\text{GeV} &= 26.7\cos\theta_H + 1.42(1+\cos 2\theta_H)\ , \\ \lambda_4 &= -0.0106 + 0.0304\cos 2\theta_H + 0.00159\cos 4\theta_H\ . \end{aligned} \tag{2.145}$$

In the SM, the Higgs cubic and quartic self-couplings are $\lambda_3^{\rm SM} = 31.5$ GeV and $\lambda_4^{\rm SM} = 0.0320$.

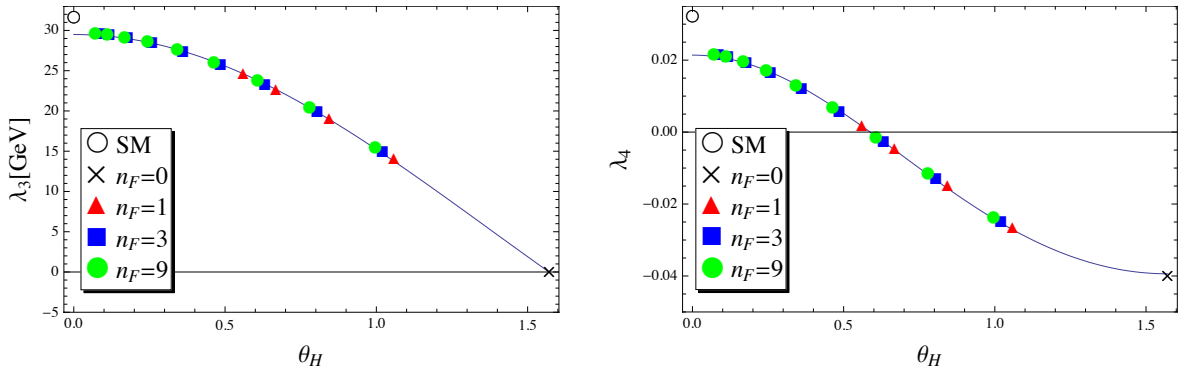

Figure 4: λ_3^H and λ_4^H as the function of θ_H for $m_H = 126$ GeV. In the SM $\lambda_3^{\rm SM} = 31.5$ GeV and $\lambda_4^{\rm SM} = 0.0320$. The fitting curves are given by (2.145). Reprinted from Ref. [27].

In contrast, no universality is found in the mass spectrum of the dark fermions. The masses of the dark fermion depends both θ_H and n_F. The mass $m_{F^{(1)}}$ is plotted in Fig. 5 for $n_F = 1, 3, 6$.

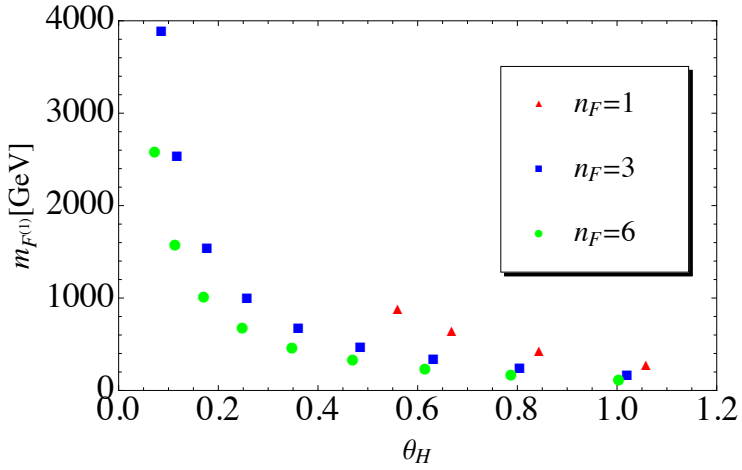

Figure 5: θ_H vs m_F for $m_H = 126$ GeV with n_F degenerate dark fermions. Reprinted from Ref. [27].

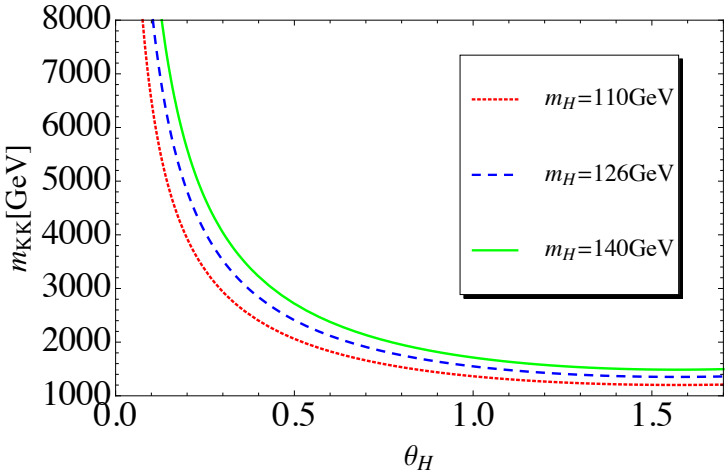

Figure 6: θ_H vs m_{KK} with various values of m_H. Reprinted from Ref. [27].

The universality relations are slightly affected by m_H. For $m_H = 110$ GeV, $m_{\rm KK}$ is approximated as $m_{\rm KK} \sim 1.20/|\sin\theta_H|^{0.733}$ TeV. For $m_H = 110, 126, 140$ GeV, $m_{\rm KK}$ is plotted in Fig. 6 as a function of θ_H.

The origin of the universality is not revealed yet. However, once θ_H is determined by some experiment such as the discovery of $Z^{(1)}$, the other physical values are simultaneously determined without the dark fermion mass $m_{F^{(1)}}$. Therefore this model is highly predictive.

2.8. Prediction of the Z' signal at the LHC

One of the important predictions of this model is the Z' signals at the LHC. In this model, there are four kinds of neutral gauge bosons which have mass $O(1)$ TeV. They are the first KK mode of the photon, the Z boson, the Z_R boson and the $A^{\hat{4}}$ boson. The $A^{\hat{4}}$ boson does not couple to SM particles so that it is not produced at the LHC. Therefore, $\gamma^{(1)}$, $Z^{(1)}$ and $Z_R^{(1)}$ are the Z' bosons. The dilepton production cross sections through the Z' from $p\bar{p}$ was studied in [27]. No significant excess have been observed in the processes at the 8 TeV LHC [6, 7]. Therefore the Z' masses are constrained and consequently the allowed range of θ_H is determined from the universality.

Table 2: Masses, total decay widths and couplings of the Z' bosons to the SM particles in the first generation for $\theta_H = 0.114$. The couplings to μ are almost same value as those to e. Reprinted from Ref. [27].

Z'	m(TeV)	Γ(GeV)	$g_{Z'u_Lu_L}$	$g_{Z'd_Ld_L}$	$g_{Z'e_Le_L}$	$g_{Z'u_Ru_R}$	$g_{Z'd_Rd_R}$	$g_{Z'e_Re_R}$
Z	0.0912	2.44	0.257	−0.314	−0.200	−0.115	0.0573	0.172
$Z_R^{(1)}$	5.73	482	0	0	0	0.641	−0.321	−0.978
$Z^{(1)}$	6.07	342	−0.0887	0.108	0.0690	−0.466	0.233	0.711
$\gamma^{(1)}$	6.08	886	−0.0724	0.0362	0.109	0.846	−0.423	−1.29
$Z^{(2)}$	9.14	1.29	−0.0073	0.0089	0.0057	−0.0055	0.0027	0.0086

Table 3: Masses, total decay widths and couplings of the Z' bosons to the SM particles in the first generation for $\theta_H = 0.073$. Reprinted from Ref. [27].

Z'	m(TeV)	Γ(GeV)	$g_{Z'u_Lu_L}$	$g_{Z'd_Ld_L}$	$g_{Z'e_Le_L}$	$g_{Z'u_Ru_R}$	$g_{Z'd_Rd_R}$	$g_{Z'e_Re_R}$
$Z_R^{(1)}$	8.00	553	0	0	0	0.588	−0.294	−0.896
$Z^{(1)}$	8.61	494	−0.100	0.123	0.0780	−0.426	0.213	0.650
$\gamma^{(1)}$	8.61	1.04×10^3	−0.0817	0.0408	0.123	0.775	−0.388	−1.18

The relevant couplings of the Z' bosons to calculate the production and decay rates are tabulated in Table 2 and Table 3. As shown in those tables, the couplings of $\gamma^{(1)}$, $Z^{(1)}$ and $Z_R^{(1)}$ to the right-handed fermions are larger than those to the left-handed fermions. This difference comes from a feature of the RS metric. The mode functions of left-handed fermions are written by $C_L(z;\lambda)$ and $S_L(z;\lambda)$ and those of right-handed fermions are written by $C_R(z;\lambda)$ and $S_R(z;\lambda)$, respectively. $C_L(z;\lambda)$ and $S_L(z;\lambda)$ have large values near the Planck brane, in contrast $C_R(z;\lambda)$ and $S_R(z;\lambda)$ have large values near the TeV brane. These mode functions for the top quark are shown in Fig 7(a) and 7(b). Considering the mode functions of the Z', the mode functions of $\gamma^{(1)}$, $Z^{(1)}$ and $Z_R^{(1)}$ include $C(z;\lambda)$. For the first KK modes, $C(z;\lambda)$ have a large value near the TeV brane as shown in Fig. 8. This behaviour is a consequence of the RS metric and leads to the large Z' couplings to the right-handed fermions.

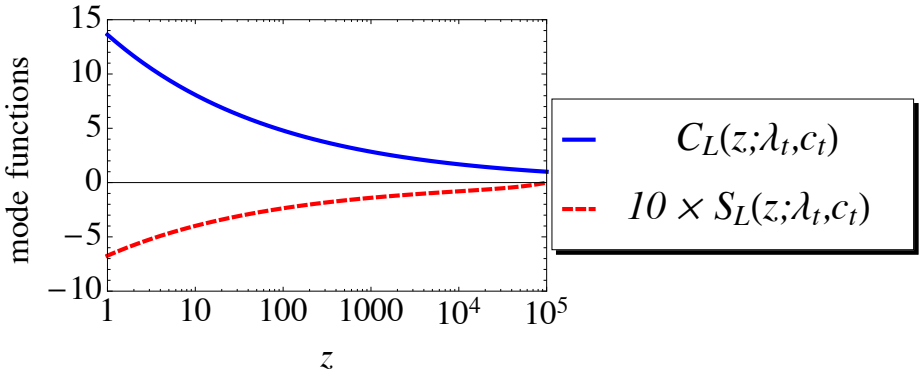

(a) Behaviour of the mode functions for the left-handed top quark, $C_L(z;\lambda,c_t)$ and $10\times S_L(z;\lambda,c_t)$ are represented by the blue solid and red dashed curve, respectively where the factor 10 is for convenience.

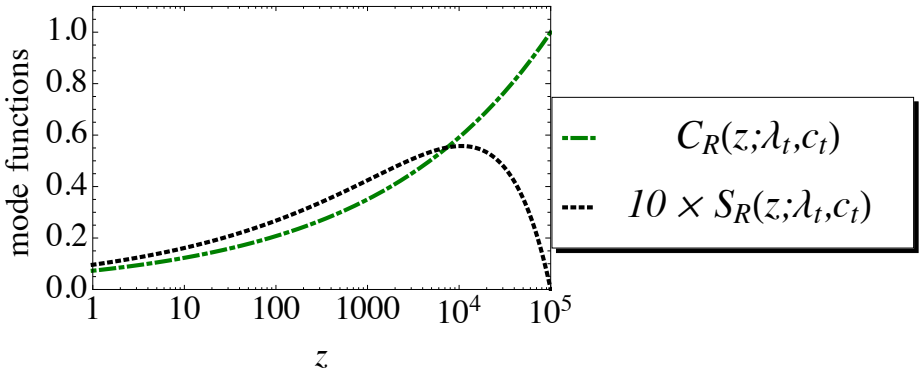

(b) Behaviour of the mode functions for the left-handed top quark, $C_R(z;\lambda,c_t)$ and $10\times S_R(z;\lambda,c_t)$ are represented by the green dot-dashed and grey dotted curve, respectively where the factor 10 is for convenience.

Figure 7: Behaviour of the mode functions for the left-handed and right-handed top quark are plotted where $z_L = 10^5$ and $c_t = 0.227$.

The decay width of the Z' boson is given by

$$\Gamma_{Z'} = \sum_i \frac{m_{Z'}}{12\pi}\left(\frac{\left(g_{Z'i_Li_L}\right)^2+\left(g_{Z'i_Ri_R}\right)^2}{2} + 2g_{Z'i_Li_L}g_{Z'i_Ri_R}\frac{m_i^2}{m_{Z'}^2}\right)\sqrt{1-\frac{4m_i^2}{m_{Z'}^2}}\ . \tag{2.146}$$

Here i runs over all fermions including the SM fermions and the dark fermions. The contribution of its decay to W^+W^- is very small and negligible because the couplings $Z'WW$ are small enough as shown in Table 12. By Eq. (2.146), the decay widths $\Gamma_{Z'}$ are calculated and the results are summarised in Table 2 and Table 3. It is found that all of $Z_R^{(1)}$, $Z^{(1)}$, and $\gamma^{(1)}$ have large decay widths. Especially $\gamma^{(1)}$ has large decay width around 1 TeV for $\theta_H \simeq 0.1$.

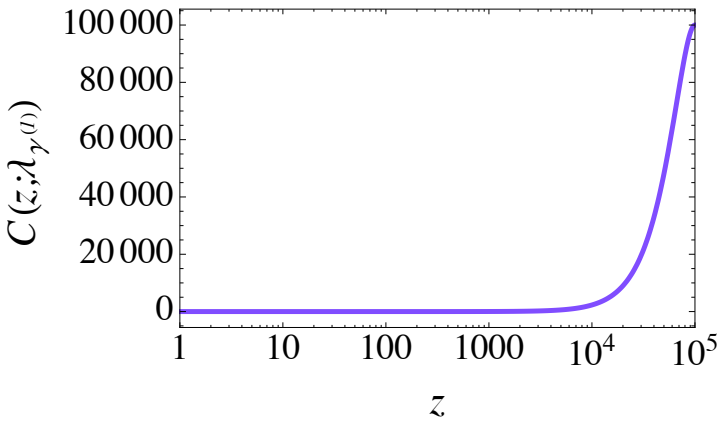

Figure 8: Behaviour of the $C(z;\lambda)$ for the first KK photon where $z_L = 10^5$, $\theta_H = 0.114$ and $m_{\gamma^{(1)}} = 6.08$ TeV.

The dependence of the cross section $\sigma(pp \to \ell^+\ell^- X)$ on the final state invariant mass $M_{\ell\ell}$ is described as

$$\frac{d\sigma(pp \to \ell^+\ell^- X)}{dM_{\ell\ell}} = \sum_q \int_{-1}^{1} d\cos\theta \int_{\frac{M_{\ell\ell}^2}{E_{\rm CMS}^2}}^{1} dx_1 \frac{2M_{\ell\ell}}{x_1 E_{\rm CMS}^2} \times f_q(x_1, M_{\ell\ell}^2) f_{\bar{q}}\left(\frac{M_{\ell\ell}^2}{x_1 E_{\rm CMS}^2}, M_{\ell\ell}^2\right) \frac{d\sigma(\bar{q}q \to \ell^+\ell^-)}{d\cos\theta}, \tag{2.147}$$

where $E_{\rm CMS}$ is the center-of-mass energy of the LHC and f_q's are the parton distribution functions (PDFs) for q quark. In our analysis, CTEQ5M [35] are employed for the PDFs.

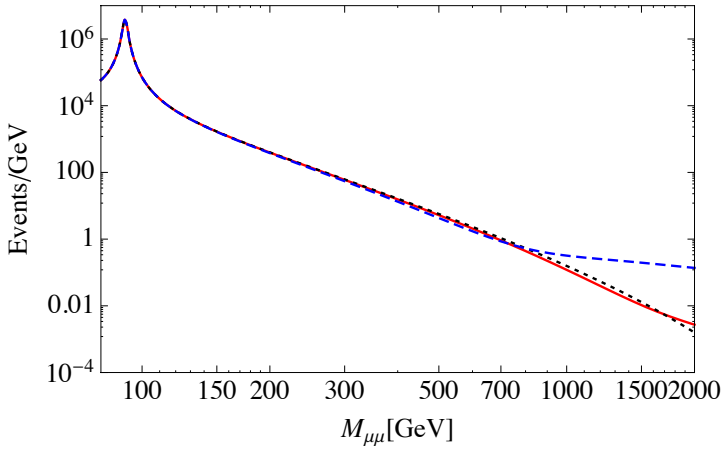

Figure 9: The differential cross section multiplied by a luminosity of 20.6 fb^{-1} for $pp \to \mu^+\mu^- X$ at the 8 TeV LHC for $\theta_H = 0.114$ (red solid curve) and for $\theta_H = 0.251$ (blue dashed curve). The black dotted line represents the SM background. Reprinted from Ref. [27].

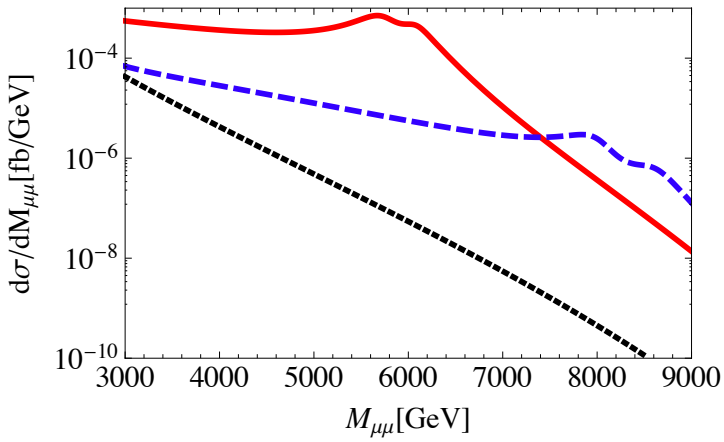

Figure 10: The differential cross section for $pp \to \mu^+\mu^- X$ at the 14 TeV LHC for $\theta_H = 0.114$ (red solid curve) and for $\theta_H = 0.073$ (blue dashed curve). The black dotted line represents the SM background. Reprinted from Ref. [27].

In Figure 9, the differential cross sections for $pp \to \mu^+\mu^- X$ are shown in the $\theta_H = 0.251$ and $\theta_H = 0.114$ cases. The values of the photon and Z boson couplings to the SM particles are almost equal to the SM value, so that the cross section in this model does not deviate largely from that in the SM below 1 TeV. However the decay widths of Z' bosons are very wide. In the $\theta_H = 0.251$ case, the deviation from the SM is large above 1 TeV. Therefore the $\theta_H = 0.251$ case is excluded by the 8 TeV LHC experiments but the $\theta_H = 0.114$ case is not excluded. In Figure 10, the predictions for the 14 TeV LHC are shown in the $\theta_H = 0.114$ and 0.073 cases. Because of the wide decay widths of Z''s, the large peak is predicted.

3. Higgs decay

In this section the decay rates $\Gamma(H \to \gamma\gamma)$ and $\Gamma(H \to Z\gamma)$ in the $SO(5) \times U(1)$ GHU model is evaluated. These processes occur at the one loop level. Therefore an infinite numbers of the KK mode contribution might be significant. However amazing cancellation occurs in their contributions and negligible. The decay rates in this model is approximately suppressed by $\cos^2\theta_H$ from the SM value. Therefore the branching ratios of the Higgs boson are consistent with the SM. In the following, the amplitudes are calculated in the unitary gauge.

3.1. $H \to \gamma\gamma$

At first, the decay rate $\Gamma(H \to \gamma\gamma)$ is calculated. The decay rate in the SM is given by

$$\Gamma(H \to \gamma\gamma)_{\rm SM} = \frac{\alpha^2 g_w^2}{1024\pi^3}\frac{m_H^3}{m_W^2}\left|\sum_i N_{c\,i} e_i^2 F_i(\tau_i)\right|^2 , \quad \tau_i = \frac{4m_i^2}{m_H^2} , \tag{3.1}$$

where we follow the notation of Ref. [36]. $N_{c\,i}$ is the number of the color degrees of freedom and e_i is the electromagnetic charge in units of e. Functions $F_1(\tau)$ and $F_{1/2}(\tau)$ are defined by

$$\begin{aligned} F_1(\tau) &= 2 + 3\tau + 3\tau(2-\tau)f(\tau) , \\ F_{1/2}(\tau) &= -2\tau[1 + (1-\tau)f(\tau)] , \\ f(\tau) &= \begin{cases} \left[\sin^{-1}\left(\sqrt{1/\tau}\right)\right]^2 & \text{for } \tau \geq 1 , \\ -\frac{1}{4}\left[\ln\frac{1+\sqrt{1-\tau}}{1-\sqrt{1-\tau}} - i\pi\right]^2 & \text{for } \tau < 1 , \end{cases} \end{aligned} \tag{3.2}$$

and assigned for gauge bosons and fermions, respectively. In the large τ limit, these functions reaches to $F_{1/2} \to -\frac{4}{3}$ and $F_1 \to 7$.

In the $SO(5) \times U(1)$ GHU model, the KK number is conserved by the electromagnetic interaction. Therefore the KK number in the loop is conserved and the calculation of the decay rate in the GHU is straightforward. The result is

$$\Gamma(H \to \gamma\gamma) = \frac{\alpha^2 g_w^2}{1024\pi^3}\frac{m_H^3}{m_W^2}\left|\mathcal{F}_W + \frac{4}{3}\mathcal{F}_t + n_F\mathcal{F}_F\right|^2 , \tag{3.3}$$

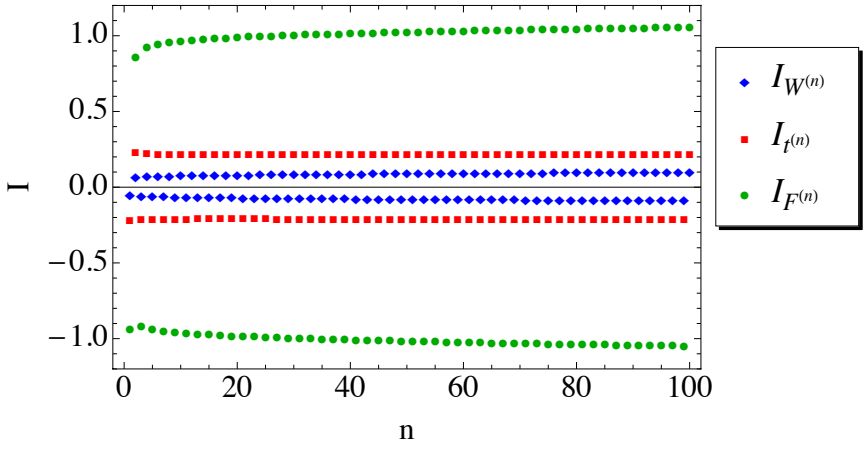

Figure 11: Behaviors of $I_{W^{(n)}} = g_{HW^{(n)}W^{(n)}}/g_w m_{W^{(n)}} \cos\theta_H$, $I_{t^{(n)}} = y_{t^{(n)}t^{(n)}}/y_t^{\rm SM} \cos\theta_H$ and $I_{F^{(n)}} = y_{F^{(n)}F^{(n)}}/y_t^{\rm SM} \sin\frac{\theta_H}{2}$ in the case of $n_F = 4$, $z_L = 10^5$ for which $\theta_H = 0.1153$. Reprinted from Ref. [29].

where

$$\begin{aligned}
\mathcal{F}_W &= \sum_{n=0}^{\infty} \frac{g_{HW^{(n)}W^{(n)}}}{g_w m_W} \frac{m_W^2}{m_{W^{(n)}}^2} F_1(\tau_{W^{(n)}}) = \sum_{n=0}^{\infty} I_{W^{(n)}} \frac{m_W}{m_{W^{(n)}}} \cos\theta_H F_1(\tau_{W^{(n)}}) \ , \\
\mathcal{F}_t &= \sum_{n=0}^{\infty} \frac{y_{t^{(n)}t^{(n)}}}{y_t^{\rm SM}} \frac{m_t}{m_{t^{(n)}}} F_{1/2}(\tau_{t^{(n)}}) = \sum_{n=0}^{\infty} I_{t^{(n)}} \frac{m_t}{m_{t^{(n)}}} \cos\theta_H F_{1/2}(\tau_{t^{(n)}}) \ , \\
\mathcal{F}_F &= \sum_{n=1}^{\infty} \frac{y_{F^{(n)}F^{(n)}}}{y_t^{\rm SM}} \frac{m_t}{m_{F^{(n)}}} F_{1/2}(\tau_{F^{(n)}}) = \sum_{n=1}^{\infty} I_{F^{(n)}} \frac{m_t}{m_{F^{(n)}}} \sin\frac{\theta_H}{2} F_{1/2}(\tau_{F^{(n)}}) \ . \qquad (3.4)
\end{aligned}$$

Here $I_{W^{(n)}}$, $I_{t^{(n)}}$ and $I_{F^{(n)}}$ are defined as $I_{W^{(n)}} = g_{HW^{(n)}W^{(n)}}/g_w m_{W^{(0)}} \cos\theta_H$, $I_{t^{(n)}} = y_{t^{(n)}t^{(n)}}/y_t^{\rm SM} \cos\theta_H$ and $I_{F^{(n)}} = y_{F^{(n)}F^{(n)}}/y_t^{\rm SM} \sin\frac{\theta_H}{2}$. Contributions from other quarks and leptons and their KK modes are negligible.

In the $SO(5) \times U(1)$ GHU, the Higgs couplings to the zero modes are approximated as $g_{HW^{(0)}W^{(0)}}/g_w m_{W^{(0)}} \simeq y_{t^{(0)}t^{(0)}}/y_t^{\rm SM} \simeq \cos\theta_H$, etc [24]. The Higgs couplings to the KK modes are obtained by the numerical calculation. In Fig. 11, the values of $I_{W^{(n)}}$, $I_{t^{(n)}}$ and $I_{F^{(n)}}$ are shown in the $N_F = 4$ and $\theta_H = 0.1153$ case. They approximately behave as

$$\begin{aligned}
I_{W^{(n)}} &\simeq (-1)^n \left\{ 0.0759 - 0.0065 \ln n + 0.0022 (\ln n)^2 \right\} \ , \\
I_{t^{(n)}} &\simeq (-1)^n \left\{ 0.2304 - 0.0108 \ln n + 0.0017 (\ln n)^2 \right\} \ , \\
I_{F^{(n)}} &\simeq (-1)^n \left\{ 1.0341 - 0.0457 \ln n + 0.0108 (\ln n)^2 \right\} \ , \qquad (3.5)
\end{aligned}$$

for $51 \le n \le 200$. Note that the sign changes alternatively for n. The masses of the KK modes of the W boson, top quark and the dark fermion are approximately $m_n \simeq n \cdot m_{\rm KK}/2$ for large n. Therefore the contributions of the KK modes to $\mathcal{F}$ behave

as $\sum(-1)^n(\ln n)^\alpha/n$ $(\alpha = 0, 1, 2)$ and converges. In addition, the contributions from $n \geq 1$ are suppressed by $m_{\rm EW}/m_{\rm KK}$. Hence the ratio of $\mathcal{F}$ to the zero-mode contribution becomes

$$\begin{aligned}
\frac{\mathcal{F}_W}{\mathcal{F}_{W^{(0)}\text{only}}} &= \quad 0.9997 \ , \\
\frac{\mathcal{F}_t}{\mathcal{F}_{t^{(0)}\text{only}}} &= \quad 0.9983 \ , \\
\frac{\mathcal{F}_F}{\mathcal{F}_{t^{(0)}\text{only}}} &= -\, 0.0032 \ ,
\end{aligned} \tag{3.6}$$

for $\theta_H = 0.114$ and $n_F = 4$ respectively. The ratio of the amplitude to that with only zero modes is

$$\frac{\mathcal{F}_W + \frac{4}{3}\mathcal{F}_t + 4\mathcal{F}_F}{\mathcal{F}_{W^{(0)}\text{only}} + \frac{4}{3}\mathcal{F}_{t^{(0)}\text{only}}} = 1.0027. \tag{3.7}$$

Therefore the contributions of the KK modes and the dark fermions are less than 1% and negligible. Because the zero mode couplings are approximately given by $g_{HWW} \simeq g^{\rm SM}_{HWW}\cos\theta_H = g_w m_W \cos\theta_H$ and $y_t \simeq y_t^{\rm SM}\cos\theta_H$, the decay rate in the GHU is approximately $\cos^2\theta_H$ times that in the SM. Thus the deviation from the SM is 1% for $\theta_H \sim 0.1$.

The production process $gg \to H$ also occurs at the one loop level. In the production process, only the quarks and its KK mode contribute to the process and the contributions of the light quarks are negligible as the $H \to \gamma\gamma$ process. Therefore the cross section $\sigma(gg \to H)$ is approximately obtained as

$$\frac{\sigma(gg \to H)_{\rm GHU}}{\sigma(gg \to H)_{\rm SM}} = \left(\frac{\mathcal{F}_t}{\mathcal{F}_{t^{(0)}\text{only}}}\right)^2 \cos^2\theta_H \simeq \cos^2\theta_H. \tag{3.8}$$

3.2. $H \to Z\gamma$

In this subsection, the decay rate $\Gamma(H \to Z\gamma)$ is calculated. The calculation is not so straightforward as the $H \to \gamma\gamma$ case, because the KK number might be changed by the interaction to the Z and H. Besides, there are also loops involving the W_R boson.

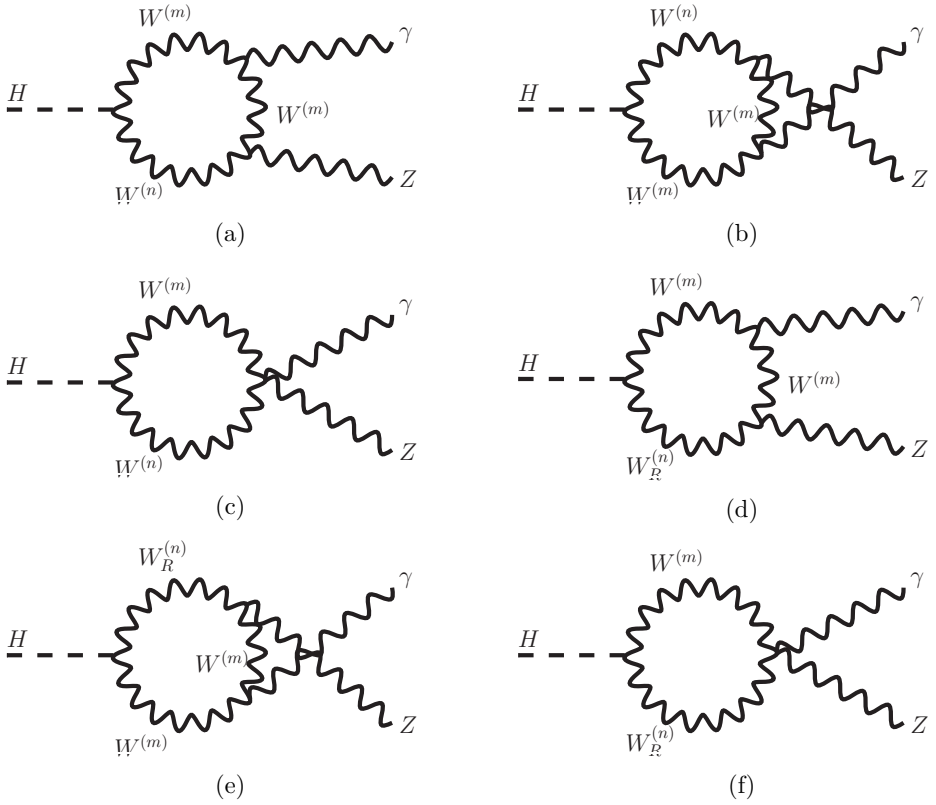

Figure 12: The gauge boson loop processes for $H \to Z\gamma$ in the $SO(5)\times U(1)$ gauge-Higgs unification is shown. W_R is the $SU(2)_R$ gauge boson and has no zero mode. Note that $HW_R^{(m)}W_R^{(n)}$ couplings does not exist. Reprinted from Ref. [29].

3.2.1. Boson loops

The gauge boson loop processes for $H \to Z\gamma$ are shown in Fig. 12. Note that there are no H-W_R-W_R interaction. The amplitude of W boson loop Figs. 12(a)(b)(c) is given by

$$
\begin{aligned}
&i\mathcal{M}^{(a)}_{W^{(m)},W^{(n)}} + i\mathcal{M}^{(b)}_{W^{(m)},W^{(n)}} + i\mathcal{M}^{(c)}_{W^{(m)},W^{(n)}} \\
&= e g_{HW^{(m)}W^{(n)}} g_{ZW^{(m)}W^{(n)}} \epsilon^*_\mu(k_1)\epsilon^*_\nu(k_2) \int \frac{d^4p}{(2\pi)^4}\, D_{\tau\alpha}(p, m_{W^{(m)}}) D_\sigma{}^\tau(p-k_1-k_2, m_{W^{(n)}}) \\
&\times \Big[2D_{\beta\rho}(p-k_1, m_{W^{(m)}}) \Big\{ 2\eta^{\alpha\beta}p^\mu - \eta^{\beta\mu}(p-2k_1)^\alpha - \eta^{\alpha\mu}(p+k_1)^\beta \Big\} \\
&\quad \times \Big\{ 2\eta^{\rho\sigma}(p-k_1)^\nu - \eta^{\sigma\nu}(p-k_1-2k_2)^\rho - \eta^{\rho\nu}(p-k_1+k_2)^\sigma \Big\} \\
&\quad - (2\eta^{\mu\nu}\eta^{\alpha\sigma} - \eta^{\mu\alpha}\eta^{\nu\sigma} - \eta^{\mu\sigma}\eta^{\nu\alpha}) \Big] , \\
&\quad D_{\mu\nu}(p,m) = \left(\eta_{\mu\nu} - \frac{p_\mu p_\nu}{m^2}\right) \frac{1}{p^2 - m^2 + i\epsilon} ,
\end{aligned}
\tag{3.9}
$$

where k_1 and k_2 are the photon and the Z boson momenta, respectively. The amplitude (3.9) is divergent. However, by adding the $m \leftrightarrow n$ diagrams and using $g_{HW^{(m)}W^{(n)}} = g_{HW^{(n)}W^{(m)}}$ and $g_{ZW^{(m)}W^{(n)}} = g_{ZW^{(n)}W^{(m)}}$, the amplitude is finite. The summation of the amplitude is

$$
\begin{aligned}
& i\Big\{\mathcal{M}^{(a)}_{W^{(m)},W^{(n)}} + \mathcal{M}^{(b)}_{W^{(m)},W^{(n)}} + \mathcal{M}^{(c)}_{W^{(m)},W^{(n)}} + (m \longleftrightarrow n)\Big\} \\
=& e g_{HW^{(m)}W^{(n)}} g_{ZW^{(m)}W^{(n)}} \epsilon^*_\mu(k_1)\epsilon^*_\nu(k_2) \left(\eta^{\mu\nu} - \frac{k_2^\mu k_1^\nu}{k_1\cdot k_2}\right) \frac{i}{16\pi^2} \frac{1}{m^2_{W^{(m)}} m^2_{W^{(n)}}} \\
& \times \Bigg\{ \Big(m^4_{W^{(m)}} + m^4_{W^{(n)}} + 10 m^2_{W^{(m)}} m^2_{W^{(n)}}\Big) E_+(m_{W^{(m)}}, m_{W^{(n)}}) \\
& \quad + \Big((m^2_{W^{(m)}} + m^2_{W^{(n)}})(m_H^2 - m_Z^2) - m_H^2 m_Z^2\Big) E_-(m_{W^{(m)}}, m_{W^{(n)}}) \\
& \quad - \Big(4 m^2_{W^{(m)}} m^2_{W^{(n)}}(m_H^2 - m_Z^2) + 2 m_Z^4 (m^2_{W^{(m)}} + m^2_{W^{(n)}})\Big) \\
& \qquad \times \left(C_0(m_{W^{(m)}}, m_{W^{(n)}}) + C_0(m_{W^{(n)}}, m_{W^{(m)}})\right) \Bigg\}
\end{aligned}
\tag{3.10}
$$

where

$$
\begin{aligned}
C_0(m_1^2, m_2^2) &\equiv C_0(0, m_H^2, m_Z^2, m_1^2, m_1^2, m_2^2) \ , \\
E_\pm(m_1, m_2) &\equiv 1 + \frac{m_Z^2}{m_H^2 - m_Z^2}\Big\{B_0(m_H^2, m_1^2, m_2^2) - B_0(m_Z^2, m_1^2, m_2^2)\Big\} \\
&\qquad \pm \Big\{m_1^2 C_0(m_1^2, m_2^2) + m_2^2 C_0(m_2^2, m_1^2)\Big\} \ ,
\end{aligned}
\tag{3.11}
$$

with the Passarino-Veltman functions [37, 38] defined by

$$
\begin{aligned}
& B_0(k^2, m_1^2, m_2^2) \equiv \frac{(2\pi)^{4-D}}{i\pi^2} \int d^D q \frac{1}{(q^2 - m_1^2)\{(q+k)^2 - m_2^2\}} \ , \\
& C_0(k_1^2, (k_1 - k_2)^2, k_2^2, m_1^2, m_2^2, m_3^2) \\
& \qquad \equiv \frac{(2\pi)^{4-D}}{i\pi^2} \int d^D q \frac{1}{(q^2 - m_1^2)\{(q+k_1)^2 - m_2^2\}\{(q+k_2)^2 - m_3^2\}} \ ,
\end{aligned}
\tag{3.12}
$$

In the $D \to 4$ limit, B_0 is divergent. However, the divergence are cancelled in C_0 and $E_\pm$, so that the amplitude (3.10) is finite.

To obtain the amplitude quantitatively, the couplings $g_{HW^{(m)}W^{(n)}}$ and $g_{ZW^{(m)}W^{(n)}}$ have to be evaluated numerically. The details are summarised in Appendix. For convenience the dimensionless coupling $J_{W^{(m)}W^{(n)}}$ is defined by

$$
J_{W^{(m)}W^{(n)}} \equiv \frac{g_{HW^{(m)}W^{(n)}} g_{ZW^{(m)}W^{(n)}}}{g_w^2 \cos\theta_W \cos\theta_H \sqrt{m_{W^{(m)}} m_{W^{(n)}}}} \ ,
\tag{3.13}
$$

and the value of $J_{W^{(m)}W^{(n)}}$ is tabulated in Table 4. $J_{W^{(m)}W^{(n)}}$ with $|m-n| \geq 2$ is found to be smaller than $J_{W^{(n)}W^{(n)}}$ by a factor 10^{-2}, whereas $J_{W^{(n)}W^{(n)}}$ and $J_{W^{(n)}W^{(n\pm1)}}$ are of

Table 4: $J_{W^{(m)}W^{(n)}}$ defined in (3.13) is shown for $0 \leq m, n \leq 7$ and for $101 \leq m, n \leq 108$ in the $N_F = 4$, $z_L = 10^5$ case. Only the values larger than that of $O(10^{-4})$ are shown with three significant figures. Reprinted from Ref. [29].

	0	1	2	3	4	5	6	7
0	1.00	$O(10^{-4})$	$O(10^{-9})$	$O(10^{-6})$	$O(10^{-11})$	$O(10^{-8})$	$O(10^{-12})$	$O(10^{-9})$
1	$O(10^{-4})$	-0.0580	0.0595	$O(10^{-6})$	$O(10^{-5})$	$O(10^{-10})$	$O(10^{-7})$	$O(10^{-9})$
2	$O(10^{-9})$	0.0595	0.0218	-0.0413	$O(10^{-8})$	$O(10^{-5})$	$O(10^{-9})$	$O(10^{-5})$
3	$O(10^{-6})$	$O(10^{-6})$	-0.0413	-0.0625	0.0637	$O(10^{-6})$	$O(10^{-5})$	$O(10^{-10})$
4	$O(10^{-11})$	$O(10^{-5})$	$O(10^{-8})$	0.0637	0.0226	-0.0432	$O(10^{-7})$	$O(10^{-5})$
5	$O(10^{-8})$	$O(10^{-10})$	$O(10^{-5})$	$O(10^{-6})$	-0.0432	-0.0652	0.0648	$O(10^{-6})$
6	$O(10^{-12})$	$O(10^{-7})$	$O(10^{-9})$	$O(10^{-5})$	$O(10^{-7})$	0.0648	0.0233	-0.0434
7	$O(10^{-9})$	$O(10^{-9})$	$O(10^{-5})$	$O(10^{-10})$	$O(10^{-5})$	$O(10^{-6})$	-0.0434	-0.0673

	101	102	103	104	105	106	107	108
101	-0.0932	0.0705	$O(10^{-6})$	$O(10^{-4})$	$O(10^{-12})$	$O(10^{-5})$	$O(10^{-8})$	$O(10^{-6})$
102	0.0705	0.0328	-0.0406	$O(10^{-6})$	$O(10^{-4})$	$O(10^{-12})$	$O(10^{-5})$	$O(10^{-9})$
103	$O(10^{-6})$	-0.0406	-0.0934	0.0706	$O(10^{-6})$	$O(10^{-4})$	$O(10^{-12})$	$O(10^{-5})$
104	$O(10^{-4})$	$O(10^{-6})$	0.0706	0.0329	-0.0405	$O(10^{-6})$	$O(10^{-4})$	$O(10^{-12})$
105	$O(10^{-12})$	$O(10^{-4})$	$O(10^{-6})$	-0.0405	-0.0937	0.0706	$O(10^{-6})$	$O(10^{-4})$
106	$O(10^{-5})$	$O(10^{-12})$	$O(10^{-4})$	$O(10^{-6})$	0.0706	0.0330	-0.0405	$O(10^{-6})$
107	$O(10^{-8})$	$O(10^{-5})$	$O(10^{-12})$	$O(10^{-4})$	$O(10^{-6})$	-0.0405	-0.0940	0.0707
108	$O(10^{-6})$	$O(10^{-9})$	$O(10^{-5})$	$O(10^{-12})$	$O(10^{-4})$	$O(10^{-6})$	0.0707	0.0331

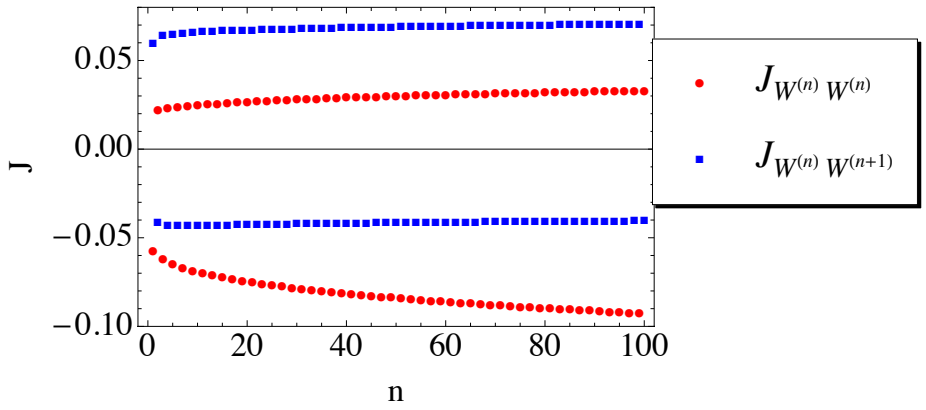

Figure 13: $J_{W^{(n)}W^{(n)}}$ and $J_{W^{(n)}W^{(n+1)}}$ are plotted for $1 \leq n \leq 100$ in the $N_F = 4$, $z_L = 10^5$ case. The red circles and blue squares represent $J_{W^{(n)}W^{(n)}}$ and $J_{W^{(n)}W^{(n+1)}}$, respectively. Reprinted from Ref. [29].

the same order. $J_{W^{(n)}W^{(n)}}$ and $J_{W^{(n)}W^{(n+1)}}$ are plotted in Fig. 13 for $1 \le n \le 100$ in the $N_F = 4$, $z_L = 10^5$ case. $J_{W^{(n)}W^{(n)}}$ and $J_{W^{(n)}W^{(n+1)}}$ for $101 \le n \le 200$ are approximately given by

$$\begin{aligned} J_{W^{(n)}W^{(n)}} &\simeq -0.0272 + 0.00320(\ln n) - 0.00083(\ln n)^2 \\ &\quad + (-1)^{n-1}\left(-0.0563 + 0.00654(\ln n) - 0.00173(\ln n)^2\right) \ , \\ J_{W^{(n)}W^{(n+1)}} &\simeq \ 0.0135 - 0.00160(\ln n) + 0.00041(\ln n)^2 \\ &\quad + (-1)^{n-1}\left(\ 0.0567 - 0.00106(\ln n) + 0.00018(\ln n)^2\right) \ . \end{aligned} \tag{3.14}$$

The diagonal ($m = n$) part of the amplitude in (3.10) for $n \gg 1$ is rewritten as

$$\begin{aligned} & i\mathcal{M}^{(a)}_{W^{(n)},W^{(n)}} + i\mathcal{M}^{(b)}_{W^{(n)},W^{(n)}} + i\mathcal{M}^{(c)}_{W^{(n)},W^{(n)}} \\ &= eg_w^2 \cos\theta_W \cos\theta_H \epsilon^*_\mu(k_1)\epsilon^*_\nu(k_2)\left(\eta^{\mu\nu} - \frac{k_2^\mu k_1^\nu}{k_1\cdot k_2}\right)\frac{i}{16\pi^2}\frac{J_{W^{(n)}W^{(n)}}}{2m^3_{W^{(n)}}} \\ &\quad \times\Bigg\{ -\frac{m_H^2 - m_Z^2}{2m^2_{W^{(n)}}}\Big(12m^4_{W^{(n)}} + 2m^2_{W^{(n)}}(m_H^2 - m_Z^2) - m_H^2 m_Z^2\Big) I_1(\tau_{W^{(n)}}, \lambda_{W^{(n)}}) \\ &\qquad + 4\Big(4m^2_{W^{(n)}}(m_H^2 - m_Z^2) - m_H^2 m_Z^2 + m_Z^4\Big) I_2(\tau_{W^{(n)}}, \lambda_{W^{(n)}})\Bigg\}, \end{aligned} \tag{3.15}$$

where

$$\begin{aligned} I_1(a,b) &= \frac{ab}{2(a-b)} + \frac{a^2b^2}{2(a-b)^2}\Big[f(a) - f(b)\Big] + \frac{a^2 b}{(a-b)^2}\Big[g(a) - g(b)\Big], \\ I_2(a,b) &= -\frac{ab}{2(a-b)}[f(a) - f(b)] \ , \\ g(\tau) &= \begin{cases} \sqrt{\tau - 1}\sin^{-1}\left(\sqrt{1/\tau}\right) & \text{for } \tau \ge 1 \ , \\ \frac{1}{2}\sqrt{1-\tau}\left[\ln\frac{1+\sqrt{1-\tau}}{1-\sqrt{1-\tau}} - i\pi\right] & \text{for } \tau < 1 \ . \end{cases} \end{aligned} \tag{3.16}$$

and $\lambda_i \equiv 4m_i^2/m_Z^2$. τ_i and $f(a)$ are defined in (3.1) and (3.2). Here, we have used

$$\begin{aligned} & \frac{m_Z^2}{m_H^2 - m_Z^2}\Big(B_0(m_H^2, m^2_{W^{(n)}}, m^2_{W^{(n)}}) - B_0(m_Z^2, m^2_{W^{(n)}}, m^2_{W^{(n)}})\Big) \\ &\qquad = -1 - \frac{m_H^2 - m_Z^2}{2m^2_{W^{(n)}}} I_1(\tau_{W^{(n)}}, \lambda_{W^{(n)}}) + 2I_2(\tau_{W^{(n)}}, \lambda_{W^{(n)}}) \ , \\ & C_0(0, m_H^2, m_Z^2, m^2_{W^{(n)}}, m^2_{W^{(n)}}, m^2_{W^{(n)}}) = -\frac{1}{m^2_{W^{(n)}}} I_2(\tau_{W^{(n)}}, \lambda_{W^{(n)}}) \ . \end{aligned} \tag{3.17}$$

The functions I_1, I_2 in (3.17) approach constants for $m_{W^{(n)}} \to \infty$. The whole amplitude

of the W boson loop is

$$i\mathcal{M}_W = \frac{i}{2}\sum_{m,n}^{\infty}\left\{\mathcal{M}^{(a)}_{W^{(m)},W^{(n)}} + \mathcal{M}^{(b)}_{W^{(m)},W^{(n)}} + \mathcal{M}^{(c)}_{W^{(m)},W^{(n)}} + (n \longleftrightarrow m)\right\} . \tag{3.18}$$

Since $J_{W^{(m)}W^{(n)}}$ for $|m-n| \geq 2$ are negligible comparing to $J_{W^{(m)}W^{(n)}}$ for $|m-n| \leq 1$, only the amplitude for $|m-n| \leq 1$ need to be considered. For $n \gg 1$, $m_{W^{(n\pm1)}} \simeq m_{W^{(n)}}$. By this approximation, the whole amplitude of the W boson loop is

$$\begin{aligned}
&\frac{1}{2}\sum_m \left(i\mathcal{M}^{(a)}_{W^{(m)},W^{(n)}} + i\mathcal{M}^{(b)}_{W^{(m)},W^{(n)}} + i\mathcal{M}^{(c)}_{W^{(m)},W^{(n)}} + (n \longleftrightarrow m)\right) \\
&\simeq e g_w^2 \cos\theta_W \cos\theta_H \epsilon^*_\mu(k_1)\epsilon^*_\nu(k_2)\left(\eta^{\mu\nu} - \frac{k_2^\mu k_1^\nu}{k_1\cdot k_2}\right)\frac{i}{16\pi^2} \\
&\quad\times \frac{1}{2m^3_{W^{(n)}}}\left(J_{W^{(n)}W^{(n)}} + J_{W^{(n+1)}W^{(n)}} + J_{W^{(n-1)}W^{(n)}}\right) \\
&\quad\times \Bigg\{ -\frac{m_H^2 - m_Z^2}{2m^2_{W^{(n)}}}\Big(12m^4_{W^{(n)}} + 2m^2_{W^{(n)}}(m_H^2 - m_Z^2) - m_H^2 m_Z^2\Big) I_1(\tau_{W^{(n)}}, \lambda_{W^{(n)}}) \\
&\qquad + 4\Big(4m^2_{W^{(n)}}(m_H^2 - m_Z^2) - m_H^2 m_Z^2 + m_Z^4\Big) I_2(\tau_{W^{(n)}}, \lambda_{W^{(n)}})\Bigg\} \\
&\approx \text{const.} \times \frac{1}{n}\left(J_{W^{(n)}W^{(n)}} + J_{W^{(n+1)}W^{(n)}} + J_{W^{(n-1)}W^{(n)}}\right) .
\end{aligned} \tag{3.19}$$

Therefore for the large n, the sum in the whole amplitude of W boson loop asymptotically behaves as

$$i\mathcal{M}_W \approx \sum_n^{\infty} \text{const.} \times \frac{1}{n}\left(J_{W^{(n)}W^{(n)}} + J_{W^{(n+1)}W^{(n)}} + J_{W^{(n-1)}W^{(n)}}\right) . \tag{3.20}$$

Nevertheless the sums $\sum J_{W^{(n)}W^{(n)}}/n$ and $\sum J_{W^{(n\pm1)}W^{(n)}}/n$ diverge respectively, the sum of them, $\sum\left(J_{W^{(n)}W^{(n)}} + J_{W^{(n+1)}W^{(n)}} + J_{W^{(n-1)}W^{(n)}}\right)/n$ behaves as

$$\begin{aligned}
&J_{W^{(n)}W^{(n)}} + J_{W^{(n+1)}W^{(n)}} + J_{W^{(n-1)}W^{(n)}} \\
&\simeq (-1)^{n-1}\Big\{ -0.0563 + 0.00654(\ln n) - 0.00173(\ln n)^2\Big\} ,
\end{aligned} \tag{3.21}$$

and therefore converges.

Next the loop process involving the W_R is considered. The dimensionless coupling $J_{W^{(m)}W_R^{(n)}}$ is also defined by

$$J_{W^{(m)}W_R^{(n)}} \equiv \frac{g_{HW^{(m)}W_R^{(n)}} g_{ZW^{(m)}W_R^{(n)}}}{g_w^2 \cos\theta_W \cos\theta_H \sqrt{m_{W^{(m)}} m_{W_R^{(n)}}}} , \tag{3.22}$$

As is seen in the Table 5, $J_{W^{(m)}W_R^{(n)}}$ is relevant only when $m/2 - n = 0, 1, 2$. The mass

Table 5: $J_{W^{(m)}W_R^{(n)}}$ in (3.22) is shown for $0 \le m \le 7$, $1 \le n \le 4$ and for $101 \le m \le 108$, $51 \le n \le 55$ in the $N_F = 4$, $z_L = 10^5$ case. Only values larger than $O(10^{-4})$ are shown explicitly with three significant figures. Reprinted from Ref. [29].

		m							
		0	1	2	3	4	5	6	7
	1	$O(10^{-5})$	$O(10^{-5})$	-0.0118	$O(10^{-7})$	$O(10^{-5})$	$O(10^{-7})$	$O(10^{-4})$	$O(10^{-7})$
	2	$O(10^{-6})$	$O(10^{-6})$	0.0296	$O(10^{-6})$	-0.0299	$O(10^{-6})$	$O(10^{-4})$	$O(10^{-8})$
n	3	$O(10^{-8})$	$O(10^{-8})$	0.0014	$O(10^{-6})$	0.0362	$O(10^{-5})$	-0.0373	$O(10^{-6})$
	4	$O(10^{-7})$	$O(10^{-8})$	$O(10^{-5})$	$O(10^{-7})$	0.0018	$O(10^{-6})$	0.0395	$O(10^{-4})$

		m							
		101	102	103	104	105	106	107	108
	51	$O(10^{-4})$	-0.0499	$O(10^{-6})$	$O(10^{-4})$	$O(10^{-7})$	$O(10^{-4})$	$O(10^{-7})$	$O(10^{-5})$
	52	$O(10^{-5})$	0.0474	$O(10^{-4})$	-0.0499	$O(10^{-6})$	$O(10^{-4})$	$O(10^{-7})$	$O(10^{-4})$
n	53	$O(10^{-7})$	0.0026	$O(10^{-5})$	0.0475	$O(10^{-4})$	-0.0499	$O(10^{-6})$	$O(10^{-4})$
	54	$O(10^{-7})$	$O(10^{-4})$	$O(10^{-7})$	0.0026	$O(10^{-5})$	0.0475	$O(10^{-4})$	-0.0499
	55	$O(10^{-8})$	$O(10^{-4})$	$O(10^{-7})$	$O(10^{-4})$	$O(10^{-7})$	0.0026	$O(10^{-5})$	0.0475

of the $W_R^{(n)}$ is approximately $m_{W_R^{(n)}} \simeq n \cdot m_{\rm KK}$, and the W mass is $m_{W^{(n)}} \simeq n \cdot m_{\rm KK}/2$. Therefore for $m/2 - n = 0, 1, 2$, $m_{W^{(m)}} \simeq m_{W_R^{(n)}} \simeq n \cdot m_{\rm KK}$ is satisfied. Hence the whole amplitude of the loop Figs. 12(d)(e)(f) is given by

$$\begin{aligned} i\mathcal{M}_{W_R} &= \sum_{m,n}^{\infty} \Big(i\mathcal{M}^{(d)}_{W^{(m)},W_R^{(n)}} + i\mathcal{M}^{(e)}_{W^{(m)},W_R^{(n)}} + i\mathcal{M}^{(f)}_{W^{(m)},W_R^{(n)}} \\ &\qquad + i\mathcal{M}^{(d)}_{W_R^{(n)},W^{(m)}} + i\mathcal{M}^{(e)}_{W_R^{(n)},W^{(m)}} + i\mathcal{M}^{(f)}_{W_R^{(n)},W^{(m)}} \Big) \\ &\approx \sum_{n}^{\infty} \text{const.} \times \frac{1}{n} \left(J_{W^{(n)}W_R^{(n/2)}} + J_{W^{(n)}W_R^{(n/2+1)}} + J_{W^{(n)}W_R^{(n/2+2)}} \right) . \end{aligned} \tag{3.23}$$

$J_{W^{(n)}W_R^{(n/2)}}$, $J_{W^{(n)}W_R^{(n/2+1)}}$ and $J_{W^{(n)}W_R^{(n/2+2)}}$ are plotted in Fig. 14 for $1 \le n \le 100$ in the $N_F = 4$, $z_L = 10^5$ case. $J_{W^{(n)}W_R^{(n/2)}}, J_{W^{(n)}W_R^{(n/2+1)}}, J_{W^{(n)}W_R^{(n/2+2)}}$are approximately

$$\begin{aligned} J_{W^{(n)}W_R^{(n/2)}} &\simeq -0.0425 - 0.00268(\ln n) + 0.00023(\ln n)^2 \\ J_{W^{(n)}W_R^{(n/2+1)}} &\simeq \quad 0.0411 + 0.00227(\ln n) - 0.00019(\ln n)^2 \\ J_{W^{(n)}W_R^{(n/2+2)}} &\simeq \quad 0.0021 + 0.00017(\ln n) - 0.00001(\ln n)^2. \end{aligned} \tag{3.24}$$

$J_{W^{(n)}W_R^{(n/2)}} + J_{W^{(n)}W_R^{(n/2+1)}} + J_{W^{(n)}W_R^{(n/2+2)}}$ almost vanishes.

To summarise, the whole amplitude of the gauge boson loop contributions $i\mathcal{M}_{\rm boson} \equiv i\mathcal{M}_W + i\mathcal{M}_{W_R}$ are convergent.

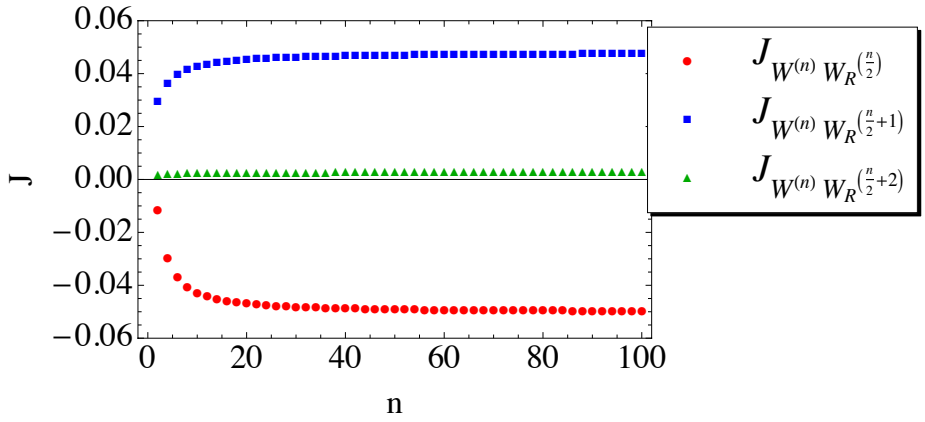

Figure 14: $J_{W^{(n)}W_R^{(n/2)}}$, $J_{W^{(n)}W_R^{(n/2+1)}}$ and $J_{W^{(n)}W_R^{(n/2+2)}}$ are plotted for $1 \leq n \leq 100$ in the $N_F = 4$, $z_L = 10^5$ case. The red circles, blue squares, green triangles represent $J_{W^{(n)}W_R^{(n/2)}}$, $J_{W^{(n)}W_R^{(n/2+1)}}$ and $J_{W^{(n)}W_R^{(n/2+2)}}$, respectively. Reprinted from Ref. [29].

3.2.2. Fermion loops

Next, the amplitude of the fermion loops in Fig. 15 are calculated similarly. The contributions from the top quark, charged dark fermions and their KK excitations are significant. The contributions from other quarks and leptons are negligible.

The diagrams of fermion loops Fig. 15 (a, b) (or (c,d)), give

$$
\begin{aligned}
& i\mathcal{M}^{(a)}_{f^{(m)},f^{(n)}} + i\mathcal{M}^{(b)}_{f^{(m)},f^{(n)}} \\
&= -\,Q_f e\,\epsilon^*_\mu(k_1)\epsilon^*_\nu(k_2)\int \frac{d^4p}{(2\pi)^4}\frac{1}{p^2-m^2_{f^{(m)}}}\frac{1}{(p-k_1)^2-m^2_{f^{(m)}}}\frac{1}{(p-k_1-k_2)^2-m^2_{f^{(n)}}} \\
&\quad\times \mathrm{Tr}\Big[\Big(y_{f^{(m)}f^{(n)}}+\hat{y}_{f^{(m)}f^{(n)}}\gamma^5\Big)(\not{p}+m_{f^{(m)}})\gamma^\mu(\not{p}-\not{k}_1+m_{f^{(m)}})\gamma^\nu \\
&\qquad\times\Big(g^V_{Zf^{(m)}f^{(n)}}+g^A_{Zf^{(m)}f^{(n)}}\gamma^5\Big)(\not{p}-\not{k}_1-\not{k}_2+m_{f^{(n)}}) \\
&\qquad+\Big(y_{f^{(m)}f^{(n)}}+\hat{y}_{f^{(n)}f^{(m)}}\gamma^5\Big)(-\not{p}+\not{k}_1+\not{k}_2+m_{f^{(n)}})\gamma^\nu \\
&\qquad\times\Big(g^V_{Zf^{(m)}f^{(n)}}+g^A_{Zf^{(n)}f^{(m)}}\gamma^5\Big)(-\not{p}+\not{k}_1+m_{f^{(m)}})\gamma^\mu(-\not{p}+m_{f^{(m)}})\Big]\,,
\end{aligned}
\tag{3.25}
$$

where $f^{(m)}$ is arbitrary fermion. The Yukawa couplings $y_{f^{(m)}f^{(n)}}$ and $\hat{y}_{f^{(m)}f^{(n)}}$ for $f^{(m)} = t^{(m)}$ and $F^{(m)}$ are given in (B.45) and (B.57), respectively. The amplitude (3.25) is divergent, but by adding the $m \leftrightarrow n$ diagrams and making use of $y_{f^{(m)}f^{(n)}} = y_{f^{(n)}f^{(m)}}$

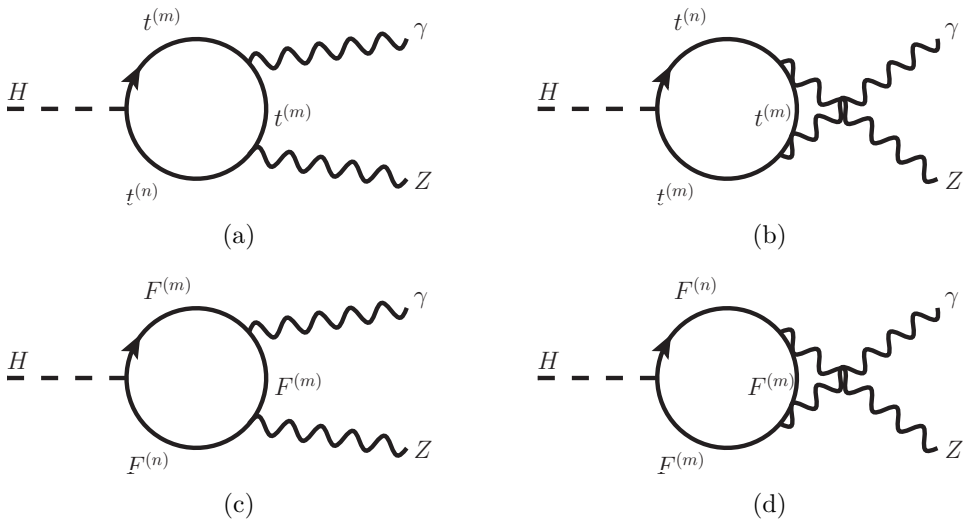

Figure 15: The fermion loop processes of $H \to Z\gamma$ decay in the $SO(5)\times U(1)$ gauge-Higgs unification. F^+ is the charged dark fermion. Reprinted from Ref. [29].

and $\hat{y}_{f^{(m)}f^{(n)}} = -\hat{y}_{f^{(n)}f^{(m)}}$, the amplitude becomes

$$
\begin{aligned}
& i\mathcal{M}^{(a)}_{f^{(m)},f^{(n)}} + i\mathcal{M}^{(b)}_{f^{(m)},f^{(n)}} + (m \longleftrightarrow n) \\
&= -\frac{iQ_f e}{4\pi^2}\epsilon^*_\mu(k_1)\epsilon^*_\nu(k_2)\left(\eta^{\mu\nu} - \frac{k_2^\mu k_1^\nu}{k_1\cdot k_2}\right) \\
&\quad \times \left\{ y_{f^{(m)}f^{(n)}} g^V_{Zf^{(m)}f^{(n)}} G_+(m_{f^{(m)}}, m_{f^{(n)}}) - \hat{y}_{f^{(m)}f^{(n)}} g^A_{Zf^{(m)}f^{(n)}} G_-(m_{f^{(m)}}, m_{f^{(n)}}) \right\} , \\
& G_\pm(m_1, m_2) = 2(m_1 \pm m_2) + \frac{2m_Z^2(m_1 \pm m_2)}{m_H^2 - m_Z^2}\Big(B_0(m_H^2, m_1^2, m_2^2) - B_0(m_Z^2, m_1^2, m_2^2)\Big) \\
&\qquad + m_1(2m_1^2 \pm 2m_1m_2 - m_H^2 + m_Z^2)C_0(0, m_H^2, m_Z^2, m_1^2, m_1^2, m_2^2) \\
&\qquad \pm m_2(2m_2^2 \pm 2m_1m_2 - m_H^2 + m_Z^2)C_0(0, m_H^2, m_Z^2, m_2^2, m_2^2, m_1^2) \ . \qquad (3.26)
\end{aligned}
$$

and this amplitude is finite as the gauge boson case.

We define $J_{t^{(m)}t^{(n)}}$ and $J_{F^{+(m)}F^{+(n)}}$ by

$$
J_{t^{(m)}t^{(n)}} \equiv \frac{g^V_{Zt^{(m)}t^{(n)}} y_{t^{(m)}t^{(n)}} \cos\theta_W}{g_w y_t \cos\theta_H} \ , \qquad (3.27)
$$

$$
J_{F^{+(m)}F^{+(n)}} \equiv \frac{g^V_{ZF^{+(m)}F^{+(n)}} y_{F^{(m)}F^{(n)}} \cos\theta_W}{g_w y_t \sin\frac{\theta_H}{2}} \qquad (3.28)
$$

The value of the $J_{t^{(m)}t^{(n)}}$ and $J_{F^{+(m)}F^{+(n)}}$ by the numerical calculation are shown in the Table 6 and Table 7. As in the case of $J_{W^{(n)}W^{(n)}}$, $J_{t^{(m)}t^{(n)}}$ and $J_{F^{+(m)}F^{+(n)}}$ for $|m-n| \geq 2$ is negligible. In addition, the ratio $(\hat{y}_{f^{(m)}f^{(n)}}/y_{f^{(m)}f^{(n)}}) \cdot (g^A_{Zf^{(m)}f^{(n)}}/g^V_{Zf^{(m)}f^{(n)}})$ is smaller than 10^{-4}. Hence the $\hat{y}_{f^{(m)}f^{(n)}} g^A_{Zf^{(m)}f^{(n)}}$ term in (3.26) is negligible.

Table 6: $J_{t^{(m)}t^{(n)}}$ is shown for $0 \leq m, n \leq 7$ and for $101 \leq m, n \leq 108$ in the $N_F = 4$, $z_L = 10^5$ case. Only the values larger than $O(10^{-4})$ are shown with three significant figures. Reprinted from Ref. [29].

	0	1	2	3	4	5	6	7
0	0.0988	-0.0041	$O(10^{-4})$	$O(10^{-5})$	$O(10^{-7})$	$O(10^{-6})$	$O(10^{-6})$	$O(10^{-7})$
1	-0.0041	-0.0790	0.0638	$O(10^{-5})$	$O(10^{-4})$	$O(10^{-9})$	$O(10^{-10})$	$O(10^{-8})$
2	$O(10^{-4})$	0.0638	-0.0350	-0.0071	$O(10^{-6})$	$O(10^{-6})$	$O(10^{-9})$	$O(10^{-5})$
3	$O(10^{-5})$	$O(10^{-5})$	-0.0071	-0.0763	0.0616	$O(10^{-6})$	$O(10^{-4})$	$O(10^{-9})$
4	$O(10^{-7})$	$O(10^{-4})$	$O(10^{-6})$	0.0616	-0.0338	-0.0071	$O(10^{-6})$	$O(10^{-6})$
5	$O(10^{-6})$	$O(10^{-9})$	$O(10^{-6})$	$O(10^{-6})$	-0.0071	-0.0754	0.0609	$O(10^{-6})$
6	$O(10^{-6})$	$O(10^{-10})$	$O(10^{-9})$	$O(10^{-4})$	$O(10^{-6})$	0.0609	-0.0334	-0.0070
7	$O(10^{-7})$	$O(10^{-8})$	$O(10^{-5})$	$O(10^{-9})$	$O(10^{-6})$	$O(10^{-6})$	-0.0070	-0.0751

	101	102	103	104	105	106	107	108
101	-0.0761	0.0610	$O(10^{-6})$	$O(10^{-4})$	$O(10^{-13})$	$O(10^{-7})$	$O(10^{-8})$	$O(10^{-6})$
102	0.0610	-0.0337	-0.0068	$O(10^{-6})$	$O(10^{-6})$	$O(10^{-13})$	$O(10^{-5})$	$O(10^{-9})$
103	$O(10^{-6})$	-0.0068	-0.0761	0.0610	$O(10^{-6})$	$O(10^{-4})$	$O(10^{-13})$	$O(10^{-7})$
104	$O(10^{-4})$	$O(10^{-6})$	0.0610	-0.0337	-0.0068	$O(10^{-6})$	$O(10^{-6})$	$O(10^{-13})$
105	$O(10^{-13})$	$O(10^{-6})$	$O(10^{-6})$	-0.0068	-0.0761	0.0610	$O(10^{-6})$	$O(10^{-4})$
106	$O(10^{-7})$	$O(10^{-13})$	$O(10^{-4})$	$O(10^{-6})$	0.0610	-0.0337	-0.0068	$O(10^{-6})$
107	$O(10^{-8})$	$O(10^{-5})$	$O(10^{-13})$	$O(10^{-6})$	$O(10^{-6})$	-0.0068	-0.0762	0.0610
108	$O(10^{-6})$	$O(10^{-9})$	$O(10^{-7})$	$O(10^{-13})$	$O(10^{-4})$	$O(10^{-6})$	0.0610	-0.0337

Table 7: $J_{F^{+(m)}F^{+(n)}}$ is shown for $0 \leq m, n \leq 7$ and for $101 \leq m, n \leq 108$ in the $N_F = 4$, $z_L = 10^5$ case. Only the values larger than $O(10^{-4})$ are shown with three significant figures. Reprinted from Ref. [29].

	1	2	3	4	5	6	7
1	0.2256	-0.0272	$O(10^{-5})$	-0.0040	$O(10^{-8})$	$O(10^{-5})$	$O(10^{-7})$
2	-0.0272	0.2378	0.0824	$O(10^{-6})$	$O(10^{-5})$	$O(10^{-8})$	$O(10^{-5})$
3	$O(10^{-5})$	0.0824	0.2204	-0.3188	$O(10^{-6})$	0.0036	$O(10^{-8})$
4	-0.0040	$O(10^{-6})$	-0.3188	0.2554	0.0866	$O(10^{-6})$	$O(10^{-5})$
5	$O(10^{-8})$	$O(10^{-5})$	$O(10^{-6})$	0.0866	0.2245	-0.3263	$O(10^{-6})$
6	$O(10^{-5})$	$O(10^{-8})$	-0.0036	$O(10^{-6})$	-0.3263	0.2612	0.0874
7	$O(10^{-7})$	$O(10^{-5})$	$O(10^{-8})$	$O(10^{-5})$	$O(10^{-6})$	0.0874	0.2271

	101	102	103	104	105	106	107	108
101	0.2505	-0.3528	$O(10^{-6})$	-0.0033	$O(10^{-11})$	$O(10^{-5})$	$O(10^{-8})$	$O(10^{-5})$
102	-0.3528	0.2918	0.0848	$O(10^{-5})$	$O(10^{-5})$	$O(10^{-12})$	$O(10^{-5})$	$O(10^{-8})$
103	$O(10^{-6})$	0.0848	0.2508	-0.3531	$O(10^{-6})$	-0.0033	$O(10^{-11})$	$O(10^{-5})$
104	-0.0033	$O(10^{-5})$	-0.3530	0.2921	0.0848	$O(10^{-5})$	$O(10^{-5})$	$O(10^{-12})$
105	$O(10^{-11})$	$O(10^{-5})$	$O(10^{-6})$	0.0848	0.2510	-0.3533	$O(10^{-6})$	-0.0033
106	$O(10^{-5})$	$O(10^{-12})$	-0.0033	$O(10^{-5})$	-0.3533	0.2924	0.0847	$O(10^{-5})$
107	$O(10^{-8})$	$O(10^{-5})$	$O(10^{-11})$	$O(10^{-5})$	$O(10^{-6})$	0.0847	0.2512	-0.3535
108	$O(10^{-5})$	$O(10^{-8})$	$O(10^{-5})$	$O(10^{-12})$	-0.0033	$O(10^{-5})$	-0.3535	0.2927

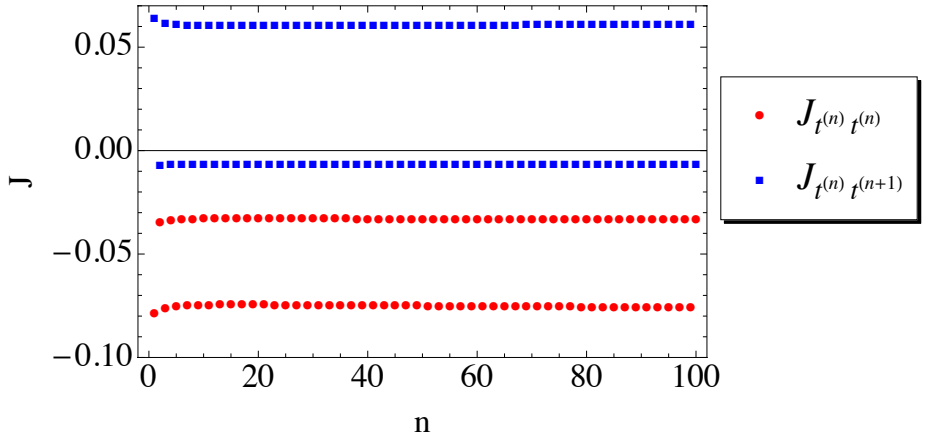

Figure 16: $J_{t^{(n)}t^{(n)}}$ and $J_{t^{(n)}t^{(n+1)}}$ are plotted for $1 \leq n \leq 100$ in the $N_F = 4$, $z_L = 10^5$ case. The red circles and blue squares express $J_{t^{(n)}t^{(n)}}$ and $J_{t^{(n)}t^{(n+1)}}$, respectively. Reprinted from Ref. [29].

From the numerical calculation, only the terms $J_{t^{(m)}t^{(n)}}$ and $J_{F^{+(m)}F^{+(n)}}$ for the $|m-n| \leq 1$ is significant. For $|m-n| \leq 1$ and $n \gg 1$, $m_{f^{(n\pm1)}} \simeq m_{f^{(n)}}$ is satisfied and the amplitudes are

$$\begin{aligned}
&\frac{1}{2}\sum_m \left\{ i\mathcal{M}^{(a)}_{t^{(m)},t^{(n)}} + i\mathcal{M}^{(b)}_{t^{(m)},t^{(n)}} + i\mathcal{M}^{(c)}_{F^{+(m)},F^{+(n)}} + i\mathcal{M}^{(d)}_{F^{+(m)},F^{+(n)}} + (m \leftrightarrow n) \right\} \\
&\approx \frac{i}{4\pi^2}\epsilon^*_\mu(k_1)\epsilon^*_\nu(k_2)\left(\eta^{\mu\nu} - \frac{k_2^\mu k_1^\nu}{k_1\cdot k_2}\right)\frac{e g_w y_t \cos\theta_H}{\cos\theta_W}(m_H^2 - m_Z^2) \\
&\times \left\{ \frac{2}{3}\frac{J_{t^{(n)}t^{(n)}} + J_{t^{(n+1)}t^{(n)}} + J_{t^{(n-1)}t^{(n)}}}{m_{t^{(n)}}}\left[I_1(\tau_{t^{(n)}}, \lambda_{t^{(n)}}) - I_2(\tau_{t^{(n)}}, \lambda_{t^{(n)}}) \right] \right. \\
&\left. + \frac{J_{F^{+(n)}F^{+(n)}} + J_{F^{+(n+1)}F^{+(n)}} + J_{F^{+(n-1)}F^{+(n)}}}{m_{F^{+(n)}}}\left[I_1(\tau_{F^{+(n)}}, \lambda_{F^{+(n)}}) - I_2(\tau_{F^{+(n)}}, \lambda_{F^{+(n)}}) \right] \right\} .
\end{aligned} \tag{3.29}$$

$J_{t^{(n)}t^{(n)}}$, $J_{t^{(n)}t^{(n+1)}}$, $J_{F^{+(n)}F^{+(n)}}$ and $J_{F^{+(n)}F^{+(n+1)}}$ are plotted in Figs. 16 and 17. For $101 \leq n \leq 200$, they are approximately given by

$$\begin{aligned}
J_{t^{(n)}t^{(n)}} &\simeq -0.0597 + 0.00323(\ln n) - 0.00047(\ln n)^2 \\
&\quad + (-1)^{n-1}\Big\{ -0.0230 + 0.00122(\ln n) - 0.00018(\ln n)^2 \Big\} , \\
J_{t^{(n)}t^{(n+1)}} &\simeq 0.0296 - 0.00162(\ln n) + 0.00024(\ln n)^2 \\
&\quad + (-1)^{n-1}\Big\{ 0.0362 - 0.00143(\ln n) + 0.00020(\ln n)^2 \Big\} ,
\end{aligned} \tag{3.30}$$

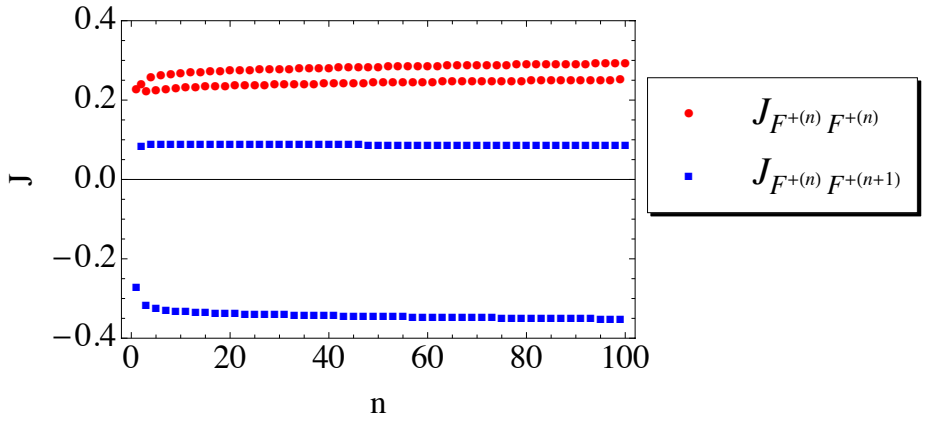

Figure 17: $J_{F^{+(n)}F^{+(n)}}$ and $J_{F^{+(n)}F^{+(n+1)}}$ are plotted for $1 \leq n \leq 100$ in the $N_F = 4$, $z_L = 10^5$ case. The red circles and blue squares express $J_{F^{+(n)}F^{+(n)}}$ and $J_{F^{+(n)}F^{+(n+1)}}$, respectively. Reprinted from Ref. [29].

$$
\begin{aligned}
J_{F^{+(n)}F^{+(n)}} &\simeq 0.280 - 0.0172(\ln n) + 0.00331(\ln n)^2 \\
&\quad + (-1)^{n-1}\Big\{ - 0.0212 + 0.00131(\ln n) - 0.00026(\ln n)^2 \Big\} , \\
J_{F^{+(n)}F^{+(n+1)}} &\simeq -0.138 + 0.0084(\ln n) - 0.00163(\ln n)^2 \\
&\quad + (-1)^{n-1}\Big\{ - 0.2218 + 0.00558(\ln n) - 0.00107(\ln n)^2 \Big\} .
\end{aligned} \tag{3.31}
$$

Consequently, by adding them, it is found that

$$
\begin{aligned}
&J_{t^{(n)}t^{(n)}} + J_{t^{(n+1)}t^{(n)}} + J_{t^{(n-1)}t^{(n)}} \simeq (-1)^{n-1}\Big\{ - 0.0230 + 0.00122(\ln n) - 0.00018(\ln n)^2 \Big\}, \\
&J_{F^{+(n)}F^{+(n)}} + J_{F^{+(n+1)}F^{+(n)}} + J_{F^{+(n-1)}F^{+(n)}} \\
&\qquad\qquad \simeq (-1)^{n-1}\Big\{ - 0.0212 + 0.00131(\ln n) - 0.00026(\ln n)^2 \Big\} .
\end{aligned} \tag{3.32}
$$

Since $i\mathcal{M}_f \propto \sum_n (J_{f^{(n)}f^{(n)}} + J_{f^{(n+1)}f^{(n)}} + J_{f^{(n-1)}f^{(n)}})/n$ for large n, the amplitude of the fermion loops converges as in the case of the gauge boson loops. Therefore the whole amplitude of the fermion contributions $i\mathcal{M}_{\text{fermion}}$ defined as

$$
\begin{aligned}
i\mathcal{M}_{\text{fermion}} &\equiv i\mathcal{M}_t + i\mathcal{M}_F \\
&= \frac{i}{2}\sum_{m,n}^{\infty}\Big\{ \mathcal{M}^{(a)}_{t^{(m)},t^{(n)}} + \mathcal{M}^{(b)}_{t^{(m)},t^{(n)}} + \mathcal{M}^{(c)}_{F^{+(m)},F^{+(n)}} + \mathcal{M}^{(d)}_{F^{+(m)},F^{+(n)}} + (m \leftrightarrow n) \Big\} ,
\end{aligned} \tag{3.33}
$$

is finite.

3.2.3. Total amplitude

The ratio of the sum of the all boson contributions to the W boson contribution and that of the all fermion contributions to the top quark contribution are given by

$$\frac{\mathcal{M}_{\rm boson}}{\mathcal{M}_{W^{(0)}{\rm only}}} = 0.9994, \quad \frac{\mathcal{M}_{\rm fermion}}{\mathcal{M}_{t^{(0)}{\rm only}}} = 1.0023, \tag{3.34}$$

respectively for $z_L = 10^5$, $n_F = 4$, and $\theta_H = 0.1153$. In the case, the ratio of the whole contribution to the W boson and top quark contributions is

$$\frac{\mathcal{M}_{\rm boson} + \mathcal{M}_{\rm fermion}}{\mathcal{M}_{W^{(0)}{\rm only}} + \mathcal{M}_{t^{(0)}{\rm only}}} = 0.9993 \ . \tag{3.35}$$

Therefore the KK mode contributions are found to be negligible. The zero mode couplings are approximated as $g_{HW^{(0)}W^{(0)}} \simeq g_w \cos\theta_H$ and $y_{t^{(0)}} \simeq y_{t\rm SM} \cos\theta_H$, the decay width is approximated by

$$\Gamma(H \to Z\gamma)_{\rm GHU} \simeq \Gamma(H \to Z\gamma)_{\rm SM} \times \cos^2\theta_H \ . \tag{3.36}$$

In the $SO(5)\times U(1)$ gauge-Higgs unification, the decay width of $H \to WW$, $H \to ZZ$, $H \to bb$ and $H \to \tau\tau$ are suppressed by $\cos^2\theta_H$ at the tree level. The decay width of the $H \to \gamma\gamma$ and $H \to Z\gamma$ are also suppressed by $\cos^2\theta_H$ at the one-loop level. Therefore the branching ratios of the Higgs decay modes in this model are almost the same as in the SM. The dominant process in the Higgs boson production is $gg \to H$, and the production cross section is also suppressed by $\cos^2\theta_H$. Therefore the signal strength, $[\sigma(gg \to H)B(H \to Z\gamma)]_{\rm GHU}/[\sigma(gg \to H)B(H \to Z\gamma)]_{\rm SM}$, is approximately $\cos^2\theta_H$. For $\theta_H \sim 0.1$, the deviation from the SM is only 1%.

The $H \to gg$, $\gamma\gamma$ and $H \to Z\gamma$ processes occur at the one-loop level and an infinite number of the KK modes contribute to the processes. By the non-trivial cancellations among the KK mode contributions, the infinite sums of the KK mode contributions converge and their contributions turn out negligible. Especially, in the $H \to Z\gamma$ process, the miraculous cancellations occur. The KK numbers of the particles can change by the interaction with the Z boson, so that the whole amplitude is obtained by summing up the two KK numbers. The mere infinite sum of the amplitudes in which the KK numbers are conserved diverges. However, the cancellations occur among the amplitude of the process in which the KK number is conserved in the loop and the amplitude of the process in which the KK number is not conserved in the loop. Consequently, the whole amplitude converges by summing up all of the contributions of the KK modes. These amazing cancellations are remarkable and attractive features of this model. The origin of the cancellations is to be clarified. It seems to originate from the five-dimensional gauge symmetry.

4. Dark mater

The existence of the dark matter (DM) [39] is one of the important clues to the physics beyond the SM and studied in the several models [40–43]. In this section, the relic density and the direct detection constraint of the neutral dark fermion are considered. The dark fermions do not have the zero mode from the boundary condition and the lightest mode are almost $SU(2)_R$ doublet and the $SU(2)_L$ doublet is slightly mixed. Thus the neutral dark fermions are DM candidates.

In this section, the first KK modes of the dark fermions $F_i^{(n)}$ are denoted as F_i.

4.1. Relic density

4.1.1. Pair annihilations and relic density of dark fermions

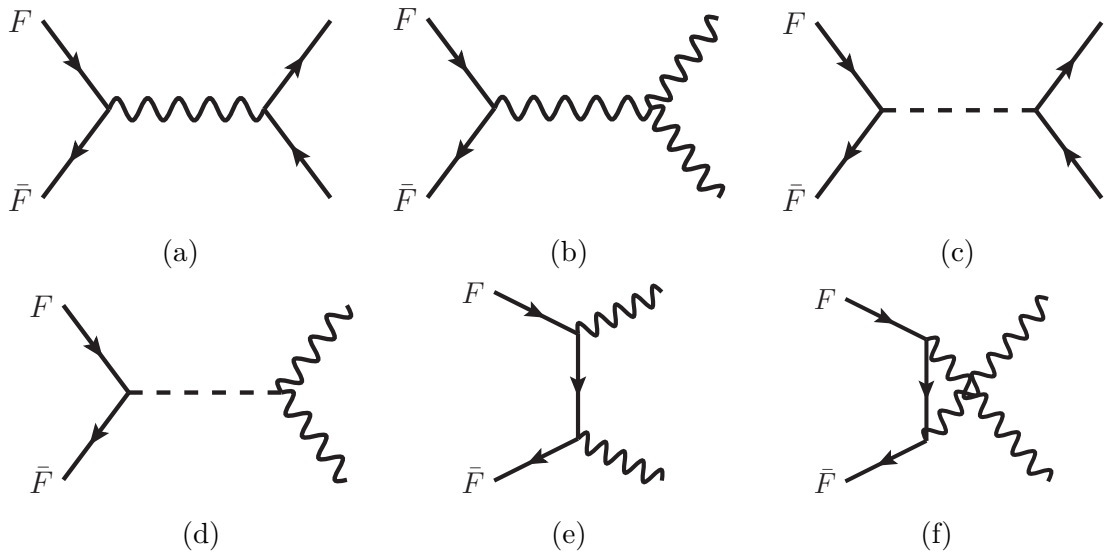

Figure 18: $F\bar{F}$ annihilation diagrams. (a) s-channel annihilation to fermions through a vector boson. (b) s-channel annihilation to vector bosons through a vector boson. (c) s-channel annihilation to a fermion-pair through the Higgs boson. (d) s-channel annihilation to a boson-pair through the Higgs boson. (e) t-channel annihilation to two vector bosons. (f) u-channel annihilation to two vector bosons. Reprinted from Ref. [28].

To obtain the relic density of the dark fermion, the annihilation cross sections of the dark fermions are calculated. Here, it should be emphasised that the lowest KK dark fermions are mostly $SU(2)_R$ doublets. Consequently, the WFF and ZFF couplings are small and Z_RWW couplings are also small.

At first the neutral dark fermion annihilations are considered. The s-channel annihilation to fermions through Z and $Z^{(n)}$ in Fig. 18(a) are suppressed by the small $ZF\bar{F}$ and

$Z^{(n)}F\bar{F}$ couplings. The s-channel annihilation to two vector bosons shown in Fig. 18(b) are suppressed by the small $\bar{F}FZ^{(n)}$ and $Z_R^{(n)}WW$ couplings. The s-channel annihilation through the Higgs boson in Fig. 18(c)(d) are negligible because of the small Higgs Yukawa couplings of $F\bar{F}$. The t- and u-channel processes shown in Fig. 18(e)(f) are also negligible because of the small $\bar{F}FW$ and $\bar{F}FZ$.

Considering the charged dark fermion, γ and $\gamma^{(1)}$ contribute to the processes. The s-channel annihilation to fermions through γ in Fig. 18(a) are small because of the heavy dark fermion mass. The s-channel annihilation $F^+\overline{F}^- \to \gamma^{(1)} \to W^+W^-$ in Fig. 18(b) are suppressed by the small $\gamma^{(1)}WW$ coupling shown in Table 12. The t- and u-channel processes $F^+\overline{F}^- \to \gamma\gamma$ and $F^+\overline{F}^- \to Z\gamma$ in Fig. 18(e)(f) are also negligible because of the large dark fermion mass and small ZFF coupling, respectively.

Thus unsuppressed processes are the s-channel annihilation processes $F^0\overline{F}^0 \to Z^{(1)} \to f\bar{f}$, $F^+\overline{F}^- \to Z^{(1)} \to f\bar{f}$ and $F^+\overline{F}^- \to \gamma^{(1)} \to f\bar{f}$. The couplings of $Z_R^{(1)}$ to quarks and leptons are large as shown in Table 2 and 3.

There are the also the co-annihilation processes. In this model, the annihilation of charged and neutral dark fermions is the co-annihilation and all of the co-annihilation processes are either vanishing or suppressed. The s-channel co-annihilation, $F^+\bar{F}^0$ to fermions through W and $W^{(n)}$ in Fig. 18(a) are suppressed by the small $WF^+\bar{F}^{(0)}$ and $W^{(n)}F^+\bar{F}^{(0)}$ couplings and the s-channel co-annihilation to fermions through $W_R^{(n)}$ is forbidden because $W_R\bar{f}f$ couplings are banished. The s-channel co-annihilation to two vector bosons shown in Fig. 18(b) are suppressed by the small $WF^+\bar{F}^{(0)}$, $W^{(n)}F^+\bar{F}^{(0)}$ and $W_R^{(n)}WZ$ couplings. The t- and u-channel processes $F^+\overline{F}^0 \to W^+\gamma$ and $F^+\overline{F}^0 \to W^+Z$ in Fig. 18(e)(f) are also suppressed by small $F^+\bar{F}^0W^-$ couplings.

Therefore the relevant processes for the dark fermion annihilation are the following s-channel processes

$$\begin{array}{rcccl} F^0\bar{F}^0 & \to & Z_R^{(1)} & \to & q\bar{q},\ l\bar{l},\ \nu\bar{\nu}, \\ F^+\bar{F}^- & \to & \gamma^{(1)} & \to & q\bar{q},\ l\bar{l}, \\ F^+\bar{F}^- & \to & Z_R^{(1)} & \to & q\bar{q},\ l\bar{l},\ \nu\bar{\nu}, \end{array} \tag{4.1}$$

and all other annihilation and co-annihilation processes are negligible. In addition, these processes could be enhanced by the Breit-Wigner resonance [43].

For charged dark fermions, the annihilation cross section of $F_i^+F_i^-$ to the SM fermions

is given by

$$
\begin{aligned}
&\sum_f \sigma(F_i^+ F_i^- \to \{\gamma^{(1)},\ Z_R^{(1)}\} \to \bar{f} f) \\
&= \frac{1}{64\pi\beta}\Bigg[\frac{s}{(s-m^2_{Z_R^{(1)}})^2 + m^2_{Z_R^{(1)}}\Gamma^2_{Z_R^{(1)}}} g_w^4 \Bigg(\sum_f \left[\left(g_{Z_R^{(1)} f_L}\right)^2 + \left(g_{Z_R^{(1)} f_R}\right)^2\right]\Bigg) \\
&\qquad \times \left\{\left(1+\frac{\beta^2}{3}\right)\left[\left(g_{Z_R^{(1)} F_L^+}\right)^2 + \left(g_{Z_R^{(1)} F_R^+}\right)^2\right] + 8\frac{m_F^2}{s} g_{Z_R^{(1)} F_L^+} g_{Z_R^{(1)} F_R^+}\right\} \\
&\quad + \frac{s}{(s-m^2_{\gamma^{(1)}})^2 + m^2_{\gamma^{(1)}}\Gamma^2_{\gamma^{(1)}}} e^4 \left(\sum_f \left[\left(g_{\gamma^{(1)} f_L}\right)^2 + \left(g_{\gamma^{(1)} f_R}\right)^2\right]\right) \\
&\qquad \times \left\{\left(1+\frac{\beta^2}{3}\right)\left[\left(g_{\gamma^{(1)} F_L^+}\right)^2 + \left(g_{\gamma^{(1)} F_R^+}\right)^2\right] + 8\frac{m_F^2}{s} g_{\gamma^{(1)} F_L^+} g_{\gamma^{(1)} F_R^+}\right\} \\
&\quad + 2\cdot \frac{(s-m^2_{Z_R^{(1)}})(s-m^2_{\gamma^{(1)}}) + m_{Z_R^{(1)}} m_{\gamma^{(1)}} \Gamma_{Z_R^{(1)}} \Gamma_{\gamma^{(1)}}}{[(s-m^2_{Z_R^{(1)}})^2 + m^2_{Z_R^{(1)}}\Gamma^2_{Z_R^{(1)}}][(s-m^2_{\gamma^{(1)}})^2 + m^2_{\gamma^{(1)}}\Gamma^2_{\gamma^{(1)}}]} \cdot s \\
&\qquad \times g_w^2 e^2 \left(\sum_f \left[g_{Z_R^{(1)} f_L} g_{\gamma^{(1)} f_L} + g_{Z_R^{(1)} f_R} g_{\gamma^{(1)} f_R}\right]\right) \\
&\qquad \times \Bigg\{\left(1+\frac{\beta^2}{3}\right)\left[g_{Z_R^{(1)} F_L^+} g_{\gamma^{(1)} F_L^+} + g_{Z_R^{(1)} F_L^+} g_{\gamma^{(1)} F_R^+}\right] \\
&\qquad\quad + 4\frac{m_F^2}{s}\left[g_{Z_R^{(1)} F_L^+} g_{\gamma^{(1)} F_R^+} + g_{Z_R^{(1)} F_R^+} g_{\gamma^{(1)} F_L^+}\right]\Bigg\}\Bigg], \qquad (4.2)
\end{aligned}
$$

where $g_{VF_L^+/F_R^+}$ and g_{Vf_L/f_R} are abbreviation of $g_{VF_L^+F_L^+}$, etc. $\beta \equiv \sqrt{1-4m_F^2/s}$ and s is the invariant mass of $F\bar{F}$. $F_i^0\bar{F}_i^0$ annihilation cross section $\sum_f \sigma(F^0\bar{F}^0 \to Z_R^{(1)} \to \bar{f}f)$ is obtained from (4.2) by replacing $g_{VF_L^+/F_R^+}$ with $g_{VF_L^0/F_R^0}$ and ignoring e^2 and e^4 terms.

The Boltzmann equation for F_i^0 is given by

$$
\begin{aligned}
\frac{dn_{(F_i^0)}}{dt} = -3Hn_{(F_i^0)} &- \sum_{X,X'}\left[\langle\sigma(\bar{F}_i^0 F_i^0 \to XX')v\rangle\left(n_{(F_i^0)}n_{(\bar{F}_i^0)} - n_{(F_i^0),\mathrm{eq}}n_{(\bar{F}_i^0),\mathrm{eq}}\right)\right] \\
&- \sum_{X,X'}\left[\langle\sigma(F_i^- F_i^0 \to XX')v\rangle\left(n_{(F_i^0)}n_{(\bar{F}_i^+)} - n_{(F_i^0),\mathrm{eq}}n_{(\bar{F}_i^+),\mathrm{eq}}\right)\right] \\
&- \sum_{j}\left[\langle\sigma(\bar{F}_i^0 F_i^0 \to F_j^+ F_j^-)v\rangle\left(n_{(F_i^0)}n_{(\bar{F}_i^0)} - n_{(F_i^0),\mathrm{eq}}n_{(\bar{F}_i^0),\mathrm{eq}}\right)\right] \\
&- \sum_{X,X'}\Big\{\langle\sigma(F_i^0 X \to F_i^+ X')v\rangle n_{(F_i^0)}n_{(X)} \\
&\qquad - \langle\sigma(F_i^+ X' \to F_i^0 X)v\rangle n_{(F_i^+)}n_{(X')}\Big\}, \qquad (4.3)
\end{aligned}
$$

where H is the Hubble constant, $n_{(F)}$ denotes the number density of F, and X represents

a SM field. The last term corresponds to the decay $F_i^+ \to F_i^0 W^+ \to F_i^0 f \bar{f}'$ where f and f' denotes the SM fermions. Similar relations are obtained for $\bar{F}_i^0$ and $F_i^\pm$. The number density of F in the thermal equilibrium is given by $n_{(x)}^{\rm eq} = g_x (m_x T/2\pi)^{3/2} \exp(-m_x/T)$ where g_x and m_x are the number of the degrees of freedom and mass of x, respectively.

The number-density of F_i^0 and $\bar{F}_i^0$ [F_i^+ and $\bar{F}_i^+$] ($i = 1, \ldots, n_F$) are denoted by n_0 [n_+]. Because the co-annihilations are suppressed, the third term in the right-hand side of (4.3) are negligible. The Boltzmann equation for the total number density of the DM, $n \equiv 2n_F(n_0 + n_+)$, is given by

$$\frac{dn}{dt} = -3Hn - 2n_F \langle \sigma_0 v \rangle (n_0^2 - n_{0,eq}^2) - 2n_F \langle \sigma_+ v \rangle (n_+^2 - n_{+,eq}^2), \tag{4.4}$$

where σ_0 [σ_+] be the annihilation cross section of F_i^0 [F_i^+] and $n_{0/+,eq}$ is approximately given by $n_{0/+,eq} \approx g_{0/+} (m_{F^{0/\pm}} T/2\pi)^{3/2} \exp(-m_{F^{0/\pm}}/T)$ and $g_{0/+} = 2$ for F_i^0 and F_i^+. Using the relations $n_{0,+}/n_{0,+eq} = n/n_{eq}$ and $n_{0,eq}/n_{eq} = n_{+,eq}/n_{eq} = 1/4n_F$, we obtain

$$\frac{dn}{dt} = -3Hn - \langle \sigma_{eff} v \rangle (n^2 - n_{eq}^2), \quad \sigma_{eff} v \equiv \frac{\sigma_0 v + \sigma_+ v}{8n_F}. \tag{4.5}$$

From the above definition, the relic density of the dark fermions at the present time is given by

$$\Omega_{DM} h^2 = \frac{1.04 \times 10^9}{M_{Pl}} \frac{1}{\sqrt{g_*}} \frac{1}{J_f}, \tag{4.6}$$

where g_* is the degree of freedom at the freeze-out temperature T_f and we take $g_* = 92$,

$$J_f \equiv \int_0^{x_f} \langle \sigma_{eff} v \rangle (x) dx \ , \tag{4.7}$$

The value of the x_f is determined by the relation

$$x_f^{-1} = \ln \left(\frac{5}{4} \sqrt{\frac{45}{8}} \frac{2 \cdot 4n_F}{2\pi^3} \frac{m_F M_{Pl} x_f^{1/2} \langle \sigma_{eff} v \rangle}{g_*^{1/2}} \right), \tag{4.8}$$

which can be solved by numerical iteration.

To obtain the thermal-averaged cross section $\langle \sigma v \rangle$, σv is expanded in v^2 as

$$\sigma v = a + b v^2 + \cdots = a + b[(s - 4m_F^2)/m_F^2] + \cdots \ , \tag{4.9}$$

then, we obtain

$$\begin{aligned}\langle\sigma v\rangle &= 4\pi\left(\frac{m_F}{4\pi T}\right)^{3/2}\int_0^\infty dv\, v^2 e^{-m_F v^2/4T}\sigma v \\ &= a + 6bT/m_F + \cdots .\end{aligned} \tag{4.10}$$

In the present case $x_f \sim 1/30$ and therefore only the first term in the v^2 expansion in Eq. (4.9) is kept in the following analysis. In the case where the Breit-Wigner resonance enhance the DM relic density, a careful treatment may be required [44]. In our case, because of the large decay widths of $V = Z^{(1)}, Z_R^{(1)}, \gamma^{(1)}$, the approximation can be justified.

4.1.2. Relic density of degenerate dark fermions

First we consider the case in which all dark fermions are degenerate. In Fig. 19 the relic density of the degenerate dark fermions for $n_F = 3, 4, 5$ and 6 is plotted. In the plot, the

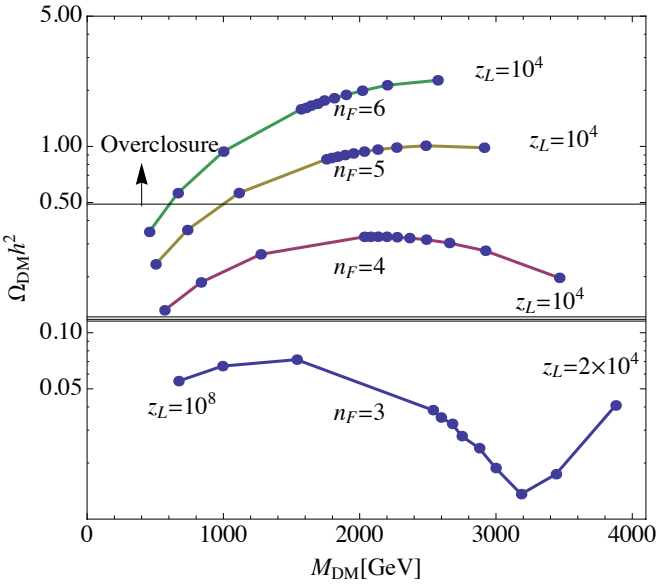

Figure 19: Relic density of the n_F degenerate dark fermions ($n_F = 3, 4, 5, 6$) are plotted. Data points are, from right to left, $z_L = 10^4$ (2×10^4) to 10^5 with a step of 10^4, 10^6, 10^7 and 10^8 for $n_F = 4, 5, 6$ ($n_F = 3$). The horizontal lines represent the observed relic density of the DM and the lower bound of the overclosure of the universe. Reprinted from Ref. [28].

best value [68% confidence level (CL) limits] of the relic density of the cold DM observed by Planck [8]:

$$\Omega_{CDM}h^2 = 0.11805 \quad [0.1186 \pm 0.0031], \tag{4.11}$$

has been also shown. From the Z' search (Sec. 2.8) in dilepton events, the allowed region of z_L is $z_L \lesssim 10^6$. For $z_L \lesssim 10^6$, no parameter regions can explain the relic abundance of the DM. For $n_F = 3$, $\Omega_{\rm DM}h^2 \simeq 0.01$ around $z_L \simeq 4 \times 10^4$ are obtained. For $n_F \geq 4$, the obtained values of the relic density is too large.

4.1.3. Relic density of non-degenerate dark fermions

In the above discussion, all of the c_{F_i} are the same value. Thus all of the dark fermion masses are degenerate, but the dark fermion masses need not be degenerate. From here, the possibility of the non-degenerate dark fermions as DM is discussed. In the scenario, some of them are heavier than others, only the lightest $F_i^{0(1)}$ becomes the DM.

Let us denote the mass eigenstates of the lightest particles of heavy and light dark fermions by (F_h^+, F_h^0) and (F_l^+, F_l^0), respectively. To make the (F_h^+, F_h^0) unstable, F_h^0 decay $F_h^0 \to F_l^0 + Z$ or as $F_h^0 \to F_l^+ + W^- \to F_l^0 + W^+ + W^-$ have to be realised.

The boundary condition of the Ψ_{F_l} are set as $\eta_{F_l} = +1$ in (2.14), whereas that of the Ψ_{F_h} are set as $\eta_{F_h} = -1$. By the boundary conditions, the lowest mode $(F_h^{+(1)}, F_h^{0(1)})$ is mostly an $SU(2)_L$ doublet, whereas $(F_l^{+(1)}, F_l^{0(1)})$ is mostly an $SU(2)_R$ doublet. The KK spectra for both Ψ_{F_h} and Ψ_{F_l} are given by (2.128).

The gauge eigenstates of the lightest modes of Ψ_{F_h}, Ψ_{F_l} are denoted by $\hat{F}_h^+, \hat{F}_h^0, \hat{F}_l^+, \hat{F}_l^0$. The most general form of bulk mass terms for Ψ_{F_h} and Ψ_{F_l} is

$$\mathcal{L}_F^{5D\ mass} = -\sigma'(y)\Big\{c_{F_h}\bar{\Psi}_{F_h}\Psi_{F_h} + c_{F_l}\bar{\Psi}_{F_l}\Psi_{F_l}\Big\} - \tilde{\Delta}\Big\{\bar{\Psi}_{F_h}\Psi_{F_l} + \bar{\Psi}_{F_l}\Psi_{F_h}\Big\}\ . \tag{4.12}$$

Note that $\bar{\Psi}_{F_h}\Psi_{F_h}$ and $\bar{\Psi}_{F_l}\Psi_{F_l}$ are odd under parity $y \to -y$, whereas $\bar{\Psi}_{F_h}\Psi_{F_l}$ is even. The $\tilde{\Delta}$ term induces mass mixing among $\hat{F}_h^+$ and $\hat{F}_l^+$, and among $\hat{F}_h^0$ and $\hat{F}_l^0$. c_{F_h} and c_{F_l} generate masses $\hat{m}_h$ and $\hat{m}_l$ for $(\hat{F}_h^+, \hat{F}_h^0)$ and $(\hat{F}_l^+, \hat{F}_l^0)$. Their bulk mass parameters c_{F_h} and c_{F_l} are supposed to be $c_{F_h} < c_{F_l}$ so that $\hat{m}_h > \hat{m}_l$. As mentioned above, the charged dark fermions acquire radiative corrections by photon, and becomes heavier than the neutral ones. The mass difference $m_{F^+} - m_{F^0}$ is denoted as $a \cdot \hat{m}_h$ $(a \cdot \hat{m}_l)$ for $\hat{F}_h^+$ $(\hat{F}_l^+)$ where a is $O(10^{-3} \sim 10^{-2})$.

Hence the mass matrices are given by

$$\begin{aligned}
&\mathcal{L}_F^{4D\ mass} = -\Big(\bar{\hat{F}}_h^+, \bar{\hat{F}}_l^+\Big)\mathcal{M}_+ \begin{pmatrix}\hat{F}_h^+ \\ \hat{F}_l^+\end{pmatrix} - \Big(\bar{\hat{F}}_h^0, \bar{\hat{F}}_l^0\Big)\mathcal{M}_0 \begin{pmatrix}\hat{F}_h^0 \\ \hat{F}_l^0\end{pmatrix}, \\
&\mathcal{M}_+ = \begin{pmatrix}(1+a)\hat{m}_h & \Delta \\ \Delta & (1+a)\hat{m}_l\end{pmatrix}\ ,\ \ \mathcal{M}_0 = \begin{pmatrix}\hat{m}_h & \Delta \\ \Delta & \hat{m}_l\end{pmatrix}.
\end{aligned} \tag{4.13}$$

We suppose that $\Delta \ll \hat{m}_h, \hat{m}_l$. By diagonalising the two matrices, we obtain

$$\begin{aligned}
\mathcal{L}_F^{4D\ mass} &= -m_{F_h^+}\bar{F}_h^+F_h^+ - m_{F_l^+}\bar{F}_l^+F_l^+ - m_{F_h^0}\bar{F}_h^0F_h^0 - m_{F_l^0}\bar{F}_l^0F_l^0 \ , \\
\begin{pmatrix} F_h^+ \\ F_l^+ \end{pmatrix} &= V\left(\frac{1}{2}\alpha_+\right)\begin{pmatrix} \hat{F}_h^+ \\ \hat{F}_l^+ \end{pmatrix}, \quad \begin{pmatrix} F_h^0 \\ F_l^0 \end{pmatrix} = V\left(\frac{1}{2}\alpha_0\right)\begin{pmatrix} \hat{F}_h^0 \\ \hat{F}_l^0 \end{pmatrix}, \\
\begin{pmatrix} m_{F_h^+} \\ m_{F_l^+} \end{pmatrix} &= \frac{1}{2}(1+a)(\hat{m}_h+\hat{m}_l) \pm \sqrt{\frac{1}{4}(1+a)^2(\hat{m}_h-\hat{m}_l)^2+\Delta^2} \ , \\
V(\alpha) &= \begin{pmatrix} \cos\alpha & \sin\alpha \\ -\sin\alpha & \cos\alpha \end{pmatrix}, \quad \tan\alpha_+ = \frac{2\Delta}{(1+a)(\hat{m}_h-\hat{m}_l)} \ .
\end{aligned} \tag{4.14}$$

The masses $(m_{F_h^0}, m_{F_l^0})$ and angle α_0 are obtained from $(m_{F_h^+}, m_{F_l^+})$ and α_+ by taking $a \to 0$.

The couplings to Z (the neutral currents) are given originally by

$$Z_\mu \sum_{j=h,l}\left\{g_{ZF_{jL}^+}\bar{\hat{F}}_{jL}^+\gamma^\mu\hat{F}_{jL}^+ + g_{ZF_{jR}^0}\bar{\hat{F}}_{jL}^0\gamma^\mu\hat{F}_{jL}^0\right\} + (L\to R) \ . \tag{4.15}$$

Similarly the couplings to W (the charged currents) are given by

$$W_\mu \sum_{j=h,l}\left\{g_{WF_{jL}}\bar{\hat{F}}_{jL}^+\gamma^\mu\hat{F}_{jL}^0 + g_{WF_{jR}}\bar{\hat{F}}_{jR}^+\gamma^\mu\hat{F}_{jR}^0\right\} + (\text{h.c.}). \tag{4.16}$$

In terms of mass eigenstates, the neutral current becomes

$$\begin{aligned}
&(\bar{F}_{hL}^0, \bar{F}_{lL}^0)\left\{\frac{g_{ZF_{hL}^0}+g_{ZF_{lL}^0}}{2} + \frac{g_{ZF_h^0L}-g_{ZF_l^0L}}{2}U(\alpha_0)\right\}\gamma^\mu\begin{pmatrix} F_{hL}^0 \\ F_{lL}^0 \end{pmatrix} \\
&+(\bar{F}_{hL}^+, \bar{F}_{lL}^+)\left\{\frac{g_{ZF_{hL}^+}+g_{ZF_{lL}^+}}{2} + \frac{g_{ZF_h^+L}-g_{ZF_l^+L}}{2}U(\alpha_+)\right\}\gamma^\mu\begin{pmatrix} F_{hL}^+ \\ F_{lL}^+ \end{pmatrix} + (L\to R) \ ,
\end{aligned} \tag{4.17}$$

where

$$U(\alpha) = \begin{pmatrix} \cos\alpha & -\sin\alpha \\ -\sin\alpha & -\cos\alpha \end{pmatrix}. \tag{4.18}$$

The charged current is

$$\begin{aligned}
&(\bar{F}_{hL}^+, \bar{F}_{lL}^+)\left\{\frac{g_{WF_{hL}}+g_{WF_{lL}}}{2}V\left(\frac{\alpha_+-\alpha_0}{2}\right) + \frac{g_{WF_{hL}}-g_{WF_{lL}}}{2}U\left(\frac{\alpha_++\alpha_0}{2}\right)\right\}\gamma^\mu\begin{pmatrix} F_{hL}^0 \\ F_{lL}^0 \end{pmatrix} \\
&+(L\to R) \ .
\end{aligned} \tag{4.19}$$

Thus the mixing neutral and charged currents of the heavy and light dark fermions are generated.

Table 8: Parameters in the non-degenerate case of dark fermions. $(n_F^{\rm light}, n_F^{\rm heavy})$, bulk mass parameter c_{F_l}, the masses m_{F_h} and m_{F_l} are tabulated for various $\Delta c_F \equiv c_{F_l} - c_{F_h}$ and z_L. Reprinted from Ref. [28].

Δc_F		0.04			0.06		
$(n_F^{\rm light}, n_F^{\rm heavy})$	z_L	c_{F_l}	m_{F_h} [TeV]	m_{F_l} [TeV]	c_{F_l}	m_{F_h} [TeV]	m_{F_l} [TeV]
(1,3)	10^6	0.404	1.32	1.13	0.418	1.34	1.06
	10^5	0.362	2.09	1.86	0.377	2.12	1.77
	3×10^4	0.329	2.72	2.46	0.344	2.76	2.36
	10^4	0.286	3.54	3.24	0.240	3.58	3.14
(2,2)	10^5	0.352	2.15	1.92	0.361	2.21	1.86
	10^4	0.276	3.61	3.32	0.285	3.69	3.25
(3, 1)	10^5	0.342	2.21	1.98	0.346	2.30	1.95
	10^4	0.266	3.68	3.39	0.270	3.80	3.36

In the case of $\Delta \ll \hat{m}_h - \hat{m}_l$ so that $\alpha_+, \alpha_0 \ll 1$. The Z coupling of $F^0_{lL/R}$ is $\sim g_{ZF^0_{lL/R}} + g_{ZF^0_{hL/R}}(\frac{1}{2}\alpha_0)^2$. We assume that $(\frac{1}{2}\alpha_0)^2 \ll |g_{ZF^0_{lL}}/g_{F^0_{hL}}|, |g_{ZF^0_{lR}}/g_{ZF^0_{hR}}|$ so that the value of $g_{ZF^0_{lL/R}}$ is almost equal to the value in the degenerate case. However by this coupling, F^0_{hL} decays sufficiently fast.

By the above setup, the heavy dark fermion can decays to the light dark fermion and only the lightest $F_i^{0(1)}$ becomes the DM. In the following, the relic density of the lightest dark fermion is evaluated. The n_F dark fermions (F_i^+, F_i^0) $(i = 1, \cdots, n_F)$ are divided to $n_F^{\rm light}$ light fermions (F_l^+, F_l^0) with c_{F_h} and $n_F^{\rm heavy}$ heavy fermions (F_h^+, F_h^0) with c_{F_h}. The mass parameters c_{F_l} and c_{F_h} are chosen so as to retain the values of θ_H and m_H unchanged. In Table. 8, the values of c_{F_l}, $\Delta c_F \equiv c_{F_l} - c_{F_h}$ and the corresponding fermion masses are tabulated.

For $m_{F_h} - m_{F_l} = O(100)$ GeV, the heavy dark fermions decay or annihilate sufficiently fast. Thus the Boltzmann equation of the light dark fermion is given by

$$\begin{aligned} \frac{dn}{dt} &= -3Hn\langle\sigma^{\rm ND}_{\rm eff}v\rangle(n^2 - n_{\rm eq}^2), \\ \sigma^{\rm ND}_{\rm eff}v &= \frac{1}{8n_F^{\rm light}}\left[\sigma_{l0}v + \sigma_{l+}v\right], \end{aligned} \tag{4.20}$$

where σ_{l0} and σ_{l+} are the cross section of $F^0_{l,i}\bar{F}^0_{l,i}$, $F^+_{l,i}\bar{F}^+_{l,i}$ annihilations, respectively.

In Fig. 20 the relic density of the dark fermion is plotted for $\Delta c_F = 0.04$ and 0.06 in the case of $n_F = 4$ with $(n_F^{\rm light}, n_F^{\rm heavy}) = (1, 3)$. For $\Delta c_F < 0.04$, the approximated formula (4.20) is not valid because the mass difference $m_{F_h} - m_{F_l}$ is not large enough and the relic-density can be larger than those for $\Delta c_F \gtrsim 0.04$. By inter- and extra-polating the $\Omega_{\rm DM}h^2$ with respect to Δc_F and z_L, the parameter region $(\Delta c_F, z_L)$ allowed by

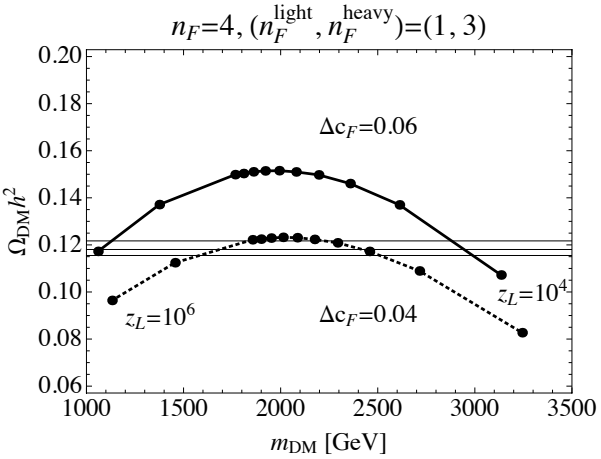

Figure 20: Relic density of the dark fermion for $(n_F^{\rm light}, n_F^{\rm heavy}) = (1, 3)$. The solid and dotted lines represent $\Delta c_F \equiv c_{F_l} - c_{F_h} = 0.06$ and 0.04, respectively. Data points are, from right to left, $z_L = 10^4$ to 10^5 with a step of 10^4, 3×10^5 and 10^6. Horizontal lines around $\Omega_{\rm DM}h^2 \sim 0.12$ represent the observed 68% CL limit of the relic density of the cold DM. Reprinted from Ref. [28].

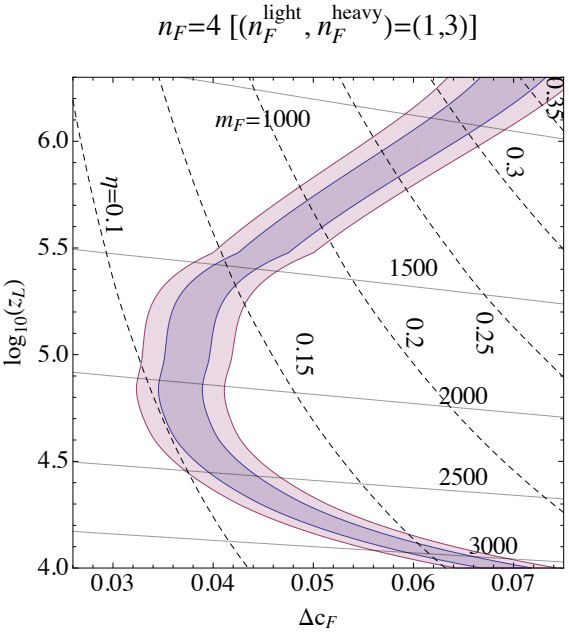

Figure 21: Parameter region $(\Delta c_F, z_L)$ allowed by the limits of the relic density. The purple and light purple regions represent the allowed regions by the 68% CL limit and twice of the 68% CL limit $\Omega_{\rm DM}h^2 \subset [0.1186 \pm 2 \times 0.0031]$, respectively. Mass of the light dark fermion m_{F_l} and a mass ratio $\eta \equiv (m_{F_h} - m_{F_l})/m_{F_l}$ are also shown as solid and dashed lines, respectively. Reprinted from Ref. [28].

the experimental limit on the current relic density is plotted in Fig. 21. It is seen that the observed current relic density is obtained when $10^4 \lesssim z_L \lesssim 10^6$ in the range $0.04 \lesssim \Delta c_F \lesssim 0.07$ where $0.07 \lesssim \theta_H \lesssim 0.17$ and $1000 \lesssim m_{F_l} \lesssim 3100$ GeV. For $n_F = 5, 6$ and $n_F = 4$ with $(n_F^{\rm light}, n_F^{\rm heavy}) = (2,2)$, $(3,1)$, we find no parameter region which explains the current DM density.

4.2. Direct detection

In this subsection, the elastic scattering of the neutral dark fermion off a nucleus is calculated [45]. The dominant and subdominant processes are shown in Fig. 22. The dominant process of the F^0-nucleus scattering is the Z boson exchange. The subdominant processes are the processes of $Z_R^{(1)}$ and Higgs exchange. Contributions from other processes are negligible. The Z-F^0 coupling is very small because the F^0 is almost $SU(2)_R$ component. The $Z_R^{(n)}$-F^0 coupling is large, but $Z_R^{(n)}$ is heavy. The H-F^0 coupling is small. Therefore the elastic scattering cross section is small.

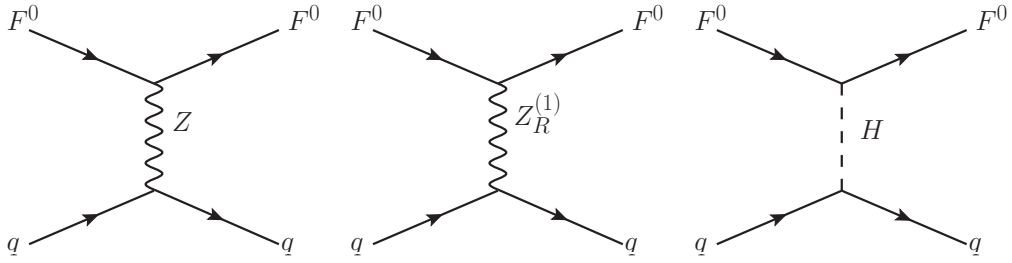

Figure 22: Dominant and subdominant processes of the F^0 scattering off the nucleus with large atomic numbers. Reprinted from Ref. [28].

In the scattering of F^0 on nuclei with large mass number A, the spin-independent scattering is dominant. Therefore pseudo-scalar and axial-vector coupling are neglected and the effective Lagrangian at low energies is given by

$$\mathcal{L}_{\rm int} \simeq \sum_q \left\{ -\left(\frac{g_w^2 v_{Zq} v_{ZF}}{m_Z^2 \cos^2\theta_W} + \frac{g_w^2 v_{Z_R^{(1)}q} v_{Z_R^{(1)}F}}{m_{Z_R^{(1)}}^2} \right) \bar{q}\gamma^0 q \ \bar{F^0}\gamma_0 F^0 + \frac{y_q y_F}{m_H^2} \bar{q} q \bar{F^0} F^0 \right\}, \quad (4.21)$$

where v_{Zq} and v_{ZF} are g^V_{Zqq} and $g^V_{ZF^{0(1)}F^{0(1)}}$ in the unit of $g_w/\cos\theta_W$, and $v_{Z_R^{(1)}q}$ and $v_{Z_R^{(1)}F}$ are $g^V_{Z_R^{(1)}qq}$ and $g^V_{Z_R^{(1)}F^{0(1)}F^{0(1)}}$ in the unit of g_w.

In the GHU model, quark couplings satisfy $v_{Zq}|_{\rm GHU} \simeq v_{Zq}|_{\rm SM}$ and

$$y_q|_{\rm GHU} \simeq y_q|_{\rm SM} \cos\theta_H = \frac{g_w}{2m_W} m_q \cos\theta_H, \quad (4.22)$$

to good accuracy. The contributions of the Higgs exchange process is evaluated by using

the nucleon matrix element

$$\langle N|m_q\bar{q}q|N\rangle = m_N f_{Tq}^{(N)}, \tag{4.23}$$

where $N = p, n$. For the heavy quarks ($Q = c,\ b,\ t$) one has

$$f_{TQ}^{(N)} = \frac{2}{27}\left(1 - \sum_{q=u,d,s} f_{Tq}^{(N)}\right). \tag{4.24}$$

Therefore, by dropping the small momentum dependence of the form factor, the spin-independent cross section of the F^0-nucleus elastic scattering becomes

$$\begin{aligned}\sigma_0 &\equiv \int_0^{4M_r^2 v^2} \left.\frac{d\sigma}{d|\mathbf{q}|^2}\right|_{|\mathbf{q}|=0} d|\mathbf{q}|^2 \\ &= \frac{M_r^2}{\pi}\Big\{Z\,(b_p + f_p) + (A - Z)\,(b_n + f_n)\Big\}^2,\end{aligned} \tag{4.25}$$

where M_r is the F^0-nucleus reduced mass and Z (A) is the atomic (mass) number of the nucleus. $|\mathbf{q}|$ is the momentum transfer and

$$\begin{aligned}&b_p = 2b_u + b_d\ ,\quad b_n = b_u + 2b_d\ , \\ &b_q = -4\sqrt{2}G_F\left(v_{Zq}v_{ZF} + \frac{m_W^2}{m_{Z_R^{(1)}}^2} v_{Z_R^{(1)}q} v_{Z_R^{(1)}F}\right)\ , \\ &f_N = \frac{y_F}{m_H^2}\sum_q \langle N|y_q\bar{q}q|N\rangle = \frac{y_F}{m_H^2}\frac{g_w m_N}{2m_W}\cos\theta_H\left(\frac{2}{9} + \frac{7}{9}\sum_{q=u,d,s} f_{Tq}^{(N)}\right)\ .\end{aligned} \tag{4.26}$$

The spin-independent cross section of the F^0-nucleon elastic scattering σ_N can be written as

$$\sigma_N \equiv \frac{1}{A^2}\frac{m_r^2}{M_r^2}\sigma_0\ , \tag{4.27}$$

where m_r is the F^0-nucleon reduced mass.

The F^0-nucleon cross sections σ_N are shown in Table 9, 10 and Figure 23. In the numerical evaluation, we have employed the values given by [41]

$$\begin{aligned}&f_{Tu}^{(p)} = 0.020\ ,\quad f_{Td}^{(p)} = 0.026\ ,\quad f_{Ts}^{(p)} = 0.118\ , \\ &f_{Tu}^{(n)} = 0.014\ ,\quad f_{Td}^{(n)} = 0.036\ ,\quad f_{Ts}^{(n)} = 0.118\ .\end{aligned} \tag{4.28}$$

Because the dominant process is the Z boson exchange process, the uncertainty of the nucleon matrix element are negligible.

Table 9: F^0 mass m_F and the spin-independent cross section σ_N of the F^0-nucleon scattering for $n_F = 4, 5, 6$ degenerate dark fermions. Reprinted from Ref. [28].

$n_F = 4$

z_L	θ_H	m_F (TeV)	σ_N (cm^2)
10^5	0.115	2.03	5.33×10^{-44}
5×10^4	0.101	2.36	3.78×10^{-44}
3×10^4	0.092	2.66	2.99×10^{-44}
2×10^4	0.085	2.92	2.53×10^{-44}
10^4	0.074	3.46	2.03×10^{-44}

$n_F = 5$

z_L	θ_H	m_F (TeV)	σ_N (cm^2)
10^5	0.114	1.75	3.67×10^{-44}
10^4	0.073	2.91	1.01×10^{-44}

$n_F = 6$

z_L	θ_H	m_F (TeV)	σ_N (cm^2)
10^5	0.113	1.57	2.96×10^{-44}
10^4	0.072	2.56	0.72×10^{-44}

Table 10: m_{F_l}, $m_{Z_R^{(1)}}$, the couplings of F_l^0 and the spin-independent cross section σ_N of the F_l^0-nucleon scattering for $n_F = 4$ and $(n_F^{\text{light}}, n_F^{\text{heavy}}) = (1, 3)$. Reprinted from Ref. [28].

$\Delta c_F = 0.04$

z_L	θ_H	m_{F_l} (TeV)	$m_{Z_R^{(1)}}$ (TeV)	v_{ZF}	$v_{Z_R^{(1)}u}$	$v_{Z_R^{(1)}d}$	$v_{Z_R^{(1)}F}$	y_F	σ_N (cm^2)
4×10^4	0.097	2.29	6.47	-0.00108	0.474	-0.237	1.11	-0.0299	2.69×10^{-44}
3×10^4	0.092	2.46	6.74	-0.00100	0.469	-0.234	1.11	-0.0293	2.35×10^{-44}
2×10^4	0.085	2.72	7.15	-0.00092	0.461	-0.231	1.10	-0.0286	1.96×10^{-44}
10^4	0.074	3.24	7.92	-0.00081	0.450	-0.225	1.08	-0.0280	1.53×10^{-44}

$\Delta c_F = 0.06$

z_L	θ_H	m_{F_l} (TeV)	$m_{Z_R^{(1)}}$ (TeV)	v_{ZF}	$v_{Z_R^{(1)}u}$	$v_{Z_R^{(1)}d}$	$v_{Z_R^{(1)}F}$	y_F	σ_N (cm^2)
2×10^4	0.085	2.61	7.15	-0.00086	0.461	-0.231	1.09	-0.0266	1.76×10^{-44}
10^4	0.074	3.13	7.92	-0.00075	0.450	-0.225	1.07	-0.0261	1.35×10^{-44}

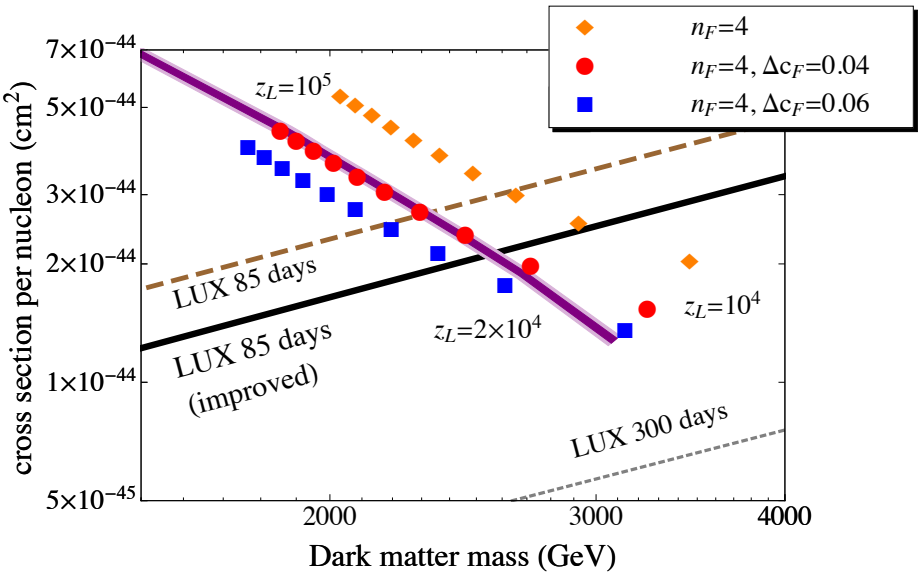

Figure 23: The spin-independent cross section of the F^0-nucleon elastic scattering for $10^4 \leq z_L \leq 10^5$. The orange diamonds represent the $n_F = 4$ cases of degenerate dark fermions with a step of 10^4 in z_L. Red circles and blue squares represent the cases of non-degenerate dark fermions $(n_F^{\rm light}, n_F^{\rm heavy}) = (1, 3)$ with $\Delta c_F = 0.04$ and 0.06, respectively. The brown dashed and black solid line are the 90% confidence limits set by the first result of the LUX experiment [9] and the improved result of the LUX experiment [10]. The purple and light purple bands represent the regions allowed by the limit of the relic density of DM at the 68 % CL depicted in Fig. 21 and by twice of that. The allowed region of the dark fermion mass is $2.6 < m_{F_l} < 3.1$ TeV.

As seen in the previous section, when all dark fermions are degenerate, there are no parameter regions which realise the observed relic density of the DM. When $n_F^{\rm light}$ light dark fermions and $n_F^{\rm heavy}$ heavy dark fermions are introduced, the parameter set of $(n_F^{\rm light}, n_F^{\rm heavy}) = (1, 3)$, the region $0.04 < \Delta c_F < 0.07$, $z_L < 10^6$ are allowed to explain the relic density as shown in Fig. 21. The spin-independent cross section for the F^0-nucleon elastic scattering for the allowed region is shown in Fig. 23. The purple and light purple bands there represent the regions allowed by the limit of the relic abundance of DM at the 68 % CL and by twice of that, respectively. The result is that the allowed region by the direct detection experiments of LUX [10] is $2.6 \lesssim m_{F_l} < 3.1$ TeV. The corresponding the value of the warp factor and the Wilson line phase are $10^4 < z_L \lesssim 2 \times 10^4$ and $0.07 < \theta_H \lesssim 0.09$. The mass of Z' is from $7.4 \lesssim m_{Z'} < 8.5$ TeV. In the allowed region, the value spin-independent cross section is larger than the expected limit by the 300-day run of the LUX experiment.

5. Summary and discussion

In this paper, the phenomenological study of the $SO(5) \times U(1)$ gauge-Higgs unification is summarised. In Ref. [26], the unstable Higgs boson with mass 126 GeV was realised by introducing the $SO(5)$-spinor representation fermion, named the dark fermion.

In Ref. [27], the universality of the parameters and the Z' signals at the LHC are studied. The universality is that the $m_{Z^{(1)}}$, $m_{Z_R^{(1)}}$, $m_{\gamma^{(1)}}$, $m_{\rm KK}$, the Higgs cubic coupling λ_3 and quartic couplings λ_4 are almost independent of the number of the dark fermion, n_F and determined only by the θ_H. The Z' in this model are $Z^{(1)}$, $Z_R^{(1)}$ and $\gamma^{(1)}$. Their decay rates are large, especially $\Gamma_{\gamma^{(1)}}$ is almost 1 TeV for $\theta_H = 0.073$. Because of the large decay width, the wide peaks are predicted in the dilepton events. By the 8 TeV LHC result, the Z' mass must be larger than 4 TeV and it might be detected by the 14 TeV LHC. By the universality, the constraint $m_{Z'} > 4$ TeV corresponds to $\theta_H < 0.17$. Once $m_{Z'}$ is determined, λ_3 and λ_4 is predicted. Therefore this model is predictive because of the universality.

One of the main topic of this thesis is the Higgs boson decay. The decay rate $\Gamma(H \to \gamma\gamma)$ and the production cross section $\sigma(gg \to H)$ calculated in Ref. [26]. The processes $gg \to H$ and $H \to \gamma\gamma$ do not occur at the tree level but occur at the one-loop level. Therefore an infinite number of the KK modes contribute to the processes, thus $\Gamma(H \to \gamma\gamma)$ and $\sigma(gg \to H)$ deviate from the SM value. However, the Higgs couplings to the KK W, KK top and the dark fermions depend on their KK numbers and their signs change alternatively for n. The summations of the each KK contribution finite and are negligible. Thus the whole amplitudes are approximately suppressed from the SM values by $\cos\theta_H$ which comes from the suppression of the Higgs coupling to the zero modes. In Ref. [29], the decay rate $\Gamma(H \to Z\gamma)$ is calculated. The decay also occurs at the one-loop level. In addition, the KK numbers can be changed by the interaction to the Higgs boson and the Z boson. Therefore the KK numbers in the loop might not be conserved and the decay rate seems to be even divergent. However, by summing all of the KK mode contributions, the summations of the KK mode contributions become alternative sums of the KK number n. The whole amplitude are are found to be convergent and the KK mode contributions are negligible. Again the amplitude is suppressed from the SM values by $\cos\theta_H$. Therefore the branching ratios of the Higgs boson decay are consistent with the SM. and the signal strengths of each decay mode are suppressed from the SM values by $\cos^2\theta_H$. Numerically, the deviation of the signal strength from the SM value is $O(1)\%$ for $\theta_H < 0.17$. It should be emphasised that an infinite numbers on the KK modes contribute to the processes in these decay processes, nevertheless, the non-trivial cancellations between the KK mode contributions occur and the infinite sums of the KK mode contributions are finite. These cancellations do not occur in the other models. Therefore these cancellations are remarkable feature of this model and thought to be a consequence of the gauge symmetry.

One of the other main topics of this thesis is the dark matter (DM). In Ref. [28], the possibility of the dark fermion as a DM is discussed. The dark fermions do not have the zero mode from the boundary condition and the lowest modes couple to the $SU(2)_L$ very weakly. The fermion number of the dark fermions is conserved and the neutral one is stable. Thus the neutral dark fermion is a candidate of the DM. The the charged and neutral dark fermion annihilate through $Z_R^{(1)}$ and $\gamma^{(1)}$, respectively and finally the charged one decays to the neutral one. The relic density of the dark fermion does not matches to the observed relic abundance of the DM for the degenerate case. In the $n_F = 3$ case, too little relic density is predicted and in the $n_F = 4, 5$ and 6 case the relic density is larger than the observed relic abundance. Therefore the non-degenerate dark fermions are considered. The heavy and light dark fermion is introduced and the mixing term of the heavy and light dark fermions are added in the Lagrangian. The heavy dark fermions finally decay to the light dark fermions. In the $(n_F^{\text{light}}, n_F^{\text{heavy}}) = (1, 3)$ case, the solution was found in which their relic density matches to the relic abundance of the DM. The constraint from the direct detection experiments are also considered. The elastic scattering cross section off a nucleon of the lowest dark fermion is suppressed because of the small $SU(2)_L$ coupling. The allowed region of the dark fermion mass from both the relic density and the direct detection is $2.6 < m_{F_l} < 3.1$ TeV with $(n_F^{\text{light}}, n_F^{\text{heavy}}) = (1, 3)$. In the range, the elastic scattering cross section is larger than the expected upper limit of the cross section by the 300-days run of the LUX experiment.

As shown in this thesis, the $SO(5) \times U(1)$ GHU solves the fine-tuning problem of the Higgs boson mass and explains the existence of the DM. Therefore the $SO(5) \times U(1)$ GHU is phenomenologically viable. This model is consistent with the 8 TeV LHC result and the LUX 85 live-days result. The most severe constraint for the parameter comes from the study of the DM. The allowed region of the dark matter mass is $2.6 < m_{F_l} < 3.1$ TeV, where the warp factor and the Wilson line phase are $10^4 < z_L \lesssim 2 \times 10^4$ and $0.07 < \theta_H \lesssim 0.09$. In this region, the scenario of the dark fermion as a dark matter is testable by the LUX 300-days run and the Z' mass is from 7.4 TeV to 8.5 TeV and the wide peak is predicted for the 14 TeV LHC in dilepton events. Considering the Higgs boson, the deviations of the Higgs boson couplings to the SM particle and the Higgs boson cubic coupling from the SM values are $O(1)\%$. These couplings will be measured precisely by the International Linear Collider (ILC) in the future.

The Z' signal has predicted in this model. Besides other signals such as the W' signal have to be predicted. Especially, the H-W-$W^{(1)}$ and H-Z-$Z^{(1)}$ couplings are found to be $O(1)$ times larger than the H-W-W and H-Z-Z couplings, respectively. These properties might be important to distinguish this model from the other models in the experimental viewpoint. Therefore, the predictions of this model for the LHC will be done for several events. In addition to the phenomenological studies of the gauge-Higgs unification, the theoretical studies of the gauge-Higgs unification are also important topics. There are other candidates of the dimensions, metrics, boundary conditions and gauge groups. Especially, the gauge-Higgs grand unification [46, 47] is proposed. The

three forces and the Higgs boson are unified into the one gauge group in the model. The Hosotani mechanism, the key of the symmetry breaking in gauge-Higgs unification, is studied nonperturbatively on the lattice [48]. A dynamical determination of the boundary conditions are also studied in Ref. [49]. Thus there are many important and interesting topics around the gauge-Higgs unification.

Acknowlegements

I am very grateful to my supervisor, Professor Yutaka Hosotani for his kind directions and advices. I am also grateful to my collaborators, Hisaki Hatanaka, Yuta Orikasa and Takuya Shimotani. In the study of the dark fermion as a dark matter, Assistant Professor Mitsuru Kakizaki in Toyama University and Assistant Professor Minoru Tanaka in Osaka University gave us many important comments. I appreciate these comments very much. I also thank to all of the members of the Particle Physics Theory Group, Osaka university.

A. $SO(5)$ algebra and generators

The algebra of $SO(5)$ is summarised below.

$$
\begin{aligned}
&[T^{a_L}, T^{b_L}] = i\epsilon^{abc}T^{c_L},\ [T^{a_R}, T^{b_R}] = i\epsilon^{abc}T^{c_R},\ [T^{a_L}, T^{b_R}] = 0,\\
&[T^{a_L}, T^{\hat{b}}] = \frac{i}{2}\delta^{ab} + i\epsilon^{abc}T^{\hat{c}},\ [T^{a_R}, T^{\hat{b}}] = -\frac{i}{2}\delta^{ab} + i\epsilon^{abc}T^{\hat{c}},\\
&[T^{\hat{a}}, T^{\hat{b}}] = \frac{i}{2}\epsilon^{abc}(T^{c_L} + T^{c_R}),\\
&[T^{a_L}, T^{\hat{4}}] = -\frac{i}{2}T^{\hat{a}},\ [T^{a_R}, T^{\hat{4}}] = \frac{i}{2}T^{\hat{a}},\ [T^{\hat{a}}, T^{\hat{4}}] = \frac{i}{2}(T^{a_L} - T^{a_R}),
\end{aligned}
\tag{A.1}
$$

where $a = 1, 2, 3$.

The $SO(5)$ generators in the vector representation can be written below.

$$
T^{1_L} = \frac{1}{2}\begin{pmatrix} & & & & -i \\ & & & -i & \\ & & i & & \\ & i & & & \\ i & & & & \end{pmatrix},\ T^{2_L} = \frac{1}{2}\begin{pmatrix} & & i & & \\ & & & & -i \\ & & & & \\ -i & & & & \\ & & i & & \end{pmatrix},\ T^{3_L} = \frac{1}{2}\begin{pmatrix} & -i & & & \\ i & & & & \\ & & & & -i \\ & & & i & \\ & & & & \end{pmatrix},
$$

$$
T^{1_R} = \frac{1}{2}\begin{pmatrix} & & & & i \\ & & & -i & \\ & & i & & \\ & i & & & \\ -i & & & & \end{pmatrix},\ T^{2_R} = \frac{1}{2}\begin{pmatrix} & & & i & \\ & & & & i \\ & & & & \\ -i & & & & \\ & & -i & & \end{pmatrix},\ T^{3_R} = \frac{1}{2}\begin{pmatrix} & -i & & & \\ i & & & & \\ & & & & i \\ & & & -i & \\ & & & & \end{pmatrix},
$$

$$
T^{\hat{1}} = \frac{1}{\sqrt{2}}\begin{pmatrix} & & & & -i \\ & & & & \\ & & & & \\ & & & & \\ i & & & & \end{pmatrix},\ T^{\hat{2}} = \frac{1}{\sqrt{2}}\begin{pmatrix} & & & & \\ & & & & -i \\ & & & & \\ & & & & \\ & i & & & \end{pmatrix},\ T^{\hat{3}} = \frac{1}{\sqrt{2}}\begin{pmatrix} & & & & \\ & & & & \\ & & & & -i \\ & & & & \\ & & i & & \end{pmatrix},
$$

$$
T^{\hat{4}} = \frac{1}{\sqrt{2}}\begin{pmatrix} & & & & \\ & & & & \\ & & & & \\ & & & & -i \\ & & & i & \end{pmatrix}.
\tag{A.2}
$$

The $SO(5)$ generators in the spinor representation can be written below.

$$
T^{a_L} = \frac{1}{2}\begin{pmatrix} \sigma_a & \\ & \end{pmatrix},\ T^{a_R} = \frac{1}{2}\begin{pmatrix} & \\ & \sigma_a \end{pmatrix},\ T^{\hat{a}} = \frac{1}{2\sqrt{2}}\begin{pmatrix} & i\sigma_a \\ -i\sigma_a & \end{pmatrix},\ T^{\hat{4}} = \frac{1}{2\sqrt{2}}\begin{pmatrix} & I \\ I & \end{pmatrix}.
\tag{A.3}
$$

B. Couplings

In the following, the numerical values of couplings are calculated for

$$z_L = 10^5, \theta_H = 0.1153, k = 2.357 \times 10^8 \text{ GeV}, c_t = 0.2270, c_F = 0.3321, \tag{B.1}$$

when there are nothing mentioned.

B.1. γWW, ZWW and $Z_R WW$ couplings

The $Z^{(l)}W^{(m)}W^{(n)}$ coupling is contained in

$$\begin{aligned}
&\int_1^{z_L} \frac{dz}{kz} \left(-\frac{1}{4}\right) \mathrm{Tr}\left[F_{\mu\nu}F_{\rho\sigma}\right] \eta^{\mu\rho}\eta^{\nu\sigma} \\
&\supset ig_A \int_1^{z_L} \frac{dz}{kz} \mathrm{Tr}\Big[(\partial_\mu \hat{Z}_\nu - \partial_\nu \hat{Z}_\mu)[\hat{W}^+_\rho, \hat{W}^-_\sigma] \\
&\qquad + (\partial_\mu \hat{W}^-_\nu - \partial_\nu \hat{W}^-_\mu)[\hat{Z}_\rho, \hat{W}^+_\sigma] + (\partial_\mu \hat{W}^+_\nu - \partial_\nu \hat{W}^+_\mu)[\hat{Z}_\rho, \hat{W}^-_\sigma]\Big] \eta^{\mu\rho}\eta^{\nu\sigma} \\
&\supset i \sum_{m,n} g_{Z^{(l)}W^{(m)}W^{(n)}} \eta^{\mu\rho}\eta^{\nu\sigma} \Big\{ (\partial_\mu Z^{(l)}_\nu - \partial_\nu Z^{(l)}_\mu) W^{+(m)}_\rho W^{-(n)}_\sigma \\
&- (\partial_\mu W^{+(m)}_\nu - \partial_\nu W^{+(m)}_\mu) Z^{(l)}_\rho W^{-(n)}_\sigma + (\partial_\mu W^{-(n)}_\nu - \partial_\nu W^{-(n)}_\mu) Z^{(l)}_\rho W^{+(m)}_\sigma \Big\}
\end{aligned} \tag{B.2}$$

so that one finds that

$$\begin{aligned}
&g_{Z^{(l)}W^{(m)}W^{(n)}} = g_w \sqrt{L} \int_1^{z_L} \frac{dz}{kz} \\
&\times \Big\{ h^L_{Z^{(l)}} \left(h^L_{W^{(m)}} h^L_{W^{(n)}} + \frac{\hat{h}_{W^{(m)}} \hat{h}_{W^{(n)}}}{2} \right) + h^R_{Z^{(l)}} \left(h^R_{W^{(m)}} h^R_{W^{(n)}} + \frac{\hat{h}_{W^{(m)}} \hat{h}_{W^{(n)}}}{2} \right) \\
&\quad + \hat{h}_{Z^{(l)}} \left(\frac{h^L_{W^{(m)}} \hat{h}_{W^{(n)}} + h^R_{W^{(m)}} \hat{h}_{W^{(n)}} + \hat{h}_{W^{(m)}} h^L_{W^{(n)}} + \hat{h}_{W^{(m)}} h^R_{W^{(n)}}}{2} \right) \Big\}.
\end{aligned} \tag{B.3}$$

Here $C_{W^{(m)}} = C(z; \lambda_{W^{(m)}})$ etc. Numerical values of $g_{ZW^{(m)}W^{(n)}}$ are given in Table 11.

Similarly, the $\gamma^{(l)}W^{(m)}W^{(n)}$ coupling is

$$\begin{aligned}
&g_{\gamma^{(l)}W^{(m)}W^{(n)}} = g_w \sqrt{L} \int_1^{z_L} \frac{dz}{kz} \\
&\times \Big\{ h^L_{\gamma^{(l)}} \left(h^L_{W^{(m)}} h^L_{W^{(n)}} + \frac{\hat{h}_{W^{(m)}} \hat{h}_{W^{(n)}}}{2} \right) + h^R_{\gamma^{(l)}} \left(h^R_{W^{(m)}} h^R_{W^{(n)}} + \frac{\hat{h}_{W^{(m)}} \hat{h}_{W^{(n)}}}{2} \right) .
\end{aligned} \tag{B.4}$$

Especially, $g_{\gamma^{(0)}W^{(m)}W^{(n)}}$ is $g_{\gamma^{(0)}W^{(m)}W^{(n)}} = e\ \delta^{mn}$.

The $Z^{(l)}_R W^{(m)}W^{(n)}$ coupling is obtained from (B.4) by replacing $\gamma^{(l)}$ to $Z^{(l)}_R$. Numerical values of $g_{ZW^{(m)}W^{(n)}}$, $g_{Z^{(1)}W^{(m)}W^{(n)}}$, $g_{Z^{(1)}_R W^{(m)}W^{(n)}}$ and $g_{\gamma^{(1)}W^{(m)}W^{(n)}}$ for various θ_H are given in Table 12.

Table 11: $g_{ZW^{(m)}W^{(n)}}/g_w \cos\theta_W$. Only the value larger than $O(10^{-3})$ are shown and written by three significant figures. Reprinted from Ref. [29].

	0	1	2	3	4	5	6	7
0	1.	$O(10^{-4})$	$O(10^{-7})$	$O(10^{-5})$	$O(10^{-7})$	$O(10^{-6})$	$O(10^{-8})$	$O(10^{-6})$
1	$O(10^{-4})$	0.996	0.032	$O(10^{-5})$	$O(10^{-4})$	$O(10^{-6})$	$O(10^{-5})$	$O(10^{-6})$
2	$O(10^{-7})$	0.032	0.350	-0.022	$O(10^{-7})$	$O(10^{-4})$	$O(10^{-6})$	$O(10^{-4})$
3	$O(10^{-5})$	$O(10^{-5})$	-0.022	0.996	0.032	$O(10^{-5})$	$O(10^{-4})$	$O(10^{-6})$
4	$O(10^{-7})$	$O(10^{-4})$	$O(10^{-7})$	0.032	0.350	-0.023	$O(10^{-5})$	$O(10^{-4})$
5	$O(10^{-6})$	$O(10^{-6})$	$O(10^{-4})$	$O(10^{-5})$	-0.023	0.996	0.032	$O(10^{-5})$
6	$O(10^{-8})$	$O(10^{-5})$	$O(10^{-6})$	$O(10^{-4})$	$O(10^{-5})$	0.032	0.350	-0.023
7	$O(10^{-6})$	$O(10^{-6})$	$O(10^{-4})$	$O(10^{-6})$	$O(10^{-4})$	$O(10^{-5})$	-0.023	0.996

Table 12: Triple vector-boson couplings VW^+W^- with $V = Z, Z^{(1)}, Z_R^{(1)}$ in unit of g_w and $\gamma^{(1)}W^+W^-$ in unit of the electric charge e for various θ_H.

θ_H	g_{ZWW}	$g_{Z^{(1)}WW}$	$g_{Z_R^{(1)}WW}$	$g_{\gamma^{(1)}WW}$
0.3548	0.811	1.506×10^{-2}	0.391×10^{-2}	-0.417×10^{-2}
0.1742	0.861	0.459×10^{-2}	0.114×10^{-2}	-0.115×10^{-2}
0.1153	0.870	0.225×10^{-2}	0.055×10^{-2}	-0.054×10^{-2}
0.0737	0.874	0.105×10^{-2}	0.025×10^{-2}	-0.024×10^{-2}

B.2. $\gamma\gamma WW$ and γZWW couplings

$\gamma Z^{(l)}W^{(m)}W^{(n)}$ coupling is contained in

$$
\begin{aligned}
&(g_A)^2 \int_1^{z_L} \frac{dz}{kz} \mathrm{Tr}\Big[[\hat{A}_\mu^{\gamma(A)}, \hat{W}_\nu^+] \left([\hat{Z}_\rho^{(l)}, \hat{W}_\sigma^-] - [\hat{Z}_\sigma^{(l)}, \hat{W}_\rho^-] \right) \\
&\qquad + [\hat{A}_\mu^{\gamma(A)}, \hat{W}_\nu^-] \left([\hat{Z}_\rho^{(l)}, \hat{W}_\sigma^+] - [\hat{Z}_\sigma^{(l)}, \hat{W}_\rho^+] \right) \Big] \eta^{\mu\rho}\eta^{\nu\sigma} \\
&\supset \sum_{l,m,n} g_{\gamma Z^{(l)}W^{(m)}W^{(n)}} \eta^{\mu\rho}\eta^{\nu\sigma} \\
&\times \{ A_\mu^\gamma W_\nu^{+(m)} (Z_\rho^{(l)} W_\sigma^{-(n)} - Z_\sigma^{(l)} W_\rho^{-(n)}) + A_\mu^\gamma W_\nu^{-(n)} (Z_\rho^{(l)} W_\sigma^{+(m)} - Z_\sigma^{(l)} W_\rho^{+(m)}) \}
\end{aligned}
\tag{B.5}
$$

so that

$$
\begin{aligned}
&g_{\gamma Z^{(l)}W^{(m)}W^{(n)}} = -g_w^2 L \int_1^{z_L} \frac{dz}{kz} \\
&\times \left\{ h_\gamma^L h_{W^{(m)}}^L \left(h_{Z^{(l)}}^L h_{W^{(n)}}^L + \frac{\hat{h}_{Z^{(l)}} \hat{h}_{W^{(n)}}}{2} \right) + h_\gamma^R h_{W^{(m)}}^R \left(h_{Z^{(l)}}^R h_{W^{(n)}}^R + \frac{\hat{h}_{Z^{(l)}} \hat{h}_{W^{(n)}}}{2} \right) \right. \\
&\quad \left. + \frac{h_\gamma^L + h_\gamma^R}{2} \hat{h}_{W^{(m)}} \left(\frac{h_{Z^{(l)}}^L \hat{h}_{W^{(n)}} + h_{Z^{(l)}}^R \hat{h}_{W^{(n)}} + \hat{h}_{Z^{(l)}} h_{W^{(n)}}^L + \hat{h}_{Z^{(l)}} h_{W^{(n)}}^R}{2} \right) \right\} \\
&= -e g_{Z^{(l)}W^{(m)}W^{(n)}} \ .
\end{aligned}
\tag{B.6}
$$

The relation $g_{\gamma Z^{(l)}W^{(m)}W^{(n)}} = -eg_{Z^{(l)}W^{(m)}W^{(n)}}$ follows from the gauge invariance as well.

Similarly, the $\gamma^{(0)}\gamma^{(0)}W^{(m)}W^{(n)}$ coupling is

$$\begin{aligned} g_{\gamma^{(0)}\gamma^{(0)}W^{(m)}W^{(n)}} &= -g_w^2 L \int_1^{z_L} \frac{dz}{kz} \\ &\times \left\{ \left(h_\gamma^L\right)^2 h_{W^{(m)}}^L h_{W^{(n)}}^L + \left(h_\gamma^R\right)^2 h_{W^{(m)}}^R h_{W^{(n)}}^R + \left(\frac{h_\gamma^L + h_\gamma^R}{2}\right)^2 \hat{h}_{W^{(m)}} \hat{h}_{W^{(n)}} \right\} \\ &= -e^2 \delta^{mn} \ . \end{aligned} \tag{B.7}$$

B.3. $ZZWW$ coupling

The $ZZW^{(m)}W^{(n)}$ coupling is contained in

$$\begin{aligned} &(g_A)^2 \int_1^{z_L} \frac{dz}{kz} \mathrm{Tr}\Big[[\hat{Z}_\mu, \hat{W}_\nu^+][\hat{Z}_\rho, \hat{W}_\sigma^-] - [\hat{Z}_\mu, \hat{W}_\nu^+][\hat{Z}_\sigma, \hat{W}_\rho^-] \Big] \eta^{\mu\rho}\eta^{\nu\sigma} \\ &\supset \sum_{m,n} g_{ZZW^{(m)}W^{(n)}} \eta^{\mu\rho}\eta^{\nu\sigma} \Big\{ Z_\mu W_\nu^{+(m)} (Z_\rho W_\sigma^{-(n)} - Z_\sigma W_\rho^{-(n)}) \Big\} \end{aligned} \tag{B.8}$$

so that one finds that

$$\begin{aligned} g_{ZZW^{(m)}W^{(n)}} = -g_w^2 L \int_1^{z_L} \frac{dz}{kz} \times \Bigg\{ & \left(h_Z^L h_{W^{(m)}}^L + \frac{\hat{h}_Z \hat{h}_{W^{(m)}}}{2} \right) \left(h_Z^L h_{W^{(n)}}^L + \frac{\hat{h}_Z \hat{h}_{W^{(n)}}}{2} \right) \\ & + \left(h_Z^R h_{W^{(m)}}^R + \frac{\hat{h}_Z \hat{h}_{W^{(m)}}}{2} \right) \left(h_Z^R h_{W^{(n)}}^R + \frac{\hat{h}_Z \hat{h}_{W^{(n)}}}{2} \right) \\ & + \left(\frac{h_Z^L \hat{h}_{W^{(m)}} + h_Z^R \hat{h}_{W^{(m)}} + \hat{h}_Z h_{W^{(m)}}^L + \hat{h}_Z h_{W^{(m)}}^R}{2} \right) \\ & \times \left(\frac{h_Z^L \hat{h}_{W^{(n)}} + h_Z^R \hat{h}_{W^{(n)}} + \hat{h}_Z h_{W^{(n)}}^L + \hat{h}_Z h_{W^{(n)}}^R}{2} \right) \Bigg\}. \end{aligned} \tag{B.9}$$

Numerical values of $g_{ZZW^{(m)}W^{(n)}}$ are given in Table 13.

B.4. ZWW_R and γZWW_R couplings

The $Z^{(l)}W^{(m)}W_R^{(n)}$ coupling in

$$\begin{aligned} i \sum_{l,m,n} g_{Z^{(l)}W^{(m)}W_R^{(n)}} \eta^{\mu\rho}\eta^{\nu\sigma} \Big\{ & (\partial_\mu Z_\nu^{(l)} - \partial_\nu Z_\mu^{(l)})(W_\rho^{+(m)} W_{R\,\sigma}^{-(n)} + W_\rho^{-(m)} W_{R\,\sigma}^{+(n)}) \\ & + (\partial_\mu W_\nu^{-(m)} - \partial_\nu W_\mu^{-(m)}) Z_\rho^{(l)} W_{R\,\sigma}^{+(n)} - (\partial_\mu W_\nu^{+(m)} - \partial_\nu W_\mu^{+(m)}) Z_\rho^{(l)} W_{R\,\sigma}^{-(n)} \\ & + (\partial_\mu W_{R\,\nu}^{-(n)} - \partial_\nu W_{R\,\mu}^{-(n)}) Z_\rho^{(l)} W_\sigma^{+(m)} - (\partial_\mu W_{R\,\nu}^{+(n)} - \partial_\nu W_{R\,\mu}^{+(n)}) Z_\rho^{(l)} W_\sigma^{-(m)} \Big\} \end{aligned} \tag{B.10}$$

Table 13: $g_{ZZW^{(m)}W^{(n)}}/g_w^2\cos^2\theta_W$. Only the value larger than $O(10^{-3})$ are shown and written by three significant figures.

	0	1	2	3	4	5	6	7
0	1.	-0.001	$O(10^{-5})$	$O(10^{-5})$	$O(10^{-6})$	$O(10^{-6})$	$O(10^{-7})$	$O(10^{-6})$
1	-0.001	0.992	0.042	$O(10^{-4})$	$O(10^{-4})$	$O(10^{-5})$	$O(10^{-5})$	$O(10^{-6})$
2	$O(10^{-5})$	0.042	0.125	-0.030	-0.001	-0.001	$O(10^{-5})$	$O(10^{-4})$
3	$O(10^{-5})$	$O(10^{-4})$	-0.030	0.993	0.043	$O(10^{-4})$	0.001	$O(10^{-5})$
4	$O(10^{-6})$	$O(10^{-4})$	-0.001	0.043	0.126	-0.031	-0.001	-0.001
5	$O(10^{-6})$	$O(10^{-5})$	-0.001	$O(10^{-4})$	-0.031	0.994	0.043	$O(10^{-4})$
6	$O(10^{-7})$	$O(10^{-5})$	$O(10^{-5})$	0.001	-0.001	0.043	0.126	-0.031
7	$O(10^{-6})$	$O(10^{-6})$	$O(10^{-4})$	$O(10^{-5})$	-0.001	$O(10^{-4})$	-0.031	0.994

is given by

$$g_{Z^{(l)}W^{(m)}W_R^{(n)}} = g_w\sqrt{L}\int_1^{z_L}\frac{dz}{kz}\Bigg\{h^L_{Z^{(l)}}h^L_{W^{(m)}}h^L_{W_R^{(n)}} + h^R_{Z^{(l)}}h^R_{W^{(m)}}h^R_{W_R^{(n)}} + \hat{h}_{Z^{(l)}}\hat{h}_{W^{(m)}}\frac{h^L_{W_R^{(n)}}+h^R_{W_R^{(n)}}}{2}\Bigg\}. \tag{B.11}$$

Numerical values of $g_{ZW^{(m)}W_R^{(n)}}$ are given in Table 14.

Table 14: $g_{ZW^{(m)}W_R^{(n)}}/g_w\cos\theta_W$. Only the values larger than $O(10^{-3})$ are shown and written by two significant figures. Reprinted from Ref. [29].

		m							
		0	1	2	3	4	5	6	7
	1	$O(10^{-4})$	0.003	-0.021	$O(10^{-4})$	0.009	$O(10^{-4})$	-0.008	$O(10^{-4})$
n	2	$O(10^{-5})$	$O(10^{-4})$	0.018	0.003	-0.026	$O(10^{-4})$	0.007	$O(10^{-4})$
	3	$O(10^{-6})$	$O(10^{-5})$	0.004	$O(10^{-4})$	0.020	0.004	-0.028	$O(10^{-4})$
	4	$O(10^{-6})$	$O(10^{-5})$	$O(10^{-4})$	$O(10^{-4})$	0.005	$O(10^{-4})$	0.020	0.004

Similarly $\gamma Z^{(l)}W^{(m)}W_R^{(n)}$ coupling is contained in

$$\begin{aligned}
&(g_A)^2\int_1^{z_L}\frac{dz}{kz}\eta^{\mu\rho}\eta^{\nu\sigma}\\
&\times\mathrm{Tr}\Big[[\hat{A}^{\gamma(A)}_\mu,\hat{W}^+_\nu]\left([\hat{Z}_\rho,\hat{W}^-_{R\,\sigma}]-[\hat{Z}_\sigma,\hat{W}^-_{R\,\rho}]\right)+[\hat{A}^{\gamma(A)}_\mu,\hat{W}^-_\nu]\left([\hat{Z}_\rho,\hat{W}^+_{R\,\sigma}]-[\hat{Z}_\sigma,\hat{W}^+_{R\,\rho}]\right)\\
&\qquad[\hat{A}^{\gamma(A)}_\mu,\hat{W}^-_{R\,\nu}]\left([\hat{Z}_\rho,\hat{W}^+_{R\,\sigma}]-[\hat{Z}_\sigma,\hat{W}^+_\rho]\right)+[\hat{A}^{\gamma(A)}_\mu,\hat{W}^-_{R\,\nu}]\left([\hat{Z}_\rho,\hat{W}^+_{R\,\sigma}]-[\hat{Z}_\sigma,\hat{W}^+_\rho]\right)\Big]\\
&\supset\sum_{m,n}g_{\gamma Z^{(l)}W^{(m)}W_R^{(n)}}\eta^{\mu\rho}\eta^{\nu\sigma}\\
&\quad\times\Big\{A^\gamma_\mu W^{+(m)}_\nu(Z^{(l)}_\rho W^{-(n)}_{R\,\sigma}-Z^{(l)}_\sigma W^{-(n)}_{R\,\rho})+A^\gamma_\mu W^{-(n)}_\nu(Z^{(l)}_\rho W^{+(m)}_{R\,\sigma}-Z^{(l)}_\sigma W^{+(m)}_{R\,\rho})\\
&\qquad+A^\gamma_\mu W^{+(m)}_{R\,\nu}(Z^{(l)}_\rho W^{-(n)}_\sigma-Z^{(l)}_\sigma W^{-(n)}_\rho)+A^\gamma_\mu W^{-(n)}_{R\,\nu}(Z^{(l)}_\rho W^{+(m)}_\sigma-Z^{(l)}_\sigma W^{+(m)}_\rho)\Big\}
\end{aligned}\tag{B.12}$$

so that

$$g_{\gamma Z^{(l)}W^{(m)}W_R^{(n)}} = -g_w^2\sqrt{L}\int_1^{z_L}\frac{dz}{kz}\Big\{h^L_{\gamma^{(0)}}h^L_{W^{(m)}}h^L_{Z^{(l)}}h^L_{W_R^{(n)}} + h^R_{\gamma^{(0)}}h^R_{W^{(m)}}h^R_{Z^{(l)}}h^R_{W_R^{(n)}} + \frac{1}{2}\left(h^L_{\gamma^{(0)}}+h^R_{\gamma^{(0)}}\right)\hat{h}_{W^{(m)}}\frac{1}{2}\hat{h}_{Z^{(l)}}\left(h^L_{W_R^{(n)}}+h^R_{W_R^{(n)}}\right)\Big\}$$
$$= -e g_{Z^{(l)}W^{(m)}W_R^{(n)}}. \tag{B.13}$$

The relation $g_{\gamma Z^{(l)}W^{(m)}W_R^{(n)}} = -e g_{Z^{(l)}W^{(m)}W_R^{(n)}}$ follows from the gauge invariance as well.

B.5. $A^{\hat{4}}WW$ coupling

The $A^{\hat{4}(l)}W^{(m)}W^{(n)}$ coupling is

$$g_{A^{\hat{4}(l)}W^{(m)}W^{(n)}} = ig_w\sqrt{L}\int_1^{z_L}\frac{dz}{kz} \times\left\{\hat{h}_{A^{\hat{4}(l)}}\left(\frac{h^L_{W^{(m)}}\hat{h}_{W^{(n)}} - h^R_{W^{(m)}}\hat{h}_{W^{(n)}} - \hat{h}_{W^{(m)}}h^L_{W^{(n)}} + \hat{h}_{W^{(m)}}h^R_{W^{(n)}}}{2}\right)\right\}. \tag{B.14}$$

Therefore the $A^{\hat{4}(l)}W^{(m)}W^{(n)}$ coupling vanishes for $m = n$.

B.6. HWW coupling

The Higgs coupling $HW^{(m)}W^{(n)}$ is contained in the $\mathrm{Tr}F_{\mu z}F^{\mu z}$ term

$$-ig_A k^2\int_1^{z_L}\frac{dz}{kz}\mathrm{Tr}\left[\left(\partial_z\hat{W}^-_\mu\right)\left[\hat{W}^+_\nu,\hat{H}\right]+\left(\partial_z\hat{W}^+_\mu\right)\left[\hat{W}^-_\nu,\hat{H}\right]\right]\eta^{\mu\nu}$$
$$\supset -\sum_{m,n} g_{HW^{(m)}W^{(n)}}HW^{+(m)}_\mu W^{-(n)}_\nu\ \eta^{\mu\nu} \tag{B.15}$$

so that

$$g_{HW^{(m)}W^{(n)}} = -g_A k^2\int_1^{z_L}\frac{dz}{kz}\frac{1}{2}u_H(z) \times\left\{-\left(\partial_z\hat{h}_{W^{(m)}}\right)\left(h^L_{W^{(n)}}-h^R_{W^{(n)}}\right)+\partial_z\left(h^L_{W^{(m)}}-h^R_{W^{(m)}}\right)\hat{h}_{W^{(n)}}+(m\longleftrightarrow n)\right\}\ . \tag{B.16}$$

Numerical values of $g_{HW^{(m)}W^{(n)}}$ are given in Table 15.

Table 15: $g_{HW^{(m)}W^{(n)}}/g_w \cos\theta_H$ in the unit of GeV written by three significant figures. The values smaller than $O(10)$ are abbreviated. Reprinted from Ref. [29].

	0	1	2	3	4	5	6	7
0	80.0	2.55×10^2	$O(1)$	45.4	$O(0.1)$	20.7	$O(0.1)$	10.4
1	2.55	-3.50×10^2	1.39×10^4	-1.96×10^2	1.40×10^3	$O(1)$	2.28×10^2	-24.1
2	$O(1)$	1.39×10^4	5.62×10^2	2.06×10^4	2.87×10^2	3.04×10^3	$O(1)$	1.66×10^3
3	45.4	-1.96×10^2	2.06×10^4	-8.40×10^2	2.94×10^4	-4.17×10^2	3.54×10^3	$O(1)$
4	$O(0.1)$	1.40×10^3	2.87×10^2	2.93×10^4	1.07×10^3	3.49×10^4	5.11×10^2	4.51×10^3
5	20.7	$O(1)$	3.04×10^3	-4.17×10^2	3.49×10^4	-1.36×10^3	4.46×10^4	-6.40×10^2
6	$O(0.1)$	2.28×10^2	$O(1)$	3.54×10^3	5.11×10^2	4.46×10^4	1.60×10^3	4.88×10^4
7	10.4	-24.1	1.66×10^3	$O(1)$	4.51×10^3	-6.40×10^2	4.88×10^4	-1.90×10^3

B.7. HWW_R and HW_RW_R couplings

Similarly the $HW^{(m)}W_R^{(n)}$ coupling contained in

$$
\begin{aligned}
&-ig_A k^2 \int_1^{z_L} \frac{dz}{kz} \mathrm{Tr}\left[\partial_z \hat{W}^-_{R\,\mu}\left[\hat{W}^+_\nu, \hat{H}\right] + \partial_z \hat{W}^+_\mu \left[\hat{W}^-_{R\,\nu}, \hat{H}\right]\right] \eta^{\mu\nu} \\
&\supset -\sum_{m,n} g_{HW^{(m)}W_R^{(n)}} H W^{+(m)}_\mu W^{-(n)}_{R\,\nu}\, \eta^{\mu\nu}
\end{aligned}
\tag{B.17}
$$

is given by

$$
\begin{aligned}
g_{HW^{(m)}W_R^{(n)}} &= ig_A k^2 \int_1^{z_L} \frac{dz}{kz} \\
&\times \frac{i}{2} u_H(z) \left[\partial_z\left(h^L_{W_R^{(n)}} - h^R_{W_R^{(n)}}\right)\hat{h}_{W^{(m)}} - \left(\partial_z \hat{h}_{W^{(m)}}\right)\left(h^L_{W_R^{(n)}} - h^R_{W_R^{(n)}}\right)\right] .
\end{aligned}
\tag{B.18}
$$

Numerical values of $g_{HW^{(m)}W_R^{(n)}}$ are given in Table 16. The $HW_R^{(m)}W_R^{(n)}$ couplings vanish for all m, n as a result of the Lie algebra.

Table 16: $g_{HW^{(m)}W_R^{(n)}}/g_w \cos\theta_H$ in the unit of GeV written by three significant figures. The values smaller than $O(10)$ are abbreviated. Reprinted from Ref. [29].

		m							
		0	1	2	3	4	5	6	7
	1	112	-60.7	3.47×10^3	$O(1)$	-55.8	$O(1)$	161	$O(1)$
n	2	80.9	-118	1.72×10^4	-278	1.62×10^4	-70.2	391	$O(1)$
	3	$O(1)$	$O(1)$	4.83×10^3	-260	3.32×10^4	-527	2.93×10^4	-140
	4	30.4	-19.4	1.13×10^3	-17.3	7.96×10^3	-412	4.94×10^4	-789

B.8. HZZ coupling

The Higgs coupling $HZ^{(m)}Z^{(n)}$ is contained in the $\mathrm{Tr}F_{\mu z}F^{\mu z}$ term

$$\begin{aligned}
&-ig_A k^2 \int_1^{z_L} \frac{dz}{kz} \mathrm{Tr}\left[\left(\partial_z \hat{Z}_\mu\right)\left[\hat{H}, \hat{Z}_\nu\right]\right] \eta^{\mu\nu} \\
&\supset -\frac{1}{2}\sum_n g_{HZ^{(n)}Z^{(n)}} H Z_\mu^{(n)} Z_\nu^{(n)}\ \eta^{\mu\nu} - \sum_{m<n} g_{HZ^{(m)}Z^{(n)}} H Z_\mu^{(m)} Z_\nu^{(n)}\ \eta^{\mu\nu}
\end{aligned} \tag{B.19}$$

so that

$$\begin{aligned}
g_{HZ^{(m)}Z^{(n)}} =& -g_A k^2 \int_1^{z_L} \frac{dz}{kz}\frac{1}{2} u_H(z) \\
&\times \left[-\left(\partial_z \hat{h}_{Z^{(m)}}\right)\left(h^L_{Z^{(n)}} - h^R_{Z^{(n)}}\right) + \partial_z\left(h^L_{Z^{(m)}} - h^R_{Z^{(m)}}\right)\hat{h}_{Z^{(n)}} + (m \longleftrightarrow n)\right] .
\end{aligned} \tag{B.20}$$

Numerical values of $g_{HW^{(m)}W^{(n)}}$ are given in Table 17.

Table 17: $g_{HZ^{(m)}Z^{(n)}} \cos^2\theta_W / g_w \cos\theta_H$ in the unit of GeV written by three significant figures. The values smaller than $O(10)$ are abbreviated.

		m							
		0	1	2	3	4	5	6	7
	0	80	2.55×10^2	$O(1)$	45.4	$O(10^{-1})$	20.7	$O(10^{-1})$	10
	1		-3.50×10^4	1.22×10^4	-1.96×10^2	1.23×10^3	$O(1)$	2.00×10^2	-24
	2			5.62×10^2	1.81×10^4	2.87×10^2	2.67×10^3	$O(1)$	1.45×10^3
	3				-8.39×10^2	2.58×10^4	-4.17×10^2	3.10×10^3	$O(1)$
n	4					1.07×10^3	3.06×10^4	5.11×10^2	3.97×10^3
	5						-1.36×10^3	3.92×10^4	-6.40×10^2
	6							1.60×10^3	4.29×10^4
	7								-1.90×10^3

B.9. $HHWW$ coupling

The Higgs coupling $HHW^{(m)}W^{(n)}$ is contained in the $\mathrm{Tr}F_{\mu z}F^{\mu z}$ term

$$\begin{aligned}
&-(-ig_A)^2 k^2 \int_1^{z_L} \frac{dz}{kz} \mathrm{Tr}\left[\left[\hat{W}^-_\mu, \hat{H}\right]\left[\hat{W}^+_\nu, \hat{H}\right]\right] \eta^{\mu\nu} \\
&\supset \frac{1}{4}\sum_{m,n} g_{HHW^{(m)}W^{(n)}} H H W_\mu^{+(m)} W_\nu^{-(n)}\ \eta^{\mu\nu}
\end{aligned} \tag{B.21}$$

so that

$$g_{HW^{(m)}W^{(n)}} = g_A^2 k^2 \int_1^{z_L} \frac{dz}{kz} u_H(z)^2 \left\{\left(h^L_{W^{(m)}} - h^R_{W^{(m)}}\right)\left(h^L_{W^{(n)}} - h^R_{W^{(n)}}\right) + 2\hat{h}_{W^{(m)}}\hat{h}_{W^{(n)}}\right\} . \tag{B.22}$$

Numerical values of $g_{HHW^{(m)}W^{(n)}}$ are given in Table 18.

Table 18: $g_{HHW^{(m)}W^{(n)}}/g_w^2\cos^2\theta_H$ written by three significant figures. The values smaller than $O(1)$ are abbreviated.

	0	1	2	3	4	5	6	7
0	1.01	3.19	$O(10^{-1})$	$O(10^{-1})$	$O(10^{-2})$	$O(10^{-1})$	$O(10^{-2})$	$O(10^{-1})$
1	3.19	12.5	$O(10^{-2})$	5.46	$O(10^{-3})$	1.54	$O(10^{-3})$	$O(10^{-1})$
2	$O(10^{-1})$	$O(10^{-2})$	15.6	$O(10^{-2})$	8.41	$O(10^{-2})$	1.85	$O(10^{-3})$
3	$O(10^{-1})$	5.46	$O(10^{-2})$	8.71	$O(10^{-2})$	4.94	$O(10^{-2})$	1.32
4	$O(10^{-2})$	$O(10^{-3})$	8.41	$O(10^{-2})$	15.6	$O(10^{-2})$	9.04	$O(10^{-2})$
5	$O(10^{-1})$	1.54	$O(10^{-2})$	4.94	$O(10^{-2})$	8.14	$O(10^{-2})$	4.82
6	$O(10^{-2})$	$O(10^{-3})$	1.85	$O(10^{-2})$	9.04	$O(10^{-2})$	15.6	$O(10^{-2})$
7	$O(10^{-1})$	$O(10^{-1})$	$O(10^{-3})$	1.32	$O(10^{-2})$	4.82	$O(10^{-2})$	7.96

B.10. $HHZZ$ coupling

The Higgs coupling $HHZ^{(m)}Z^{(n)}$ is contained in the $\mathrm{Tr}F_{\mu z}F^{\mu z}$ term

$$
\begin{aligned}
&-\frac{1}{2}(-ig_A)^2k^2\int_1^{z_L}\frac{dz}{kz}\mathrm{Tr}\left[\left[\hat{Z}_\mu^{(A)},\hat{H}\right]\left[\hat{Z}_\nu^{(A)},\hat{H}\right]\right]\eta^{\mu\nu}\\
&\supset\frac{1}{8}\sum_n g_{HHZ^{(n)}Z^{(n)}}HHZ_\mu^{(n)}Z_\nu^{(n)}\ \eta^{\mu\nu}+\frac{1}{4}\sum_{m<n}g_{HHZ^{(m)}Z^{(n)}}HHZ_\mu^{(m)}Z_\nu^{(n)}\ \eta^{\mu\nu}
\end{aligned}
\tag{B.23}
$$

so that

$$
g_{HZ^{(m)}Z^{(n)}}=g_A^2k^2\int_1^{z_L}\frac{dz}{kz}u_H(z)^2\left\{\left(h^L_{Z^{(m)}}-h^R_{Z^{(m)}}\right)\left(h^L_{Z^{(n)}}-h^R_{Z^{(n)}}\right)+2\hat{h}_{Z^{(m)}}\hat{h}_{Z^{(n)}}\right\}\ .
\tag{B.24}
$$

Numerical values of $g_{HHZ^{(m)}Z^{(n)}}$ are given in Table 19.

Table 19: $g_{HHZ^{(m)}Z^{(n)}}\cos^2\theta_W/g_w^2\cos^2\theta_H$ written by three significant figures. The values smaller than $O(1)$ are abbreviated.

		m							
		0	1	2	3	4	5	6	7
	0	1.01	3.19	$O(10^{-1})$	$O(10^{-1})$	$O(10^{-2})$	$O(10^{-1})$	$O(10^{-2})$	$O(10^{-1})$
	1		12.6	$O(10^{-3})$	5.47	$O(10^{-3})$	1.54	$O(10^{-3})$	$O(10^{-1})$
	2			12.0	$O(10^{-2})$	6.47	$O(10^{-3})$	1.42	$O(10^{-3})$
	3				8.73	$O(10^{-2})$	4.95	$O(10^{-2})$	1.33
n	4					12.0	$O(10^{-2})$	6.95	$O(10^{-2})$
	5						8.16	$O(10^{-2})$	4.83
	6							12.0	$O(10^{-2})$
	7								7.97

B.11. $\gamma f \bar{f}$ coupling

The $\gamma^{(l)} t^{(m)} t^{(n)}$ couplings are found to be

$$\mathcal{L} \supset -i \sum_{l,m,n} \left\{ g_{\gamma^{(l)} t_L^{(m)} t_L^{(n)}} A_\mu^{\gamma(l)} \bar{t}_L^{(m)} \gamma^\mu t_L^{(n)} + g_{\gamma^{(l)} t_R^{(m)} t_R^{(n)}} A_\mu^{\gamma(l)} \bar{t}_R^{(m)} \gamma^\mu t_R^{(n)} \right\} \tag{B.25}$$

where

$$\begin{aligned} g_{\gamma^{(l)} t_L^{(m)} t_L^{(n)}} &= g_w \sqrt{L} \int_1^{z_L} dz \Bigg\{ \frac{h^L_{\gamma^{(l)}} + h^R_{\gamma^{(l)}}}{2} f_{U_L}^{(m)} f_{U_L}^{(n)} \\ &\qquad + Q_{X_1} t_\phi h^B_{\gamma^{(l)}} \left(f_{B_L}^{(m)} f_{B_L}^{(n)} + f_{t_L}^{(m)} f_{t_L}^{(n)} + f_{t'_L}^{(m)} f_{t'_L}^{(n)} \right) + Q_{X_2} t_\phi h^B_{\gamma^{(l)}} f_{U_L}^{(m)} f_{U_L}^{(n)} \Bigg\} \\ &= \frac{2}{3} e \, \frac{\sqrt{L}}{\sqrt{r_\gamma}} \int_1^{z_L} dz \; C_\gamma(z) \left(f_{U_L}^{(m)} f_{U_L}^{(n)} + f_{B_L}^{(m)} f_{B_L}^{(n)} + f_{t_L}^{(m)} f_{t_L}^{(n)} + f_{t'_L}^{(m)} f_{t'_L}^{(n)} \right) \, . \end{aligned} \tag{B.26}$$

for the left-handed component $t_L^{(n)}$ and a similar expression for $t_R^{(n)}$. The $\gamma^{(l)} b^{(m)} b^{(n)}$ couplings are found to be

$$\mathcal{L} \supset -i \sum_{l,m,n} \left\{ g_{\gamma^{(l)} b_L^{(m)} b_L^{(n)}} A_\mu^{\gamma(l)} \bar{b}_L^{(m)} \gamma^\mu b_L^{(n)} + g_{\gamma^{(l)} b_R^{(m)} b_R^{(n)}} A_\mu^{\gamma(l)} \bar{b}_R^{(m)} \gamma^\mu b_R^{(n)} \right\} \tag{B.27}$$

where

$$\begin{aligned} g_{\gamma^{(l)} b_L^{(m)} b_L^{(n)}} &= g_w \sqrt{L} \int_1^{z_L} dz \Bigg\{ - \frac{h^L_{\gamma^{(l)}} + h^R_{\gamma^{(l)}}}{2} f_{b_L}^{(m)} f_{b_L}^{(n)} \\ &\qquad + Q_{X_2} t_\phi h^B_{\gamma^{(l)}} \left(f_{X_L}^{(m)} f_{X_L}^{(n)} + f_{D_L}^{(m)} f_{D_L}^{(n)} + f_{b'_L}^{(m)} f_{b'_L}^{(n)} \right) + Q_{X_1} t_\phi h^B_{\gamma^{(l)}} f_{b_L}^{(m)} f_{b_L}^{(n)} \Bigg\} \\ &= -\frac{1}{3} e \, \frac{\sqrt{L}}{\sqrt{r_\gamma}} \int_1^{z_L} dz \; C_\gamma(z) \left(f_{b_L}^{(m)} f_{b_L}^{(n)} + f_{X_L}^{(m)} f_{X_L}^{(n)} + f_{D_L}^{(m)} f_{D_L}^{(n)} + f_{b'_L}^{(m)} f_{b'_L}^{(n)} \right) \, . \end{aligned} \tag{B.28}$$

for the left-handed component $b_L^{(n)}$ and a similar expression for $b_R^{(n)}$. This form can be applied to the other quarks and leptons tower straightforwardly. For the SM photon, the coupling is obtained by replacing $r_\gamma \to L$ and $C_\gamma(z) \to 1$. Therefore

$$g_{\gamma^{(0)} t_L^{(m)} t_L^{(n)}} = \frac{2}{3} e \; \delta^{mn} \tag{B.29}$$

$$g_{\gamma^{(0)} b_L^{(m)} b_L^{(n)}} = -\frac{1}{3} e \; \delta^{mn}. \tag{B.30}$$

B.12. $Zf\bar{f}$ and $Z_Rf\bar{f}$ couplings

The Z couplings of the quark tower are found from

$$\begin{aligned}
&\sum_{a=1}^{2}\int_1^{z_L} dz\sqrt{G}\;\overline{\Psi}_a\left(-ig_AA_\mu - ig_BQ_{X_a}B_\mu\right)z\gamma^\mu\Psi_a \\
&\supset -ig_w\sqrt{L}\sum_l Z_\mu^{(l)}(x)\int_1^{z_L}\frac{dz}{k} \\
&\times\Bigg\{\frac{h^L_{Z^{(l)}}}{2}\left(-\bar{\tilde{B}}\gamma^\mu\tilde{B}+\bar{\tilde{t}}\gamma^\mu\tilde{t}-\bar{\tilde{b}}\gamma^\mu\tilde{b}+\bar{\tilde{U}}\gamma^\mu\tilde{U}-\bar{\tilde{D}}\gamma^\mu\tilde{D}+\bar{\tilde{X}}\gamma^\mu\tilde{X}\right) \\
&\quad+\frac{h^R_{Z^{(l)}}}{2}\left(\bar{\tilde{B}}\gamma^\mu\tilde{B}-\bar{\tilde{t}}\gamma^\mu\tilde{t}-\bar{\tilde{b}}\gamma^\mu\tilde{b}+\bar{\tilde{U}}\gamma^\mu\tilde{U}+\bar{\tilde{D}}\gamma^\mu\tilde{D}-\bar{\tilde{X}}\gamma^\mu\tilde{X}\right) \\
&\quad+\frac{\hat{h}_{Z^{(l)}}}{2}\left(\bar{\tilde{B}}\gamma^\mu\tilde{t'}+\bar{\tilde{t}}\gamma^\mu\tilde{t'}+\bar{\tilde{t'}}\gamma^\mu\tilde{B}+\bar{\tilde{t'}}\gamma^\mu\tilde{t}+\bar{\tilde{D}}\gamma^\mu\tilde{b'}+\bar{\tilde{X}}\gamma^\mu\tilde{b'}+\bar{\tilde{b'}}\gamma^\mu\tilde{D}+\bar{\tilde{b'}}\gamma^\mu\tilde{X}\right) \\
&\quad+Q_{X_1}t_\phi h^B_{Z^{(l)}}\left(\bar{\tilde{B}}\gamma^\mu\tilde{B}+\bar{\tilde{t}}\gamma^\mu\tilde{t}+\bar{\tilde{b}}\gamma^\mu\tilde{b}+\bar{\tilde{t'}}\gamma^\mu\tilde{t'}\right) \\
&\quad+Q_{X_2}t_\phi h^B_{Z^{(l)}}\left(\bar{\tilde{U}}\gamma^\mu\tilde{U}+\bar{\tilde{D}}\gamma^\mu\tilde{D}+\bar{\tilde{X}}\gamma^\mu\tilde{X}+\bar{\tilde{b}'}\gamma^\mu\tilde{b'}\right)\Bigg\}\,. \qquad \text{(B.31)}
\end{aligned}$$

The $Zt^{(m)}t^{(n)}$ couplings are found to be

$$\mathcal{L}\supset -i\sum_{m,n}\left\{g_{Zt_L^{(m)}t_L^{(n)}}Z_\mu\bar{t}_L^{(m)}\gamma^\mu t_L^{(n)}+g_{Zt_R^{(m)}t_R^{(n)}}Z_\mu\bar{t}_R^{(m)}\gamma^\mu t_R^{(n)}\right\} \qquad \text{(B.32)}$$

where

$$\begin{aligned}
g_{Zt_L^{(m)}t_L^{(n)}} &= \frac{g_w}{\cos\theta_W}\frac{\sqrt{L}}{\sqrt{2r_Z}}\int_1^{z_L}dz \\
&\times\Bigg\{C_Zf^{(m)}_{U_L}f^{(n)}_{U_L}+\cos\theta_HC_Z\left(-f^{(m)}_{B_L}f^{(n)}_{B_L}+f^{(m)}_{t_L}f^{(n)}_{t_L}\right) \\
&+\frac{-\sqrt{2}\sin\theta_H}{2}\hat{S}_Z\left(f^{(m)}_{B_L}f^{(n)}_{t'_L}+f^{(m)}_{t_L}f^{(n)}_{t'_L}+f^{(m)}_{t'_L}f^{(n)}_{B_L}+f^{(m)}_{t'_L}f^{(n)}_{t_L}\right) \\
&-2\sin^2\theta_WC_Z\frac{2}{3}\left(f^{(m)}_{U_L}f^{(n)}_{U_L}+f^{(m)}_{B_L}f^{(n)}_{B_L}+f^{(m)}_{t_L}f^{(n)}_{t_L}+f^{(m)}_{t'_L}f^{(n)}_{t'_L}\right)\Bigg\} \qquad \text{(B.33)}
\end{aligned}$$

for the left-handed component $t_L^{(n)}$ and a similar expression for $t_R^{(n)}$. Similarly, the $Zb^{(m)}b^{(n)}$ couplings are found to be

$$
\begin{aligned}
g_{Zb_L^{(m)}b_L^{(n)}} = & \frac{g_w}{\cos\theta_W}\frac{\sqrt{L}}{\sqrt{2r_Z}}\int_1^{z_L} dz \\
& \times \Bigg\{ -C_Z f_{b_L}^{(m)} f_{b_L}^{(n)} + \cos\theta_H C_Z \left(f_{X_L}^{(m)} f_{X_L}^{(n)} - f_{D_L}^{(m)} f_{D_L}^{(n)} \right) \\
& + \frac{-\sqrt{2}\sin\theta_H}{2}\hat{S}_Z \left(f_{D_L}^{(m)} f_{b'_L}^{(n)} + f_{X_L}^{(m)} f_{b'_L}^{(n)} + f_{b'_L}^{(m)} f_{D_L}^{(n)} + f_{b'_L}^{(m)} f_{X_L}^{(n)} \right) \\
& - 2\sin^2\theta_W C_Z \left(-\frac{1}{3} \right) \left(f_{D_L}^{(m)} f_{D_L}^{(n)} + f_{X_L}^{(m)} f_{X_L}^{(n)} + f_{b_L}^{(m)} f_{b_L}^{(n)} + f_{b'_L}^{(m)} f_{b'_L}^{(n)} \right) \Bigg\} \qquad \text{(B.34)}
\end{aligned}
$$

for the left-handed component $b_L^{(n)}$ and a similar expression for $b_R^{(n)}$. These forms can be applied to the other quarks and leptons tower straightforwardly. Therefore the vector and axial vector coupling are written by

$$
g^V_{Zf^{(m)}f^{(n)}} = \frac{g_{Zf_L^{(m)}f_L^{(n)}} + g_{Zf_R^{(m)}f_R^{(n)}}}{2}, \qquad g^A_{Zf^{(m)}f^{(n)}} = \frac{g_{Zf_L^{(m)}f_L^{(n)}} - g_{Zf_R^{(m)}f_R^{(n)}}}{2} \qquad \text{(B.35)}
$$

Numerical values of $g^V_{Zt^{(m)}t^{(n)}}$ are given in Table 20.

Table 20: $g^V_{Zt^{(m)}t^{(n)}} = \frac{1}{2}\{g_{Zt_L^{(m)}t_L^{(n)}} + g_{Zt_R^{(m)}t_R^{(n)}}\}$ in the unit of $g/\cos\theta_W$. The values larger than $O(10^{-3})$ are shown. $g^A_{Zt^{(m)}t^{(n)}} = \frac{1}{2}\{g_{Zt_L^{(m)}t_L^{(n)}} - g_{Zt_R^{(m)}t_R^{(n)}}\}$ in the unit of $g/\cos\theta_W$ is smaller than $O(10^{-3})$ in the range of $m, n \leq 10$, except for $g^A_{Zt^{(0)}t^{(0)}} = -0.2501$. Reprinted from Ref. [29].

	0	1	2	3	4	5	6	7
0	0.095	-0.008	0.001	$O(10^{-4})$	$O(10^{-5})$	$O(10^{-4})$	$O(10^{-5})$	$O(10^{-5})$
1	-0.008	0.337	0.059	$O(10^{-4})$	0.002	$O(10^{-5})$	$O(10^{-6})$	$O(10^{-6})$
2	0.001	0.059	-0.149	-0.010	$O(10^{-5})$	$O(10^{-4})$	$O(10^{-5})$	$O(10^{-4})$
3	$O(10^{-4})$	$O(10^{-4})$	-0.010	0.338	0.056	$O(10^{-5})$	0.002	$O(10^{-6})$
4	$O(10^{-5})$	0.002	$O(10^{-5})$	0.056	-0.149	-0.010	$O(10^{-5})$	$O(10^{-4})$
5	$O(10^{-4})$	$O(10^{-5})$	$O(10^{-4})$	$O(10^{-5})$	-0.010	0.338	0.056	$O(10^{-4})$
6	$O(10^{-5})$	$O(10^{-6})$	$O(10^{-5})$	0.002	$O(10^{-5})$	0.056	-0.150	-0.010
7	$O(10^{-5})$	$O(10^{-6})$	$O(10^{-4})$	$O(10^{-6})$	$O(10^{-4})$	$O(10^{-4})$	-0.010	0.338

By the same way, the $Z_R^{(1)}t^{(m)}t^{(n)}$ couplings are found to be

$$
\mathcal{L} \supset -i\sum_{m,n}\left\{ g_{Z_R^{(1)}t_L^{(m)}t_L^{(n)}} Z_{R\mu}^{(1)} \bar{t}_L^{(m)} \gamma^\mu t_L^{(n)} + g_{Z_R^{(1)}t_R^{(m)}t_R^{(n)}} Z_{R\mu}^{(1)} \bar{t}_R^{(m)} \gamma^\mu t_R^{(n)} \right\} \qquad \text{(B.36)}
$$

where

$$g_{Z_R^{(1)}t_L^{(m)}t_L^{(n)}} = g_w\sqrt{L}\int_1^{z_L} dz \times \left\{ \frac{h^L_{Z_R^{(1)}} + h^R_{Z_R^{(1)}}}{2} f^{(m)}_{U_L} f^{(n)}_{U_L} + \frac{h^L_{Z_R^{(1)}} - h^R_{Z_R^{(1)}}}{2} \left(-f^{(m)}_{B_L} f^{(n)}_{B_L} + f^{(m)}_{t_L} f^{(n)}_{t_L} \right) + Q_{X_1} t_\phi h^B_{Z_R^{(1)}} \left(f^{(m)}_{B_L} f^{(n)}_{B_L} + f^{(m)}_{t_L} f^{(n)}_{t_L} + f^{(m)}_{t'_L} f^{(n)}_{t'_L} \right) + Q_{X_2} t_\phi h^B_{Z_R^{(1)}} f^{(m)}_{U_L} f^{(n)}_{U_L} \right\} \tag{B.37}$$

for the left-handed component $t_L^{(n)}$ and a similar expression for $t_R^{(n)}$, $b_L^{(n)}$, $b_R^{(n)}$, other quarks and leptons.

B.13. $Wf\bar{f}$ and $W_Rf\bar{f}$ couplings

The W couplings of the quark tower are found from

$$\begin{aligned} &\sum_{a=1}^{2}\int_1^{z_L} dz\sqrt{G}\ \overline{\Psi}_a \left(-ig_A A_\mu - ig_B Q_{X_a} B_\mu\right) z\gamma^\mu \Psi_a \\ &\supset -ig_w\sqrt{L}\sum_l W^{+(l)}_\mu(x)\int_1^{z_L}\frac{dz}{k} \\ &\times\Big\{ h^L_{W^{(l)}}\left(\bar{\tilde{T}}\gamma^\mu\tilde{B} + \bar{\tilde{t}}\gamma^\mu\tilde{b} + \bar{\tilde{U}}\gamma^\mu\tilde{D} + \bar{\tilde{X}}\gamma^\mu\tilde{Y}\right) + h^R_{W^{(l)}}\left(\bar{\tilde{T}}\gamma^\mu\tilde{t} + \bar{\tilde{B}}\gamma^\mu\tilde{b} + \bar{\tilde{U}}\gamma^\mu\tilde{X} + \bar{\tilde{D}}\gamma^\mu\tilde{Y}\right) \\ &\quad + \hat{h}_{W^{(l)}}\left(-\bar{\tilde{T}}\gamma^\mu\tilde{t}' + \bar{\tilde{t}'}\gamma^\mu\tilde{b} - \bar{\tilde{U}}\gamma^\mu\tilde{b}' + \bar{\tilde{b}'}\gamma^\mu\tilde{D}\right)\Big\}\,. \end{aligned} \tag{B.38}$$

The $W^{(l)}t^{(m)}b^{(n)}$ couplings are found to be

$$\mathcal{L} \supset -i\sum_{m,n}\left\{ g_{W^{(l)}t_L^{(m)}b_L^{(n)}} W^{+(l)}_\mu \bar{t}^{(m)}_L \gamma^\mu b^{(n)}_L + g_{W^{(l)}t_R^{(m)}b_R^{(n)}} W^{+(l)}_\mu \bar{t}^{(m)}_R \gamma^\mu b^{(n)}_R + (\text{h.c.})\right\} \tag{B.39}$$

where

$$g_{W^{(l)}t_L^{(m)}b_L^{(n)}} = g_w\frac{\sqrt{L}}{\sqrt{2r_{W^{(l)}}}}\int_1^{z_L} dz \times \left\{ h^L_{W^{(l)}}\left(f^{(m)}_{t_L} f^{(n)}_{b_L} + f^{(m)}_{U_L} f^{(n)}_{D_L}\right) + h^R_{W^{(l)}}\left(f^{(m)}_{B_L} f^{(n)}_{b_L} + f^{(m)}_{U_L} f^{(n)}_{X_L}\right) + \hat{h}^R_{W^{(l)}}\left(f^{(m)}_{t'_L} f^{(n)}_{b_L} - f^{(m)}_{U_L} f^{(n)}_{b'_L}\right)\right\} \tag{B.40}$$

for the left-handed component $t_L^{(n)}$ and a similar expression for $t_R^{(n)}$, $b_L^{(n)}$, $b_R^{(n)}$, other quarks and leptons. Similarly, the $W_R^{(l)} t^{(m)} b^{(n)}$ couplings are found to be

$$\begin{aligned} g_{W_R^{(l)} t_L^{(m)} b_L^{(n)}} &= g_w \frac{\sqrt{L}}{\sqrt{2 r_{W_R^{(l)}}}} \int_1^{z_L} dz \\ &\quad \times \left\{ h^L_{W_R^{(l)}} \left(f^{(m)}_{t_L} f^{(n)}_{b_L} + f^{(m)}_{U_L} f^{(n)}_{D_L} \right) + h^R_{W_R^{(l)}} \left(f^{(m)}_{B_L} f^{(n)}_{b_L} + f^{(m)}_{U_L} f^{(n)}_{X_L} \right) \right\} \\ &= g_w \frac{\sqrt{L}}{\sqrt{2 r_{W_R^{(l)}} r_{t^{(m)}} r_{b^{(n)}}}} \int_1^{z_L} dz \; C(z; \lambda_{W_R^{(l)}}) C_L(z; \lambda_{t^{(m)}}) C_L(z; \lambda_{b^{(n)}}) \\ &\quad \times \left\{ (1 - \cos^2 \theta_H) \left(-\frac{\mu_2}{\tilde{\mu}} - \frac{\tilde{\mu}}{\mu_2} \right) - (1 - \cos^2 \theta_H) \left(-\frac{\mu_2}{\tilde{\mu}} - \frac{\tilde{\mu}}{\mu_2} \right) \right\} \\ &= 0 \; . \end{aligned} \tag{B.41}$$

Therefore W_R boson does not decays to the SM quarks and leptons.

B.14. $A^{\hat{4}} f \bar{f}$ coupling

The $A^{\hat{4}}$ couplings of the quark tower are found from

$$\begin{aligned} &\int_1^{z_L} dz \sqrt{G} \; \overline{\Psi}_1 \left(-i g_A A_\mu - i g_B Q_{X_a} B_\mu \right) z \gamma^\mu \Psi_1 \\ \supset &- i g_w \sum_l \sqrt{L} A_\mu^{\hat{4}(l)} \int_1^{z_L} \frac{dz}{k} \frac{i}{2} h_{A^{\hat{4}(l)}} \left(\bar{\tilde{B}} \gamma^\mu \tilde{t}' - \bar{\tilde{t}} \gamma^\mu \tilde{t}' - \bar{\tilde{t}}' \gamma^\mu \tilde{B} + \bar{\tilde{t}}' \gamma^\mu \tilde{t} \right) \; . \end{aligned} \tag{B.42}$$

The $A^{\hat{4}} t^{(m)} t^{(n)}$ couplings are found to be

$$\begin{aligned} &g_{A^{\hat{4}(l)} t_L^{(m)} t_L^{(n)}} \\ &= g_w \sqrt{L} \int_1^{z_L} \frac{dz}{k} \frac{i}{2} h_{A^{4(\hat{l})}} \left(f^{(m)}_{B_L} f^{(n)}_{t'_L} - f^{(m)}_{t'_L} f^{(n)}_{B_L} - f^{(m)}_{t_L} f^{(n)}_{t'_L} + f^{(m)}_{t'_L} f^{(n)}_{t_L} \right) \end{aligned} \tag{B.43}$$

for the left-handed component $t_L^{(n)}$ and a similar expression for $t_R^{(n)}$, other quarks and leptons. Therefore $A^{\hat{4}}$ coupling vanishes for $m = n$ case.

B.15. $Hf\bar{f}$ coupling

The Higgs couplings of the top quark tower are contained in

$$\begin{aligned}
&\int_1^{z_L} dz\sqrt{G}\ \overline{\Psi}_1\left(-ig_A kzA_z\right)\gamma^5\Psi_1 \\
&\supset -ig_w\sqrt{L}H\int_1^{z_L} dz\ u_H(z)\frac{i}{2}\left(\bar{B}\gamma^5 t' - \bar{t}\gamma^5 t' - \bar{t}'\gamma^5 B + \bar{t}'\gamma^5 t\right) \\
&= \frac{g_w k\sqrt{L}}{2}\sum_{m,n} H i t_L^{(m)\dagger} t_R^{(n)} \\
&\times\int_1^{\infty} z_L dz\ u_H(z)\left(f_{B_L}^{(m)} f_{t'_R}^{(n)} - f_{t_L}^{(m)} f_{t'_R}^{(n)} - f_{t'_L}^{(m)} f_{B_R}^{(n)} + f_{t'_L}^{(m)} f_{t_R}^{(n)}\right) + (L \leftrightarrow R) \\
&= i\sum_{m,n} H\ \left(g_{Ht_L^{(m)\dagger}t_R^{(n)}} t_L^{(m)\dagger} t_R^{(n)} - g_{Ht_R^{(m)\dagger}t_L^{(n)}} t_R^{(m)\dagger} t_L^{(n)}\right)\ . \qquad \text{(B.44)}
\end{aligned}$$

One finds that

$$\begin{aligned}
g_{Ht_R^{(m)\dagger}t_L^{(n)}} &= g_{Ht_L^{(n)\dagger}t_R^{(m)}} \\
&= -\frac{g_w\sqrt{kL}}{2}\frac{2s_H c_H}{\sqrt{(z_L^2-1)r_{t^{(m)}}r_{t^{(n)}}}} \\
&\quad\times\int_1^{z_L} dz\ z\left\{-S_R^{(m)}\frac{C_L^{(n)}(1)}{S_L^{(n)}(1)}S_L^{(n)} + \frac{C_L^{(m)}(1)}{S_L^{(m)}(1)}C_R^{(m)}C_L^{(n)}\right\}. \qquad \text{(B.45)}
\end{aligned}$$

We denote

$$y_{t^{(m)}t^{(n)}} = \frac{g_{Ht_L^{(m)\dagger}t_R^{(n)}} + g_{Ht_R^{(m)\dagger}t_L^{(n)}}}{2}\quad,\quad \hat{y}_{t^{(m)}t^{(n)}} = \frac{-g_{Ht_L^{(m)\dagger}t_R^{(n)}} + g_{Ht_R^{(m)\dagger}t_L^{(n)}}}{2}\quad. \qquad \text{(B.46)}$$

For $m = n$

$$y_{t^{(m)}t^{(m)}} = -\frac{g_w k\sqrt{kL}}{2}\frac{\sqrt{z_L^2-1}}{r_{t^{(n)}}}s_H c_H\frac{C_L^{(m)}(1)}{S_L^{(m)}(1)}\ ,\quad \hat{y}_{t^{(m)}t^{(m)}} = 0\ . \qquad \text{(B.47)}$$

Numerical values of $y_{t^{(m)}t^{(n)}}$ and $\hat{y}_{t^{(m)}t^{(n)}}$ are given in Table 21 and 22, respectively.

Table 21: $y_{t^{(m)}t^{(n)}}$ in the unit of $y_t \cos\theta_H$. Only the values larger than $O(10^{-3})$ are shown and written by three significant figures. Reprinted from Ref. [29].

	0	1	2	3	4	5	6	7
0	1.00	0.517	0.188	0.049	-0.010	0.044	0.025	0.013
1	0.517	-0.225	1.04	-0.090	0.234	$O(10^{-4})$	$O(10^{-4})$	-0.010
2	0.188	1.04	0.226	0.674	0.088	0.034	$O(10^{-4})$	0.057
3	0.049	-0.090	0.694	-0.217	1.05	-0.087	0.244	$O(10^{-4})$
4	-0.010	0.234	0.088	1.05	0.217	0.670	0.087	0.028
5	0.044	$O(10^{-4})$	0.034	-0.087	0.670	-0.214	1.05	-0.087
6	0.025	$O(10^{-4})$	$O(10^{-4})$	0.244	0.087	1.05	0.215	‘0.667
7	0.013	-0.010	0.057	$O(10^{-4})$	0.028	-0.087	0.667	-0.213

Table 22: $\hat{y}_{t^{(m)}t^{(n)}}$ in the unit of $y_t \cos\theta_H$. Only the values larger than $O(10^{-3})$ are shown and written by three significant figures. Reprinted from Ref. [29].

	0	1	2	3	4	5	6	7
0	0	-0.529	0.091	-0.043	-0.015	-0.049	0.015	-0.011
1	0.529	0	-0.040	0.014	-0.005	$O(10^{-4})$	$O(10^{-5})$	0.002
2	-0.091	0.040	0	-0.119	-0.012	-0.011	$O(10^{-4})$	-0.026
3	0.043	0.012	0.119	0	-0.024	0.008	-0.014	$O(10^{-4})$
4	0.015	$O(10^{-3})$	0.012	0.024	0	-0.060	-0.007	-0.005
5	0.049	$O(10^{-4})$	0.011	-0.008	0.062	0	-0.017	0.006
6	-0.015	$O(10^{-4})$	$O(10^{-4})$	0.014	0.007	0.017	0	-0.040

B.16. γFF coupling

The γ couplings of the dark fermion tower are given by

$$\mathcal{L} \supset -ie \sum_{l,m,n} A_\mu^{\gamma(l)} \frac{\sqrt{L}}{\sqrt{r_{\gamma(l)}}} \int_1^{z_L} dz\; C(z,\lambda_{\gamma(l)}) \Bigg[\left(f_{lL}^{(m)*} f_{lL}^{(n)} + f_{rL}^{(m)*} f_{rL}^{(n)} \right) \times \left\{ \left(Q_X + \frac{1}{2} \right) \overline{F}_L^{+(m)} \gamma^\mu F_L^{+(n)} + \left(Q_X - \frac{1}{2} \right) \overline{F}_L^{0(m)} \gamma^\mu F_L^{0(n)} \right) \right\} + (L \to R) \Bigg], \quad \text{(B.48)}$$

Therefore F^0 does not couples to photon for $Q_X = \frac{1}{2}$ case. The couplings are defined as

$$\mathcal{L} \supset -i \sum_{l,m,n} \left\{ g_{\gamma^{(l)} F_L^{+(m)} F_L^{+(n)}} A_\mu^{\gamma(l)} \overline{F}_L^{+(m)} \gamma^\mu F_L^{+(n)} + g_{\gamma^{(l)} F_R^{+(m)} F_R^{+(n)}} A_\mu^{\gamma(l)} \overline{F}_R^{+(m)} \gamma^\mu F_R^{+(n)} \right\},$$

$$g_{\gamma^{(l)} F_L^{+(m)} F_L^{+(n)}} \equiv e \frac{\sqrt{L}}{\sqrt{r_{\gamma(l)}}} \int_1^{z_L} dz\; C(z,\lambda_{\gamma(l)}) \left(f_{lL}^{(m)*} f_{lL}^{(n)} + f_{rL}^{(m)*} f_{rL}^{(n)} \right),$$

$$g_{\gamma^{(l)} F_R^{+(m)} F_R^{+(n)}} \equiv e \frac{\sqrt{L}}{\sqrt{r_{\gamma(l)}}} \int_1^{z_L} dz\; C(z,\lambda_{\gamma(l)}) \left(f_{lR}^{(m)*} f_{lR}^{(n)} + f_{rR}^{(m)*} f_{rR}^{(n)} \right). \quad \text{(B.49)}$$

Especially, the $\gamma^{(0)}$ couplings of the dark fermion tower are given by

$$g_{\gamma^{(0)}F_L^{+(m)}F_L^{+(n)}} = g_{\gamma^{(0)}F_R^{+(m)}F_R^{+(n)}} = e\delta^{mn}. \tag{B.50}$$

In Tables 23, $\gamma^{(1)}FF$ couplings for various parameter sets are tabulated.

Table 23: The mass and left- and right-handed couplings to F^+ in (B.49) in the unit of electromagnetic coupling e of the first KK photon in the case of degenerate dark fermions. Reprinted from Ref. [28].

n_F	z_L	$m_{\gamma^{(1)}}$ (TeV)	$g_{\gamma^{(1)}F_L^{+(1)}F_L^{+(1)}}$	$g_{\gamma^{(1)}F_R^{+(1)}F_R^{+(1)}}$
3	10^8	2.42	0.19	4.16
	10^6	4.26	0.28	3.61
	10^5	5.92	0.38	3.31
	2×10^4	7.55	0.52	3.09
4	10^8	2.46	0.06	4.15
	10^6	4.32	0.11	3.59
	10^5	6.00	0.15	3.28
	3×10^4	7.19	0.17	3.10
	10^4	8.52	0.21	2.93
6	10^8	2.50	-0.06	4.14
	10^6	4.40	-0.05	3.58
	10^5	6.12	-0.04	3.26
	10^4	8.68	-0.03	2.90

B.17. ZFF and Z_RFF couplings

The Z couplings of the dark fermion tower are given by

$$\begin{aligned}
&\int_1^{z_L} dz\sqrt{G}\ \overline{\Psi}_F\left(-ig_A A_\mu - ig_B Q_{X_F} B_\mu\right) z\gamma^\mu \Psi_F \\
=& -iZ_\mu \frac{g_w}{\cos\theta_W}\frac{\sqrt{L}}{\sqrt{2}\sqrt{r_Z}}\int_1^{z_L} dz \sum_{m,n} \\
&\times\Bigg[\Big\{\left(1+\cos\theta_H\right)C(z) f_{lL}^{*(m)} f_{lL}^{(n)} + \left(1-\cos\theta_H\right)C(z) f_{rL}^{*(m)} f_{rL}^{(n)} \\
&\quad -\sin\theta_H \hat{S}(z)\left(i f_{lL}^{*(m)} f_{rL}^{(n)} - i f_{rL}^{*(m)} f_{lL}^{(n)}\right)\Big\}\overline{F}_L^{(m)}\gamma^\mu I_3 F_L^{(n)} \\
&\quad -2\sin^2\theta_W\left(f_{lL}^{*(m)} f_{lL}^{(n)} + f_{rL}^{*(m)} f_{rL}^{(n)}\right)\overline{F}_L^{(m)}\gamma^\mu(I_3+Q_{X_F})F_L^{(n)} + (L\to R)\Bigg] \\
=& -iZ_\mu \sum_{m,n}\Big\{g_{ZF_L^{+(m)}F_L^{+(n)}}\overline{F}_L^{+(m)}\gamma^\mu F_L^{+(n)} + g_{ZF_R^{+(m)}F_R^{+(n)}}\overline{F}_R^{+(m)}\gamma^\mu F_R^{+(n)} \\
&\qquad + g_{ZF_L^{0(m)}F_L^{0(n)}}\overline{F}_L^{0(m)}\gamma^\mu F_L^{0(n)} + g_{ZF_R^{0(m)}F_R^{0(n)}}\overline{F}_R^{0(m)}\gamma^\mu F_R^{0(n)}\Big\}\,,
\end{aligned} \tag{B.51}$$

where $F_L^{(n)}$ is a abbreviation of the doublet $(F_L^{+(n)}, F_L^{0(n)})^T$ and I_3 is a isospin operator. Numerical values of $g^V_{ZF^{+(m)}F^{+(n)}}$ and $g^V_{ZF^{0(m)}F^{0(n)}}$ are given in Table 24 and 25, respectively.

Table 24: $g^V_{ZF^{+(m)}F^{+(n)}} = \frac{1}{2}\{g_{ZF_L^{+(m)}F_L^{+(n)}} + g_{ZF_R^{+(m)}F_R^{+(n)}}\}$ in the unit of $g/\cos\theta_W$. Only the value larger than $O(10^{-3})$ are shown and written by three significant figures. Reprinted from Ref. [29].

	1	2	3	4	5	6	7
1	-0.230	0.021	$O(10^{-5})$	-0.001	$O(10^{-6})$	$O(10^{-4})$	$O(10^{-6})$
2	0.021	0.267	0.009	$O(10^{-6})$	$O(10^{-5})$	$O(10^{-6})$	$O(10^{-5})$
3	$O(10^{-5})$	0.009	-0.230	0.024	$O(10^{-6})$	-0.001	$O(10^{-6})$
4	-0.001	$O(10^{-6})$	0.024	0.267	0.009	$O(10^{-6})$	$O(10^{-4})$
5	$O(10^{-6})$	$O(10^{-5})$	$O(10^{-6})$	0.009	-0.229	0.025	$O(10^{-6})$
6	$O(10^{-4})$	$O(10^{-6})$	-0.001	$O(10^{-6})$	0.025	0.267	0.009
7	$O(10^{-6})$	$O(10^{-5})$	$O(10^{-6})$	$O(10^{-4})$	$O(10^{-6})$	0.009	-0.229

Table 25: $g^V_{ZF^{0(m)}F^{0(n)}} = \frac{1}{2}\{g_{ZF_L^{0(m)}F_L^{0(n)}} + g_{ZF_R^{0(m)}F_R^{0(n)}}\}$ in the unit of $g/\cos\theta_W$. Only the value larger than $O(10^{-3})$ are shown and written by three significant figures. Reprinted from Ref. [29].

	1	2	3	4	5	6	7
1	-0.002	-0.021	$O(10^{-5})$	0.001	$O(10^{-6})$	$O(10^{-4})$	$O(10^{-6})$
2	-0.021	-0.498	-0.009	$O(10^{-5})$	$O(10^{-5})$	$O(10^{-6})$	$O(10^{-5})$
3	$O(10^{-5})$	-0.009	-0.002	-0.024	$O(10^{-5})$	0.001	$O(10^{-6})$
4	0.001	$O(10^{-5})$	-0.024	-0.498	-0.009	$O(10^{-5})$	$O(10^{-4})$
5	$O(10^{-6})$	$O(10^{-5})$	$O(10^{-5})$	-0.009	-0.002	-0.025	$O(10^{-5})$
6	$O(10^{-4})$	$O(10^{-6})$	0.001	$O(10^{-5})$	-0.025	-0.498	-0.009
7	$O(10^{-6})$	$O(10^{-5})$	$O(10^{-6})$	$O(10^{-4})$	$O(10^{-6})$	-0.009	-0.002

Table 26: The ZFF couplings in the unit of g_w with b.c. $\eta_F = +1$ in the case of degenerate dark fermions. Reprinted from Ref. [28].

n_F	z_L	$g_{ZF_L^{+(1)}F_L^{+(1)}}$	$g_{ZF_R^{+(1)}F_R^{+(1)}}$	$g_{ZF_L^{0(1)}F_L^{0(1)}}$	$g_{ZF_L^{0(1)}F_L^{0(1)}}$
3	10^8	-0.260	-0.242	-4.01×10^{-3}	-2.273×10^{-2}
	10^6	-0.261	-0.257	-2.18×10^{-3}	-6.96×10^{-3}
	10^5	-0.262	-0.260	-1.97×10^{-3}	-4.27×10^{-3}
	2×10^4	-0.259	-0.258	-4.13×10^{-3}	-5.84×10^{-3}
4	10^8	-0.261	-0.244	-2.52×10^{-3}	-2.049×10^{-2}
	10^6	-0.263	-0.258	-1.14×10^{-3}	-5.59×10^{-3}
	10^5	-0.263	-0.261	-7.6×10^{-4}	-2.77×10^{-3}
	3×10^4	-0.263	-0.262	-6.7×10^{-4}	-1.97×10^{-3}
	10^4	-0.263	-0.262	-6.5×10^{-4}	-1.54×10^{-3}
6	10^8	-0.263	-0.246	-1.42×10^{-3}	-1.860×10^{-2}
	10^6	-0.263	-0.259	-5.8×10^{-4}	-4.77×10^{-3}
	10^5	-0.263	-0.262	-3.4×10^{-4}	-2.19×10^{-3}
	10^4	-0.264	-0.263	-2.1×10^{-4}	-9.8×10^{-4}

Similarly the Z_R couplings of the dark fermion tower are given by

$$
\begin{aligned}
&\int_1^{z_L} dz\sqrt{G}\;\overline{\Psi}_F\left(-ig_A A_\mu - ig_B Q_{X_F} B_\mu\right) z\gamma^\mu \Psi_F \\
&= -ig_w \sum_{l,m,n} Z_{R\,\mu}^{(l)} \frac{\sqrt{L}}{\sqrt{2}\sqrt{1+\frac{\cos^2\theta_H}{\cos 2\theta_W}}\sqrt{r_{Z_R^{(l)}}}} \int_1^{z_L} dz\; C_Z(z)\overline{F}_L^{(m)}\gamma^\mu I_3 F_L^{(n)} \\
&\quad\times\left[I_3^{(c)}\left\{-\cos\theta_H\left(f_{lL}^{(m)*}f_{lL}^{(n)}+f_{rL}^{(m)*}f_{rL}^{(n)}\right)+\left(f_{lL}^{(m)*}f_{lL}^{(n)}-f_{rL}^{(m)*}f_{rL}^{(n)}\right)\right\}\right. \\
&\qquad\left.+2Q_X\frac{\sin^2\theta_W}{\cos 2\theta_W}\cos\theta_H\left(f_{lL}^{(m)*}f_{lL}^{(n)}+f_{rL}^{(m)*}f_{rL}^{(n)}\right)\right]+(L\to R). \\
&= -i\sum_{l,m,n} Z_{R\,\mu}^{(l)}\Big\{\, g_{Z_R^{(l)}F_L^{+(m)}F_L^{+(n)}}\overline{F}_L^{+(m)}\gamma^\mu F_L^{+(n)} + g_{Z_R^{(l)}F_R^{+(m)}F_R^{+(n)}}\overline{F}_R^{+(m)}\gamma^\mu F_R^{+(n)} \\
&\qquad + g_{Z_R^{(l)}F_L^{0(m)}F_L^{0(n)}}\overline{F}_L^{0(m)}\gamma^\mu F_L^{0(n)} + g_{Z_R^{(l)}F_R^{0(m)}F_R^{0(n)}}\overline{F}_R^{0(m)}\gamma^\mu F_R^{0(n)}\Big\}\,. \qquad \text{(B.52)}
\end{aligned}
$$

In Tables 26, 27, 28, 29, 30 and 31, we have summarised the $Z\bar{F}F$ and the $Z_R\bar{F}F$ couplings for various parameter sets.

B.18. WFF and W_RFF couplings

The W couplings of the dark fermion tower are given by

$$
\mathcal{L}_{4D} \supset W_\mu^{-(l)}\left(g_{W^{(l)}F_L^{(m)}F_L^{(n)}}\overline{F}_L^{0(m)}\gamma^\mu F_L^{+(n)} + g_{W^{(l)}F_R^{(m)}F_R^{(n)}}\overline{F}_R^{0(m)}\gamma^\mu F_R^{+(n)}\right) + (\text{h.c.}),
$$

Table 27: The ZFF couplings in the unit of g_w with b.c. $\eta_F = -1$ in the case of degenerate dark fermions. Reprinted from Ref. [28].

n_F	z_L	$g_{ZF_L^{+(1)}F_L^{+(1)}}$	$g_{ZF_R^{+(1)}F_R^{+(1)}}$	$g_{ZF_L^{0(1)}F_L^{0(1)}}$	$g_{ZF_L^{0(1)}F_L^{0(1)}}$
4	10^8	0.304	0.287	-0.569	-0.552
	10^6	0.306	0.301	-0.569	-0.565
	10^4	0.306	0.305	-0.570	-0.569

Table 28: The $Z^{(1)}FF$ couplings in the unit of g_w with b.c. $\eta_F = +1$ in the case of degenerate dark fermions. Reprinted from Ref. [28].

n_F	z_L	$m_{Z^{(1)}}$ (TeV)	$g_{Z^{(1)}F_L^{+(1)}F_L^{+(1)}}$	$g_{Z^{(1)}F_R^{+(1)}F_R^{+(1)}}$	$g_{Z^{(1)}F_L^{0(1)}F_L^{0(1)}}$	$g_{Z^{(1)}F_L^{0(1)}F_L^{0(1)}}$
3	10^8	2.42	-0.02	-1.07	-0.04	-0.08
	10^6	4.25	-0.06	-0.95	-0.02	-0.02
	10^5	5.92	-0.09	-0.87	-0.01	-0.01
	2×10^4	7.54	-0.12	-0.81	-0.02	-0.00
4	10^8	2.45	0.00	-1.06	-0.02	-0.08
	10^6	4.32	-0.02	-0.94	-0.01	-0.02
	10^5	6.00	-0.03	-0.86	-0.01	-0.01
	10^4	8.52	-0.05	-0.77	-0.00	-0.00
6	10^8	2.50	0.02	-1.06	-0.01	-0.07
	10^6	4.40	0.02	-0.94	-0.00	-0.01
	10^5	6.13	0.01	-0.86	-0.00	-0.01
	10^4	8.68	0.01	-0.77	-0.00	-0.00

Table 29: The $Z^{(1)}FF$ couplings in the unit of g_w with b.c. $\eta_F = -1$ in the case of degenerate dark fermions. Reprinted from Ref. [28].

n_F	z_L	$g_{Z^{(1)}F_L^{+(1)}F_L^{+(1)}}$	$g_{Z^{(1)}F_R^{+(1)}F_R^{+(1)}}$	$g_{Z^{(1)}F_L^{0(1)}F_L^{0(1)}}$	$g_{Z^{(1)}F_L^{0(1)}F_L^{0(1)}}$
4	10^8	0.00	1.25	-0.02	-2.39
	10^6	0.03	1.10	-0.06	-2.05
	10^5	0.04	1.00	-0.08	-1.87
	10^4	0.06	0.90	-0.12	-1.67

Table 30: The $Z_R^{(1)}FF$ couplings in the unit of g_w with b.c. $\eta_F = +1$ in the case of degenerate dark fermions. Reprinted from Ref. [28].

n_F	z_L	$m_{Z_R^{(1)}}$ (TeV)	$g_{Z_R^{(1)}F_L^{+(1)}F_L^{+(1)}}$	$g_{Z_R^{(1)}F_R^{+(1)}F_R^{+(1)}}$	$g_{Z_R^{(1)}F_L^{0(1)}F_L^{0(1)}}$	$g_{Z_R^{(1)}F_L^{0(1)}F_L^{0(1)}}$
3	10^8	2.34	-0.09	-1.05	0.25	2.55
	10^6	4.06	-0.13	-0.90	0.34	2.23
	10^5	5.59	-0.16	-0.82	0.42	2.06
	2×10^4	7.05	-0.20	-0.77	0.51	1.93
4	10^8	2.37	-0.07	-1.05	0.18	2.54
	10^6	4.12	-0.10	-0.89	0.24	2.22
	10^5	5.70	-0.11	-0.82	0.29	2.04
	3×10^4	6.74	-0.12	-0.78	0.32	1.94
	10^4	7.92	-0.14	-0.73	0.35	1.84
6	10^8	2.42	-0.04	-1.05	0.12	2.54
	10^6	4.20	-0.06	-0.89	0.16	2.21
	10^5	5.78	-0.07	-0.81	0.18	2.03
	10^4	8.11	-0.08	-0.73	0.21	1.83

Table 31: The $Z_R^{(1)}FF$ couplings in the unit of g_w with b.c. $\eta_F = -1$ in the case of degenerate dark fermions. Reprinted from Ref. [28].

n_F	z_L	$g_{Z_R^{(1)}F_L^{+(1)}F_L^{+(1)}}$	$g_{Z_R^{(1)}F_R^{+(1)}F_R^{+(1)}}$	$g_{Z_R^{(1)}F_L^{0(1)}F_L^{0(1)}}$	$g_{Z_R^{(1)}F_L^{0(1)}F_L^{0(1)}}$
4	10^8	0.05	0.80	0.07	0.69
	10^6	0.07	0.68	0.08	0.65
	10^5	0.08	0.62	0.09	0.61
	3×10^4	0.09	0.58	0.10	0.58
	10^4	0.11	0.55	0.11	0.55

are given by

$$g_{W^{(l)}F_L^{(m)}F_L^{(n)}} = \frac{g_w}{2\sqrt{2}}\frac{\sqrt{L}}{\sqrt{r_{W^{(l)}}}}\int_1^{z_L} dz\Big\{C(z)\Big\{(1+\cos\theta_H)f_{lL}^{(m)*}f_{lL}^{(n)} + (1-\cos\theta_H)f_{rL}^{(m)*}f_{rL}^{(n)}\Big\} - \sin\theta_H\hat{S}(z)i\Big(f_{lL}^{(m)*}f_{rL}^{(n)} - f_{rL}^{(m)*}f_{lL}^{(n)}\Big)\Big\}, \tag{B.53}$$

and $g_{W^{(l)}F_R^{(m)}F_R^{(n)}}$ is obtained by replacements $f_{l(r)L} \to f_{l(r)R}$.

Similarly the W_R couplings of the dark fermion tower are given by

$$\mathcal{L}_{4D} \supset W_{R\,\mu}^{-(l)}\left(g_{W_R^{(l)}F_L^{(m)}F_L^{(n)}}\overline{F}_L^{0(m)}\gamma^\mu F_L^{+(n)} + g_{W_R^{(l)}F_R^{(m)}F_R^{(n)}}\overline{F}_R^{0(m)}\gamma^\mu F_R^{+(n)}\right) + (\text{h.c.}),$$

$$g_{W_R^{(l)}F_L^{(m)}F_L^{(n)}} = \frac{g_w}{2\sqrt{2}}\frac{\sqrt{L}}{\sqrt{r_{W_R^{(l)}}}\sqrt{1+\cos^2\theta_H}} \times \int_1^{z_L} dz\; C(z)\Big\{(1-\cos\theta_H)f_{lL}^{(m)*}f_{lL}^{(n)} - (1+\cos\theta_H)f_{rL}^{(m)*}f_{rL}^{(n)}\Big\}, \tag{B.54}$$

and $g_{W_R^{(l)}F_R^{(m)}F_R^{(n)}}$ is obtained by replacing $f_{l(r)L}$ with $f_{l(r)R}$.

In Tables 32, 33 and 34, we have summarised the $W\bar{F}F$ and the $W_R\bar{F}F$ couplings for various parameter sets.

B.19. $A^{\hat{4}}FF$ coupling

The $A^{\hat{4}}$ couplings of the dark fermion tower are given by

$$\begin{aligned}&\int_1^{z_L} dz\sqrt{G}\;\overline{\Psi}_F\left(-ig_A A_\mu - ig_B Q_{X_F}B_\mu\right)z\gamma^\mu\Psi_F \\ &= -ig_w\sum_{l,m,n}A_\mu^{\hat{4}(l)}\overline{F}_L^{(m)}\gamma^\mu F_L^{(n)}\frac{\sqrt{L}}{\sqrt{r_{A^{\hat{4}(l)}}}}\int_1^{z_L} dz\; S(z)\frac{1}{2\sqrt{2}}\Big(f_{lL}^{(m)*}f_{rL}^{(n)} + f_{rL}^{(m)*}f_{lL}^{(n)}\Big) + (L\to R).\end{aligned} \tag{B.55}$$

Therefore $\bar{F}^{(n)}F^{(n)}A_\mu^{\hat{4}}$ couplings vanish.

Table 32: The WFF couplings in the unit of $g_w/\sqrt{2}$ with b.c. $\eta_F = +1$ in the case of degenerate dark fermions. Reprinted from Ref. [28].

n_F	z_L	$g_{WF_L^{(1)}F_L^{(1)}}$	$g_{WF_R^{(1)}F_R^{(1)}}$	$m_{W^{(1)}}$ (TeV)	$g_{W^{(1)}F_L^{(1)}F_L^{(1)}}$	$g_{W^{(1)}F_R^{(1)}F_R^{(1)}}$
3	10^8	7.0×10^{-3}	3.98×10^{-2}	2.42	6.19×10^{-2}	0.1360
	10^6	3.8×10^{-3}	1.22×10^{-2}	4.25	2.64×10^{-2}	2.80×10^{-2}
	2×10^4	7.2×10^{-3}	1.02×10^{-2}	7.54	3.15×10^{-3}	7.8×10^{-3}
4	10^8	4.4×10^{-3}	3.59×10^{-2}	2.45	4.02×10^{-2}	0.1322
	10^6	2.0×10^{-3}	9.7×10^{-3}	4.32	1.50×10^{-2}	2.68×10^{-2}
	10^4	1.1×10^{-3}	2.7×10^{-3}	8.52	6.1×10^{-3}	3.8×10^{-3}
6	10^8	2.5×10^{-3}	3.26×10^{-2}	2.50	2.34×10^{-2}	0.1273
	10^6	1.0×10^{-3}	8.4×10^{-3}	4.40	8.0×10^{-3}	2.59×10^{-2}
	10^4	0.4×10^{-3}	1.7×10^{-3}	8.68	2.3×10^{-3}	3.6×10^{-3}

Table 33: The W_RFF couplings in the unit of $g_w/\sqrt{2}$ with b.c. $\eta_F = +1$ in the case of degenerate dark fermions. Reprinted from Ref. [28].

n_F	z_L	$m_{W_R^{(1)}}$ (TeV)	$g_{W_R^{(1)}F_L^{(1)}F_L^{(1)}}$	$g_{W_R^{(1)}F_R^{(1)}F_R^{(1)}}$
3	10^8	2.34	-0.41	-3.11
	10^6	4.06	-0.57	-2.66
	2×10^4	7.05	-0.84	-2.28
4	10^8	2.37	-0.30	-3.10
	10^6	4.12	-0.41	-2.65
	10^4	7.92	-0.59	-2.18
6	10^8	2.42	-0.19	-3.10
	10^6	4.20	-0.26	-2.64
	10^4	8.07	-0.36	-2.16

Table 34: The WFF and W_RFF couplings in the unit of $g_w/\sqrt{2}$ with b.c. $\eta_F = -1$ in the case of degenerate dark fermions for $n_F = 4$ case. Reprinted from Ref. [28].

n_F	z_L	$g_{WF_L^{(1)}F_L^{(1)}}$	$g_{WF_R^{(1)}F_R^{(1)}}$	$g_{W^{(1)}F_L^{(1)}F_L^{(1)}}$	$g_{W^{(1)}F_R^{(1)}F_R^{(1)}}$	$g_{W_R^{(1)}F_L^{(1)}F_L^{(1)}}$	$g_{W_R^{(1)}F_R^{(1)}F_R^{(1)}}$
4	10^8	0.997	0.966	0.04	4.15	-0.019	0.099
	10^6	0.998	0.991	0.10	3.59	-0.008	0.020
	10^4	0.999	0.998	0.21	2.93	-0.004	0.003

B.20. HFF coupling

The Higgs couplings of the dark fermion tower are given by

$$
\begin{aligned}
&\int_1^{z_L} dz\sqrt{G}\ \overline{\Psi}_F\left(-ig_A A_z\right)\gamma^5\Psi_F \\
&\supset -ig_A k\int_1^{z_L} dz\frac{1}{2\sqrt{2}}\sum_{m,n} H(x)u_H\left(f_{lL}^{*(m)}\overline{F}_L^{(m)}\gamma^5 f_{rR}^{(n)}F_R^{(n)}+f_{rL}^{*(m)}\overline{F}_L^{(m)}\gamma^5 f_{lR}^{(n)}F_R^{(n)}\right) \\
&\qquad +(L\longleftrightarrow R) \\
&= -ig_A k\int_1^{z_L} dz\frac{1}{2\sqrt{2}}\sum_{m,n} H(x)u_H \\
&\quad (-i)\Big(f_{lL}^{*(m)}f_{rR}^{(n)}F_L^{(m)\dagger}F_R^{(n)}+f_{lR}^{*(m)}f_{rL}^{(n)}F_R^{(m)\dagger}F_L^{(n)} \\
&\qquad\qquad +f_{rL}^{*(m)}f_{lR}^{(n)}F_L^{(m)\dagger}F_R^{(n)}+f_{rR}^{*(m)}f_{lL}^{(n)}F_R^{(m)\dagger}F_L^{(n)}\Big) \\
&= iH\sum_{m,n}\left(g_{HF_L^{(m)\dagger}F_R^{(n)}}F_L^{(m)\dagger}F_R^{(n)}-g_{HF_R^{(m)\dagger}F_L^{(n)}}F_R^{(m)\dagger}F_L^{(n)}\right).
\end{aligned}
\tag{B.56}
$$

where

$$
\begin{aligned}
g_{HF_L^{(m)\dagger}F_R^{(n)}} &= g_w\frac{\sqrt{kL}}{\sqrt{r_{F^{(m)}}r_{F^{(n)}}}}\sin\frac{\theta_H}{2}\cos\frac{\theta_H}{2}\int_1^{z_L} dz\frac{1}{2}\frac{1}{\sqrt{z_L^2-1}}\ z \\
&\quad\times\left(S_L^{(m)}(1)C_L^{(m)}(z)C_L^{(n)}(1)C_R^{(n)}(z)-C_L^{(m)}(1)S_L^{(m)}(z)S_L^{(n)}(1)S_R^{(n)}(z)\right)\ , \\
g_{HF_R^{(m)\dagger}F_L^{(n)}} &= g_w\frac{\sqrt{kL}}{\sqrt{r_{F^{(m)}}r_{F^{(n)}}}}\sin\frac{\theta_H}{2}\cos\frac{\theta_H}{2}\int_1^{z_L} dz\frac{1}{2}\frac{1}{\sqrt{z_L^2-1}}\ z \\
&\quad\times\left(-S_L^{(m)}(1)S_R^{(m)}(z)C_L^{(n)}(1)S_L^{(n)}(z)+C_L^{(m)}(1)C_R^{(m)}(z)S_L^{(n)}(1)C_L^{(n)}(z)\right)\ .
\end{aligned}
\tag{B.57}
$$

One can show that $g^*_{HF_R^{(m)\dagger}F_L^{(n)}}=g_{HF_R^{(m)\dagger}F_L^{(n)}}=g_{HF_L^{(n)\dagger}F_R^{(m)}}$. We define

$$
y_{F^{(m)}F^{(n)}}=\frac{g_{HF_L^{(m)\dagger}F_R^{(n)}}+g_{HF_R^{(m)\dagger}F_L^{(n)}}}{2}\quad,\quad \hat{y}_{F^{(m)}F^{(n)}}=\frac{-g_{HF_L^{(m)\dagger}F_R^{(n)}}+g_{HF_R^{(m)\dagger}F_L^{(n)}}}{2}\ .
\tag{B.58}
$$

In particular

$$
y_{F^{(n)}F^{(n)}}=g_w\frac{\sqrt{kL}}{\sqrt{r_{F^{(m)}}r_{F^{(n)}}}}\sin\frac{\theta_H}{2}\cos\frac{\theta_H}{2}\frac{1}{4}\sqrt{z_L^2-1}S_L^{(n)}(1)C_L^{(n)}(1)\ .
\tag{B.59}
$$

Numerical values of $y_{F^{(m)}F^{(n)}}$ and $\hat{y}_{F^{(m)}F^{(n)}}$ are given in Table 35 and 36, respectively. Numerical values of $y_{F^{(n)}F^{(n)}}$ for various parameter sets are shown in 37.

Table 35: $y_{F^{(m)}F^{(n)}}$ in the unit of $y_t \sin\frac{\theta_H}{2}$. The value are written by three significant figures. Reprinted from Ref. [29].

	1	2	3	4	5	6	7
1	-0.944	-12.6	0.328	2.85	-0.006	-0.485	0.038
2	-12.6	0.856	8.73	-0.357	-0.174	0.003	0.394
3	0.328	8.73	-0.924	-12.7	0.369	2.65	-0.002
4	2.85	-0.357	-12.7	0.920	9.05	-0.376	-0.277
5	-0.006	-0.174	0.369	9.05	-0.942	-12.7	0.380
6	-0.485	0.003	2.65	-0.376	-12.7	0.941	9.13
7	0.038	0.394	-0.002	-0.277	0.380	9.13	-0.953

Table 36: $\hat{y}_{F^{(m)}F^{(n)}}$ in the unit of $y_t \sin\frac{\theta_H}{2}$. Only the value larger than $O(10^{-3})$ are shown and written by three significant figures. Reprinted from Ref. [29].

	1	2	3	4	5	6	7
1	0	-6.54	0.117	1.35	-0.017	-0.654	0.013
2	6.54	0	1.62	-0.094	0.168	0.005	0.106
3	-0.117	-1.62	0	-1.26	0.066	0.627	-0.002
4	-1.35	0.094	1.26	0	0.934	-0.057	0.027
5	0.017	-0.168	-0.066	-0.934	0	-0.668	0.044
6	0.654	0.005	-0.627	0.057	0.668	0	0.648
7	-0.013	-0.106	0.002	-0.027	-0.044	-0.648	0

Table 37: The Higgs-Yukawa couplings $y_{F_i^{(1)}F_i^{(1)}}$ in (B.58) in the case of degenerate dark fermions. Reprinted from Ref. [28].

n_F	z_L	$y_{F_i^{(1)}F_i^{(1)}}$
3	10^8	-0.106
	10^6	-0.071
	10^5	-0.064
	2×10^4	-0.089
4	10^8	-0.082
	10^6	-0.049
	10^5	-0.038
	3×10^4	-0.034
	10^4	-0.033
6	10^8	-0.060
	10^6	-0.034
	10^5	-0.024
	10^4	-0.017

References

[1] G. Aad *et al.*, [ATLAS Collaboration], "Observation of a new particle in the search for the Standard Model Higgs boson with the ATLAS detector at the LHC", Phys. Lett. **B716**, 1 (2012).

[2] S. Chatrchyan *et al.*, [CMS Collaboration], "Observation of a new boson at a mass of 125 GeV with the CMS experiment at the LHC", Phys. Lett. **B716**, 30 (2012).

[3] G. Aad *et al.*, [ATLAS and CMS Collaboration], "Combined Measurement of the Higgs Boson Mass in *pp* Collisions at $\sqrt{s} = 7$ and 8 TeV with the ATLAS and CMS Experiments", Phys. Rev. Lett. **114**, 191803 (2015).

[4] V. Khachatryan *et al.* [CMS Collaboration], "Precise determination of the mass of the Higgs boson and tests of compatibility of its couplings with the standard model predictions using proton collisions at 7 and 8 TeV", Eur. Phys. J. **C75**, 212 (2015).

[5] G. Aad *et al.* [ATLAS Collaboration], "Measurements of the Higgs boson production and decay rates and coupling strengths using *pp* collision data at $\sqrt{s} = 7$ and 8 TeV in the ATLAS experiment", Eur. Phys. J. **C76**, 6 (2016).

[6] G. Aad *et al.*, [ATLAS Collaboration], "Search for high-mass dilepton resonances in pp collisions at $\sqrt{s} = 8$ TeV with the ATLAS detector", Phys. Rev. **D90**, 052005 (2014).

[7] V. Khachatryan *et al.*, [CMS Collaboration], "Search for physics beyond the standard model in dilepton mass spectra in proton-proton collisions at $\sqrt{s} = 8$ TeV", JHEP **04**, 025 (2015).

[8] P. A. R. Ade *et al.*, [Planck Collaboration], "Planck 2013 results. XVI. Cosmological parameters", Astron. Astrophys. **571**, A16 (2014).

[9] D. S. Akerib *et al.*, [LUX Collaboration], "First results from the LUX dark matter experiment at the Sanford Underground Research Facility", Phys. Rev. Lett. **112**, 091303 (2014).

[10] D. S. Akerib *et al.* [LUX Collaboration], "Improved WIMP scattering limits from the LUX experiment", arXiv:1512.03506 [astro-ph.CO].

[11] Y. Hosotani, "Dynamical Mass Generation by Compact Extra Dimensions", Phys. Lett. **B126**, 309 (1983).

[12] Y. Hosotani, "Dynamics of Nonintegrable Phases and Gauge Symmetry Breaking", Annals Phys. **190**, 233 (1989).

[13] A. Davies and A. McLachlan, "Gauge Group Breaking by Wilson Loops", Phys. Lett. **B200**, 305 (1988).

[14] A. Davies and A. McLachlan, "Congruency Class Effects in the Hosotani Model", Nucl. Phys. **B317**, 237 (1989).

[15] H. Hatanaka, T. Inami, and C. Lim, "The Gauge hierarchy problem and higher dimensional gauge theories", Mod. Phys. Lett. **A13**, 2601 (1998).

[16] G. Burdman and Y. Nomura, "Unification of Higgs and gauge fields in five-dimensions", Nucl. Phys. **B656**, 3 (2003).

[17] C. Csaki, C. Grojean, and H. Murayama, "Standard model Higgs from higher dimensional gauge fields", Phys. Rev. **D67**, 085012 (2003).

[18] Y. Matsumoto and Y. Sakamura, "6D gauge-Higgs unification on T^2/Z_N with custodial symmetry", JHEP **1408**, 175 (2014).

[19] C. S. Lim, N. Maru, and T. Miura, 'Is the 126 GeV Higgs boson mass calculable in gauge-Higgs unification?", PTEP **2015**, 043B02 (2015).

[20] K. Agashe, R. Contino, and A. Pomarol, "The Minimal composite Higgs model", Nucl. Phys. **B719**, 165 (2005).

[21] A. D. Medina, N. R. Shah, and C. E. Wagner, "Gauge-Higgs Unification and Radiative Electroweak Symmetry Breaking in Warped Extra Dimensions", Phys. Rev. **D76**, 095010 (2007).

[22] Y. Hosotani and Y. Sakamura, "Anomalous Higgs couplings in the $SO(5)\times U(1)_{B-L}$ gauge-Higgs unification in warped spacetime", Prog. Theor. Phys. **118**, 935 (2007).

[23] Y. Hosotani, K. Oda, T. Ohnuma, and Y. Sakamura, "Dynamical Electroweak Symmetry Breaking in $SO(5)\times U(1)$ Gauge-Higgs Unification with Top and Bottom Quarks", Phys. Rev. **D78**, 096002 (2008).

[24] Y. Hosotani and Y. Kobayashi, "Yukawa Couplings and Effective Interactions in Gauge-Higgs Unification", Phys. Lett. **B674**, 192 (2009).

[25] Y. Hosotani, S. Noda, and N. Uekusa, "The Electroweak gauge couplings in $SO(5)\times U(1)$ gauge-Higgs unification", Prog. Theor. Phys. **123**, 757 (2010).

[26] S. Funatsu, H. Hatanaka, Y. Hosotani, Y. Orikasa, and T. Shimotani, "Novel universality and Higgs decay $H\to\gamma\gamma, gg$ in the $SO(5)\times U(1)$ gauge-Higgs unification", Phys. Lett. **B722**, 94 (2013).

[27] S. Funatsu, H. Hatanaka, Y. Hosotani, Y. Orikasa, and T. Shimotani, "LHC signals of the $SO(5) \times U(1)$ gauge-Higgs unification", Phys. Rev. **D89**, 095019 (2014).

[28] S. Funatsu, H. Hatanaka, Y. Hosotani, Y. Orikasa, and T. Shimotani, "Dark matter in the $SO(5) \times U(1)$ gauge-Higgs unification", PTEP **2014**, 113B01 (2014).

[29] S. Funatsu, H. Hatanaka, and Y. Hosotani, "$H \to Z\gamma$ in the gauge-Higgs unification", Phys. Rev. **D92**, 115003 (2015).

[30] L. Randall and R. Sundrum, "A Large mass hierarchy from a small extra dimension", Phys. Rev. Lett. **83**, 3370 (1999).

[31] A. Pomarol, "Gauge bosons in a five-dimensional theory with localized gravity", Phys. Lett. **B486**, 153 (2000).

[32] Y. Grossman and M. Neubert, "Neutrino masses and mixings in nonfactorizable geometry", Phys. Lett. **B474**, 361 (2000).

[33] K. Oda and A. Weiler, "Wilson lines in warped space: Dynamical symmetry breaking and restoration", Phys. Lett. **B606**, 408 (2005).

[34] A. Falkowski, "About the holographic pseudo-Goldstone boson", Phys. Rev. **D75**, 025017 (2007).

[35] J. Pumplin *et al.*, "New generation of parton distributions with uncertainties from global QCD analysis", JHEP **07**, 012 (2002).

[36] J. F. Gunion, H. E. Haber, G. L. Kane, and S. Dawson, "The Higgs Hunter's Guide", Front. Phys. **80**, 1 (2000).

[37] G. Passarino and M. Veltman, "One Loop Corrections for e^+e^- Annihilation into $\mu^+\mu^-$ in the Weinberg Model", Nucl. Phys. **B160**, 151 (1979).

[38] A. Denner, "Techniques for calculation of electroweak radiative corrections at the one loop level and results for W physics at LEP-200", Fortsch. Phys. **41**, 307 (1993).

[39] E. W. Kolb and M. S. Turner, "The Early Universe", Front. Phys. **69**, 1 (1990).

[40] G. Jungman, M. Kamionkowski and K. Griest, "Supersymmetric dark matter", Phys. Rept. **267**, 195 (1996).

[41] J. R. Ellis, A. Ferstl and K. A. Olive, "Re-evaluation of the elastic scattering of supersymmetric dark matter", Phys. Lett. **B481**, 304 (2000).

[42] G. Servant and T. M. P. Tait, "Is the lightest Kaluza-Klein particle a viable dark matter candidate?", Nucl. Phys. **B650**, 391 (2003).

[43] G. Belanger, M. Kakizaki and A. Pukhov, "Dark matter in UED: The Role of the second KK level", JCAP **1102**, 009 (2011).

[44] K. Griest and D. Seckel, "Three exceptions in the calculation of relic abundances", Phys. Rev. **D43**, 3191 (1991).

[45] M. W. Goodman and E. Witten, "Detectability of Certain Dark Matter Candidates", Phys. Rev. **D31**, 3059 (1985).

[46] Y. Hosotani and N. Yamatsu, "Gauge-Higgs Grand Unification", PTEP **2015** 111B01 (2015).

[47] N. Yamatsu, "Gauge Coupling Unification in Gauge-Higgs Grand Unification", arXiv:1512.05559 [hep-ph].

[48] G. Cossu, H. Hatanaka, Y. Hosotani, and J.-I. Noaki, "Polyakov loops and the Hosotani mechanism on the lattice", Phys. Rev. **D89** 094509 (2014).

[49] K. Yamamoto, "The formulation of gauge-Higgs unification with dynamical boundary conditions", Nucl. Phys. **B883** 45-58 (2014).